

MEASUREMENT OF SOLIDUS AND LIQUIDUS TEMPERATURE
OF BLAST FURNACE SLAG WITH AND WITHOUT
ADDITIONS OF Al_2O_3 , CaO & TiO_2

by
RAJENDRA KUMAR VERMA



DEPARTMENT OF METALLURGICAL ENGINEERING

INDIAN INSTITUTE OF TECHNOLOGY KANPUR

MAY, 1977

MEASUREMENT OF SOLIDUS AND LIQUIDUS TEMPERATURE
OF BLAST FURNACE SLAG WITH AND WITHOUT
ADDITIONS OF Al_2O_3 , CaO & TiO_2

A Thesis Submitted
In Partial Fulfilment of the Requirements
for the Degree of
MASTER OF TECHNOLOGY

by
RAJENDRA KUMAR VERMA

20862

to the


DEPARTMENT OF METALLURGICAL ENGINEERING
INDIAN INSTITUTE OF TECHNOLOGY KANPUR
MAY, 1977

LIBRARY
CENTRAL LIBRARY
Acc. No. A 50869

ME-1977-M-VER-MEA

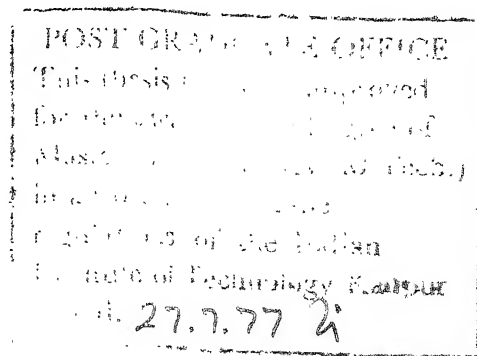
CERTIFICATE

Certified that this work on "Measurement of Solidus and Liquidus Temperature of Blast Furnace Slags With and Without Additions of Al_2O_3 , CaO and TiO_2 " has been carried out under our supervision and that it has not been submitted elsewhere for a degree.



(H.S. RAY)
Assistant Professor
Dept. of Metallurgical Engg.
Indian Institute of Technology
Kanpur.

(A. GHOSH)
Professor
Dept. of Metallurgical Engg.
Indian Institute of Technology
Kanpur.



ACKNOWLEDGEMENTS

The author wishes to express his deep sense of gratitude to Dr. A. Ghosh and Dr. H.S. Ray for their valuable guidance and constant encouragement throughout the course of this work.

The author is grateful to R & D Organization, Hindustan Steel Ltd., Ranchi for financial support for the entire work including fellowship and for periodic discussions with their personnel.

The author is grateful to Prof. P.K. Sen (I.I.T. Kharagpur), Drs. E.C. Subbarao, K.V.G.K. Gokhale, R.N. Biswas, T.R. Vishwanathan for the useful discussions he had with them.

Thanks are due to Messers N.B. Ballal, R. Mathur, R. Dixit, J.Y. Chaudhary, V.N. Sharma, A. Sharma and V.P. Gupta for their help in various ways. The author also thanks Mr. R.N. Srivastava for his flawless typing.

CONTENTS

| <u>Chapter</u> | <u>Page</u> |
|---|-------------|
| LIST OF FIGURES | vi |
| LIST OF TABLES | viii |
| 1. INTRODUCTION | 1 |
| 1.1 Importance of Liquidus Temperature | 1 |
| 1.2 Objective of Present Work | 2 |
| 1.3 Blast Furnace Slag Composition | 3 |
| 1.4 Measurement Techniques | 4 |
| 1.5 Plan of the Work | 6 |
| 2. LITERATURE REVIEW ON DIFFERENTIAL THERMAL ANALYSIS AND HOT FILAMENT MICROSCOPY | 7 |
| 2.1 Differential Thermal Analysis (DTA) | 8 |
| 2.2 Hot Filament Microscopy (HFM) | 21 |
| 3. LITERATURE REVIEW ON LIQUIDUS TEMPERATURES IN BLAST FURNACE SLAG SYSTEM | 30 |
| 3.1 Phase Diagrams of Three Component and Multicomponent Systems | 30 |
| 3.2 Synthetic Blast Furnace Slag Compositions | 39 |
| 3.3 Actual Blast Furnace Slags | 47 |
| 3.4 Crystallization of Blast Furnace Slag | 48 |
| 4. PREPARATION AND CHARACTERIZATION OF SLAG SAMPLES | 55 |
| 4.1 Preparation of Blast Furnace Slag Samples | 55 |
| 4.2 Additives-Specifications and Preparations | 56 |
| 4.3 Preparation of Various Compositions with and without Additives | 56 |

| <u>Chapter</u> | <u>Page</u> |
|--|-------------|
| 4.4 Chemical Analysis of Blast Furnace Slags | 57 |
| 4.5 Chemical Characterization of Various Compositions | 60 |
| 4.6 Annealing Procedure for Blast Furnace Slags | 60 |
| 5. DESIGN, FABRICATION AND PERFORMANCE OF HOT FILAMENT MICROSCOPE (HFM) | 65 |
| 5.1 Apparatus | 68 |
| 5.2 Performance of Apparatus | 77 |
| 6. DIFFERENTIAL THERMAL ANALYSIS (DTA): APPARATUS AND EXPERIMENTAL PROCEDURE | 79 |
| 6.1 Apparatus | 79 |
| 6.2 Experimental Procedure | 88 |
| 6.3 Performance of Apparatus at Moderate Temperatures | 90 |
| 6.4 Performance of Apparatus at High Temperatures | 90 |
| 7. RESULTS AND DISCUSSIONS | 92 |
| 7.1 DTA Traces | 92 |
| 7.2 Results | 96 |
| 7.3 Comparison with Liquidus Data Available in Literature | 99 |
| 8. SUMMARY AND CONCLUSIONS | 105 |
| 8.1 Summary | 105 |
| 8.2 Conclusions | 105 |
| REFERENCES | 106 |
| Appendix-I | 111 |

LIST OF FIGURES

| <u>Figure</u> | <u>Page</u> |
|---|-------------|
| 2.1 Simplified DTA curve | 10 |
| 2.2 DTA switching circuit by Welch | 20 |
| 2.3 DTA apparatus by Gruner | 22 |
| 2.4 Electrical circuit diagram used by Ohno and Ross | 24 |
| 2.5 All alloy platinum-rhodium thermocouple | 27 |
| 2.6 Thermocouple shapes used by several workers | 28 |
| 3.1 Representation of composition in a ternary diagram | 31 |
| 3.2 Perspective drawing of a space model of a ternary system | 33 |
| 3.3 Phase diagram for system $\text{CaO-Al}_2\text{O}_3\text{-SiO}_2$ | 35 |
| 3.4 Tetrahedron representing the quaternary system $\text{CaO-Al}_2\text{O}_3\text{-SiO}_2\text{-MgO}$ | 38 |
| 3.5 Selected saturation lines in blast furnace slags of the system $\text{Al}_2\text{O}_3\text{-CaO-MgO-SiO}_2$ | 46 |
| 3.6 Schematic diagram for the crystallization of a viscous liquid | 51 |
| 4.1 Induction melting crucible | 58 |
| 5.1 Heating and measurement circuit | 66 |
| 5.2 Hot stage microscope | 67 |
| 5.3 Solid state switching device | 71 |
| 5.4 DTA circuit using DPDT switch | 72 |
| 5.5 SPDT rotary switch | 74 |
| 5.6 Components of rotary switch | 75 |

| <u>Figure</u> | <u>Page</u> |
|--|-------------|
| 6.1 Set-up for DTA | 80 |
| 6.2 Furnace assembly | 82 |
| 6.3 Helical winding on refractory tybe | 83 |
| 6.4 DTA cell | 85 |
| 6.5 Photograph of DTA set-up | 87 |

LIST OF TABLES

| <u>Table</u> | | <u>Page</u> |
|--------------|--|-------------|
| 3.1 | Various compounds present in blast furnace slag | 40 |
| 3.2 | A comparison of slags of same desulphurizing power with and without magnesia | 42 |
| 4.1 | Slag analysis from various sources | 59 |
| 4.2 | Computed chemical analysis of region A and B | 63 |
| 7.1 | Summary of main observations from DTA traces | 93 |
| 7.2 | Slag analysis of samples in terms of four component | 100 |
| 7.3 | Comparison of some liquidus temperatures with those of Osborn et al. ²² | 102 |
| 7.4 | Comparison of some liquidus temperatures with those of Baldwin ²⁰ | 104 |

CHAPTER 1

INTRODUCTION

1.1 Importance of Liquidus Temperature:

A typical blast furnace slag is a complex system consisting of several constituents and has no well-defined melting point. In the quenched state, it consists of a glassy phase which on heating exhibits a softening range but no sharp melting point. In the softening range the viscosity of any glass gradually falls by several orders of magnitude to show transition from an apparent rigid state to a fluid one. For such slags, therefore, it is difficult to define a sharp melting point. However, one can indicate an approximate temperature at which the entire bulk is transformed into a molten state. Thus the liquidus temperature has been defined as a temperature above which the system is completely liquid.

The importance of liquidus temperature in blast furnace operation cannot be over-emphasised. If the liquidus temperature is low, then a molten slag is obtained at a lower hearth temperature. A molten slag at lower temperature allows lower operational temperature in the blast furnace leading to lower coke rate and less refractory wear. It

also yields pig iron with a lower silicon content, which is an advantage in steelmaking. It is therefore extremely important to operate blast furnaces with slag of as low a liquidus temperature as possible.

1.2 Objective of the Present Work:

The objective of the present investigation is to measure the solidus and liquidus temperatures of some slag compositions, specified by Hindustan Steel Limited, Research and Development Organization. They are interested in changing compositions of the Bosh slag by additions through tuyeres.

The bosh slag characteristics has quite a bearing with the performance of any blast furnace. Indian blast furnaces operate under an unusual slag regime characterized mainly by highly viscous bosh slag. This is because of the fact that the flux required to be charged through the burden is very high under Indian conditions of high ash in coke and high $\text{Al}_2\text{O}_3/\text{SiO}_2$ ratio. But only about 25% of coke ash, which is the major source of SiO_2 input into the blast furnace is released in the bosh zone and rest of it is released near the tuyeres. Therefore basicity of the bosh slag is very high leading to high viscosity as well. If a

portion of total lime required is injected through tuyeres, the bosh slag basicity is likely to decrease which is expected to decrease the viscosity and increase bosh permeability, resulting into higher driving rates and higher productivity.¹

Keeping in view the above, this laboratory investigation was sponsored to measure the solidus and liquidus temperatures of 23 slags compositions using Differential Thermal Analysis (DTA) and Hot Filament Microscopy (HFM). These compositions were made by making various additions to a Rourkela blast furnace slag sample according to the specifications given by the Research and Development Organization, Hindustan Steel Limited.

1.3 Blast Furnace Slag Composition:

For a blast furnace to operate smoothly and with maximum efficiency, the slag should have the following characteristics:

- a. It should be a homogeneous liquid and without any crystalline phases present.
- b. Its composition should be such that a wide latitude of variation in composition is possible without troublesome slag developing. Even under the best conditions of operation, characteristics of the raw materials exhibit variations to cause significant fluctuations in

composition of the slag. This should not lead to notable changes in its properties and performance.

- c. It should have a large capacity to retain sulphur, or in other words, the partition coefficient of sulphur between the slag and metal under conditions prevalent in the blast furnace should be high.
- d. It should have a low viscosity at the temperatures prevailing in the furnace hearth and bosh in order to melt it down and move it through and out of the furnace quickly and smoothly. This also leads to better sulphur and silicon partitioning.

1.4 Measurement Techniques:

There are three methods which have been used for the determination of liquidus and solidus temperatures.

1. Quench Method: This is the classical method for determination of solidus and liquidus temperatures. In this method a given sample is held for a very long time at a given temperature to ensure attainment of equilibrium amongst phases. It is then quenched and the phases analysed under a petrographic microscope. The method is extremely tedious and time consuming. A single liquidus temperature may take a couple of days or more for determination.

2. Hot Filament Microscopy: In this method, first developed by Ordway^{1A} and then Welch², a phase transformation is actually observed visually in a hot filament microscope.

For greater accuracy of temperature measurements, only a very minute quantity of slag is heated at the tip of a thermocouple which functions both as a heating device as well as a temperature sensing device. To achieve this dual purpose a switching circuit is used for alternate heating and temperature measurement. The switching is done at a frequency of 50 c/s or more. This method, however, depends on the visual judgement of the observer and may be subjective. Also the method yields no permanent record. Its great advantage lies in the fact that data collection can be done at a fast rate.

3. Differential Thermal Analysis: The differential thermal analysis (DTA) is a technique of recording the difference in temperature between the substance under investigation and a reference material as the two specimens are subjected to identical temperature regimes in an environment heated or cooled at a controlled rate. If the substance is thermally active in the temperature range used, then the record obtained, called the DTA curve, shows one or more peaks, the positions of which are determined by the chemical composition

and the crystalline structure of the substance and the area of which is related to the energy involved in the reaction occurring.

It has been shown that the data obtained by these three techniques on the same samples are in good agreement³, provided adequate precautions are taken.

1.5 Plan of the Work:

The entire work was divided into five parts.

1. Preparation and characterization of slag samples with and without additions.
2. Fabrication of a hot filament microscope set-up.
3. Determination of liquidus temperatures by hot filament microscopy.
4. Fabrication of DTA set-up.
5. Determination of liquidus and solidus temperatures by DTA.

CHAPTER 2

LITERATURE REVIEW ON DIFFERENTIAL THERMAL ANALYSIS AND HOT FILAMENT MICROSCOPY

The most widely used method for determination of melting and solidation points in model oxide system has been the one in which a melt of known gross composition is brought into thermal equilibrium at a high temperature. It is then rapidly quenched to room temperature to preserve the high temperature phases which are identified with the aid of a petrographic microscope. As mentioned earlier, this method is extremely tedious and must be repeated at successive temperature intervals for every composition studied. As there is no means of knowing in advance which combination of temperature and composition will yield the most useful information, it may be necessary to examine several hundreds of quenched samples while investigating a system. The other methods of melting point determination, viz., the hot filament method (HFM) and the thermal analysis methods, however, are far more rapid and yield direct determination of these temperatures for every composition. The results are reliable provided the experimental arrangements are adequate.

2.1 Differential Thermal Analysis (DTA):

"Differential Thermal Analysis (DTA) is a technique of recording the difference in temperature between a substance and a reference material as the two specimens are subjected to identical temperature regimes in an environment heated or cooled at a controlled rate. If the substance is thermally active in the temperature range used then the record obtained, called the DTA curve, shows a series of peaks, the positions of which are determined by chemical composition and crystal structure of the substance and the areas of which are related to the energy involved in the reaction occurring."⁴

Recording the DTA curve of a sample is not a difficult procedure once suitable operating conditions have been established. However, the subsequent interpretation of the peaks and the base line shifts in terms of reactions and physical changes in the sample may be far more difficult, particularly if the sample is a multicomponent system or its composition is unknown. Secondly, although the art of DTA has reached a maturity that warrants a detailed and critical examination of the experimental methods used, the current literature still reveals a lack of knowledge of such basic considerations as heat transfer and temperature gradient

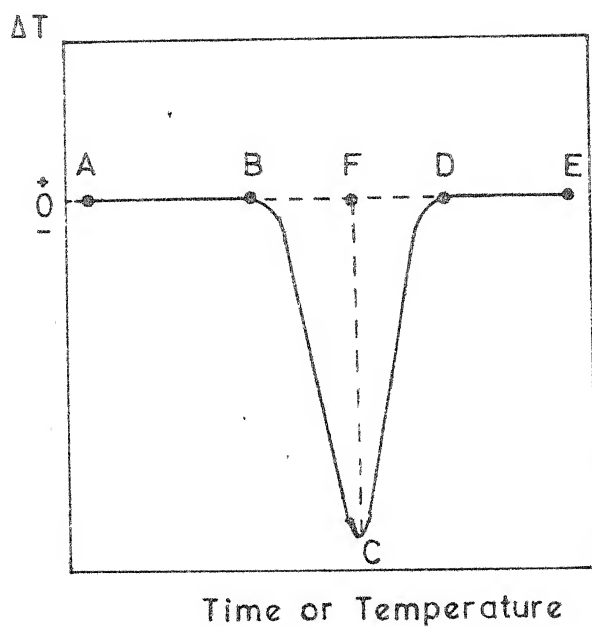
effects. The basic principles of DTA and various apparatus used have been discussed in several books, proceedings and monographs. 4-11 Accordingly, in the present write up only the more important aspects would be discussed.

2.1.1 Basic Principles:

Every chemical reaction or physical transformation liberates or absorbs heat, causing a change in temperature of the sample in DTA. Thus DTA involves recording of every enthalpy change caused by any structural change. DTA is a dynamic method in which equilibrium conditions are not attained. Thus the transition temperature obtained does not strictly correspond to equilibrium value. The differential temperature profile is characteristic of the substance under study for the given experimental conditions and may be used for its identification.

2.1.2 DTA Curve:

A simplified and formalized DTA curve for a material undergoing a simple endothermic reaction is shown in Figure 2-1. ΔT is plotted on the ordinate and time, or temperature on the abscissa. From room temperature (i.e. A to B) and again from D to E, no reaction occurs and the sample heats at the same rate as the reference material



G.2.1 Simplified and formalized DTA curve, illustrating the various attributes of the peak.

quasi-steady state of $\Delta T = 0$ is again established. Over the whole peak representing an endothermic reaction, therefore, the amount of heat supplied by the source to the sample is greater than that supplied to the reference. An exothermic peak may be analysed similarly.

In the case of physical transformations of the first order, the corresponding enthalpy change (ΔH) occurs at constant temperature, giving rise to an ideal DTA curve. In practice however DTA of majority of substances yield curves that are far from ideal. This is mainly because of temperature gradient created in the sample. In case of phase changes of higher order, the total enthalpy change occurs over a range of temperature but discontinuities in the specific heat and thermal conductivity are observed. This type of transformation includes changes in magnetic properties, transition from an ordered state to a disordered one, and devitrification. Supercooling or superheating leads to special effects on DTA curves, which are caused by the inhibition of the formation of nuclei of some new phase.

One of the simplest expression for area under the DTA curve is the following.

$$\frac{M_a \cdot \Delta H}{g \cdot \lambda_{sm}} = \int_a^c \Delta T \cdot dt \quad (2.1)$$

where M_a is the active mass of reacting substance in gms, ΔH is the enthalpy change of the reaction per gm of the active substance, g is a constant concerned with the effect of the arrangement of the sample and of the reference on the heat transfer, λ_{sm} is the coefficient of thermal conductivity of the sample, ΔT is the temperature difference and a and c are the limits of integral. The above expression relates the heat of reaction ($M_a \cdot \Delta H$) to the area under the curve when constants g and λ_{sm} are introduced. In the above equation the temperature drop in the sample and the dependance of the area on the specific heat of the sample are neglected. Small differences (approximately 3%) between calculated and measured values may be explained by the fact that the heat of reaction is not a linear function of temperature.

A series of mathematical expressions for the DTA curve based on general laws of heat and mass transport have been deduced. However, keeping in view the possible arrangements of the system, accurate solutions are complex and do not have Universal applicability.

2.1.3 Operational Parameters:

Garn³⁷ reviewed various empirical and theoretical factors involved in DTA. A number of experimental factors influencing the DTA curves are as follows:

1. Rate of temperature rise of furnace
2. Nature of sample holder
3. Depth and radius of the sample holes in the holder
4. The measurement sites of both the furnace as well as differential temperature
5. Nature and size of thermocouple
6. Nature of reference substance
7. The packing of the test sample and reference material
8. Composition of furnace atmosphere
9. Covering of the sample holes
10. Particle size of powders if powdered sample is used
11. Degree of crystallization if the sample is glassy.

The influence of only the more important parameters will be discussed here.

A. Choice of Reference Substance: Under steady heating conditions with no reaction the observed temperature depends both on the ease of heat transfer within the reference material (related to thermal conductivity) and on the amount of heat necessary to raise the temperature of the material (heat capacity). The quantities of interest are density, specific heat, thermal conductivity, and particle size. The first three of these are related in a term called the thermal diffusivity (α), which is defined as:

$$a = \frac{\lambda}{\rho c} \quad (2.2)$$

where λ is thermal conductivity, ρ is density, and c is specific heat.

For steady-state temperature difference, the following expression has been derived by Arens.⁴¹

$$\Delta T = \frac{1}{4} \frac{dT}{dt} r^2 \left(\frac{1}{a'} - \frac{1}{a} \right) \quad (2.3)$$

where dT/dt is the heating rate, r is the radius of the cavity and a' and a are the thermal diffusivities of the sample and the reference respectively.

It should also be noted that while the density and thermal conductivity are generally known for solids in large sizes, the effective density and the effective thermal conductivity will depend on particle size and packing.

Equation (2.3) shows that a zero base line can be obtained only when a and a' matched exactly at all temperatures. It is also commonly found that the base line after the reaction is not the same as before because the effective thermal diffusivity is most likely to change.

B. Packing of Powders: It has been generally found that non-reproducible packing from sample to sample causes variation between successive DTA curves and also leads to base line drifts. This is mainly attributed to the change

in thermal diffusivities of sample and reference material.³⁸ For consistent and reproducible results, it is desirable to use hard packing. However in certain types of holder - thermocouple arrangement where the thermocouple is outside the sample, packing does not affect the curve.^{39,40} Curves for materials undergoing reaction with the enveloping atmosphere are also particularly susceptible to packing differences unless the gas involved passes through the sample.³⁸ It is, therefore, essential that a reproducible method of packing should be employed. A careful packing or tapping the crucible by hand has been found to yield reproducible results within 1-2%, which is adequate for most purposes.⁴²

C. The Heating Rate: The significance of heating rate over the peak temperature not only depends on the nature of sample but also the way the sample is kept.³⁷ If the sample undergoes only a change in state the nature of sample holder is immaterial except for heat transfer problems. In such cases the effect of a change of heating rate will be small and any change or effect can be attributed principally to heat transfer considerations.⁴¹

The reactions involving weight-loss show peculiar behaviour with respect to changes in heating rates. Peak shifts of the order of 75°C or more have been reported.⁴²

Very high heating rates may completely mask a thermal event while very low heating rates may produce too small an effect to be detectable. The following table summarizes the effect of heating rates over peak temperature, and height, and width of the peak.

Effects of Slow and Fast Heating Rates³⁸

| Heating Rate | Effect |
|--------------|--|
| Slow | <p>Little base line shift;</p> <p>near equilibrium conditions;</p> <p>broad shallow peaks on T v/s time curves;</p> <p>sharp peaks on T v/s temperature curves;</p> <p>long time for determination</p> |
| ----- | |
| Fast | <p>Base line drift may be appreciable;</p> <p>conditions far from equilibrium;</p> <p>large narrow peaks on T v/s time curve;</p> <p>large broad peaks on T v/s temperature curve;</p> <p>short time for determination</p> |

For normal work 8-12°C/min rate is usually employed although rates ranging from 0.1°C/min to 200°C/min have been reported in literature.

D. Temperature Measurement and Effect of the Thermocouple

The shape of the DTA curve and the assignment of transition temperature depend on where the temperatures are measured.

Smyth⁴³ investigated the situation theoretically based on heat flow and arrived at the following conclusions.

- a. If the temperature difference, ΔT , is expressed as a function of the temperature of the surface of the sample, then the temperature of the point at which the curve first deviates from the base line corresponds to the transition temperature.
- b. If ΔT is expressed as a function of temperature of sample centre, and if the temperature of the surface increases linearly then the temperature of the peak corresponds to the temperature of change.
- c. If the temperature is measured in reference then the point of first deviation of the curve depends on the heating rate.
- d. If the change takes place continuously within a temperature interval, then it cannot be characterized by a single temperature. It may be characterized, however, by the temperature at which the rate of change under the given conditions attains its maximum value.

2.1.4 DTA Studies in Slag System:

A large number of DTA studies have been carried out in slag systems chiefly comprising of CaO , MgO , Al_2O_3 and SiO_2 .^{50,51} But these refer mainly to solid state transformations, devitrification and compound formations. Very few studies pertaining to solidus and liquidus temperature measurements are available in literature.

Solidus and liquidus determinations by DTA were undertaken by Nurse¹³, Welch³ and Grupner¹⁴. The method used by Welch involved continuous automatic recording of specimen temperature and difference temperature by a conventional photographic recorder. The mounting of specimen, however, was unorthodox. It consisted of using small amounts of material attached directly to the junction of thermocouple. Although a single thermocouple in the sample measures both absolute and difference temperatures, the measuring circuits are isolated from each other by a synchronous vibrator. The rapid switching of vibrator effectively produces continuous recording, for both T and ΔT . The schematic representation of the set-up is shown in Figure 2-2. The small sample size and intimate thermocouple contact are a definite advantage in rapidly establishing thermal and chemical equilibrium and countering the problem of drift. Grupner studied the

solidus temperature of synthetic analogues of zinc blast furnace slags. The sample holder used in this work consisted of three turns of 0.02 mm platinum wire with a thermojunction on the middle turn. The slag and the reference material (alumina) filled the interior and covered the exterior of the turns respectively. The experimental arrangement of the DTA cell is shown in Figure 2-3.

Ott and McLaren¹⁵ have studied the role of lead oxide and lead silicates in the melting of a sodium-lead-silicate glass using DTA with thermogravimetric measurements. Recently Naifziger¹⁶ investigated liquid phase relations in the portions of the system $\text{CaF}_2\text{-CaO-MgO-Al}_2\text{O}_3$ in an inert atmosphere. The DTA was employed to find out the lowest liquidus temperature for the optimum compositions of the fluxes used in electroslag process for making cobalt base superalloys.

2.2 Hot Filament Microscopy (HFM):

The principle of hot filament method (HFM) was first described by Ordway^{1A} and later modified by Welch². Subsequently it has been applied and used successfully by Byerley¹⁷ and Ohno¹⁸ with certain modifications for measurement of liquidus temperature.

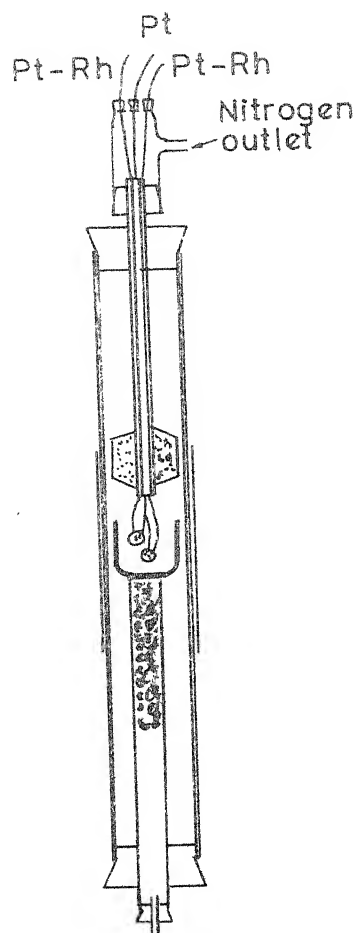


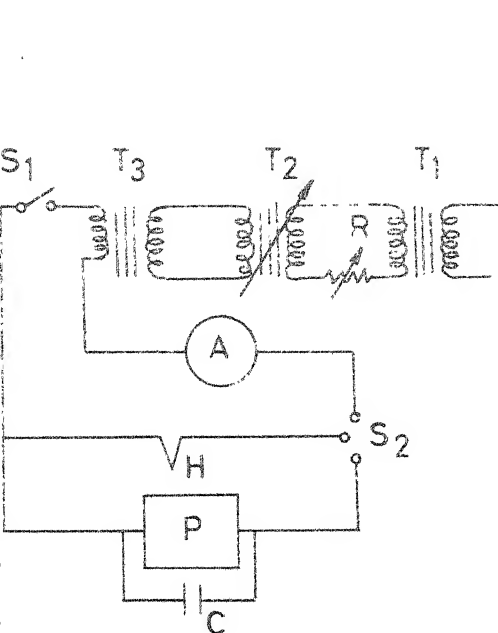
FIG.2.3 DTA apparatus by Grupner¹²

HFM apparatus consists of a small, electrically heated thermocouple bent into a loop at its extremity so as to hold the specimen in the form of a bead in contact with the thermojunction. The heating current is taken from any convenient 50 cps source and a vibrating switch driven from the same source permits the heating current to flow only during alternate half cycles, the measuring circuit being connected during the other half cycles.

Baldwin²⁰ with a similar equipment measured liquidus temperatures of over 150 blast furnace slags of varying composition. The agreement between results of liquidus measurements by HFM and quench methods were very good differing by no more than 1%.

2.2.1 Electrical Circuit:

The electrical circuit for HFM consists of a low voltage, high current power supply; and a switch, either mechanical or electrical, to change contacts to heating voltage or measuring instrument with a desired frequency. A schematic of the circuit is shown in Figure 2-4. In Figure 2-4 it is seen that one arm of the heated thermocouple is connected to common lead joining one side of the power supply and the measuring circuit. The essential feature of switch is that it should operate on break before make



- A : Ammeter
- T_1 : Constant voltage transformer
- T_2 : Variac autotransformer
- T_3 : Step transformer
- R : Variable resistance
- H : Thermocouple
- P : Potentiometer
- C : Capacitor
- S_1 : Single-pole Single throw switch
- S_2 : Rotating switch

FIG.2.4 Electrical circuit diagram used by Ohno & Ross (Ref 21)

principle to ensure isolation of the two circuits. Welch¹ used a single pole change over relay which was later found to be inadequate because relay contacts required continuous adjustment and tended to 'float' due to excessive current. Thus to obtain a steady-switching cycle Byerely¹⁷ adopted an arrangement which is simply two sets of automobile ignition contacts positioned around an eight-lobe cam so that one contact opens while the other closes, resulting in a single change over relay action. Later on this was used by Ohno¹⁸ and Ohno and Ross²¹ for liquidus measurements in synthetic blast furnace slags.

2.2.2 Thermocouple:

Instead of conventional platinum and 10% rhodium-platinum thermocouple, a relatively new platinum-rhodium alloy combination was used in HFM, viz., this thermocouple comprised of wires of 5% rhodium-platinum and 20% rhodium-platinum. The main reason for employing the above combination was to avoid cold junction errors. It also allowed a higher working temperature. This couple is very insensitive to variations in cold junction temperature although the thermoelectric output at higher temperature approximates that of conventional thermocouple alloys. Consequently the cold junction error likely to be encountered in the use of this

thermocouple will not be a significant factor within the overall accuracy expected. Comparison of EMF vs. temperature characteristics of various platinum alloy thermocouples is shown in Figure 2-5 to establish this argument.

Moreover, the 5% rhodium-platinum vs. 20% rhodium-platinum thermocouple is less susceptible to contamination than the standard platinum vs. 10% rhodium-platinum combination.

2.2.3 Optimum Thermocouple Shape:

Some possible thermocouple shapes have been described by Ohno and Ross²¹ and are shown in Figure 2-6. The wire employed for heated part of the thermocouple was 0.02 cm in diameter. This was welded to a short supporting lead, 0.05 cm in diameter, connected to external circuit by two set screws. In the thermocouple in Figure 2-6(b) a primary crystal of slag is expected to appear at the point indicated because the temperature in the fused slag would be lower at this point. In the arrangement shown in Figure 2-6(c), a primary crystal would not appear at the hot junction but at the point indicated. Therefore, in either of these two cases, it is difficult to measure the liquidus temperature of the slag accurately. The shape depicted in Figure 2-6(a) in which primary crystal of the slag is expected to appear at the hot junction ought to give the greatest accuracy in the liquidus determinations.

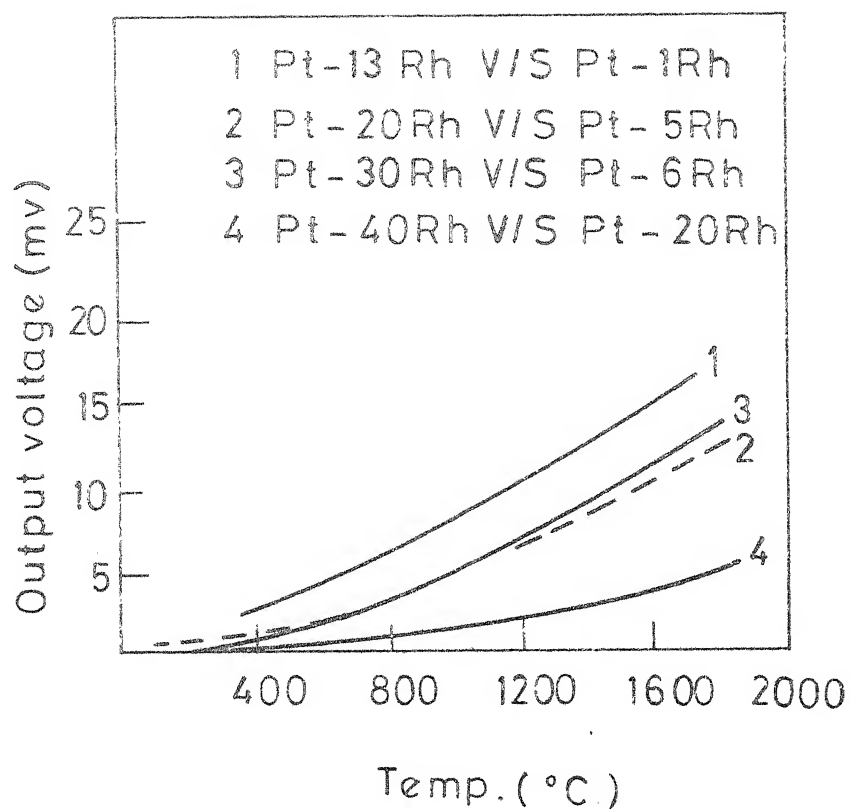
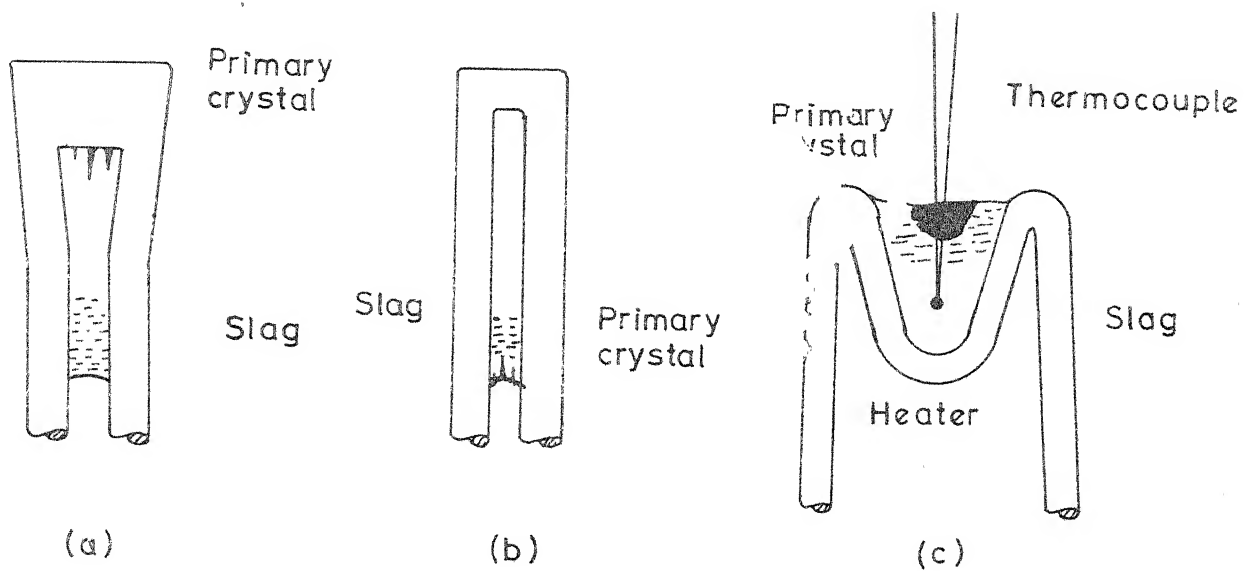


FIG. 2.5 ALL ALLOY PLATINUM - RHODIUM THERMOCOUPLES.



G. 2.6 Thermocouple shapes used by various workers (Ref. 21)

2.2.4 The Optical System:

This system consists of a long focus microscope and an illumination source. The microscope is characterized by the use of an objective of low numerical aperture, allowing for a greater depth of focus. This would give a working distance such that hot sample can be enclosed easily and damage of lenses from the high temperature can be prevented.

The major problem confronted is visibility of the crystals. The crystal formation is not visible by the light of incandescent samples. Viewing the samples in the transmitted light is the only method that would clearly illuminate the crystals which are transparent. The intense illumination is usually obtainable from tungsten ribbon filament lamp.

CHAPTER 3

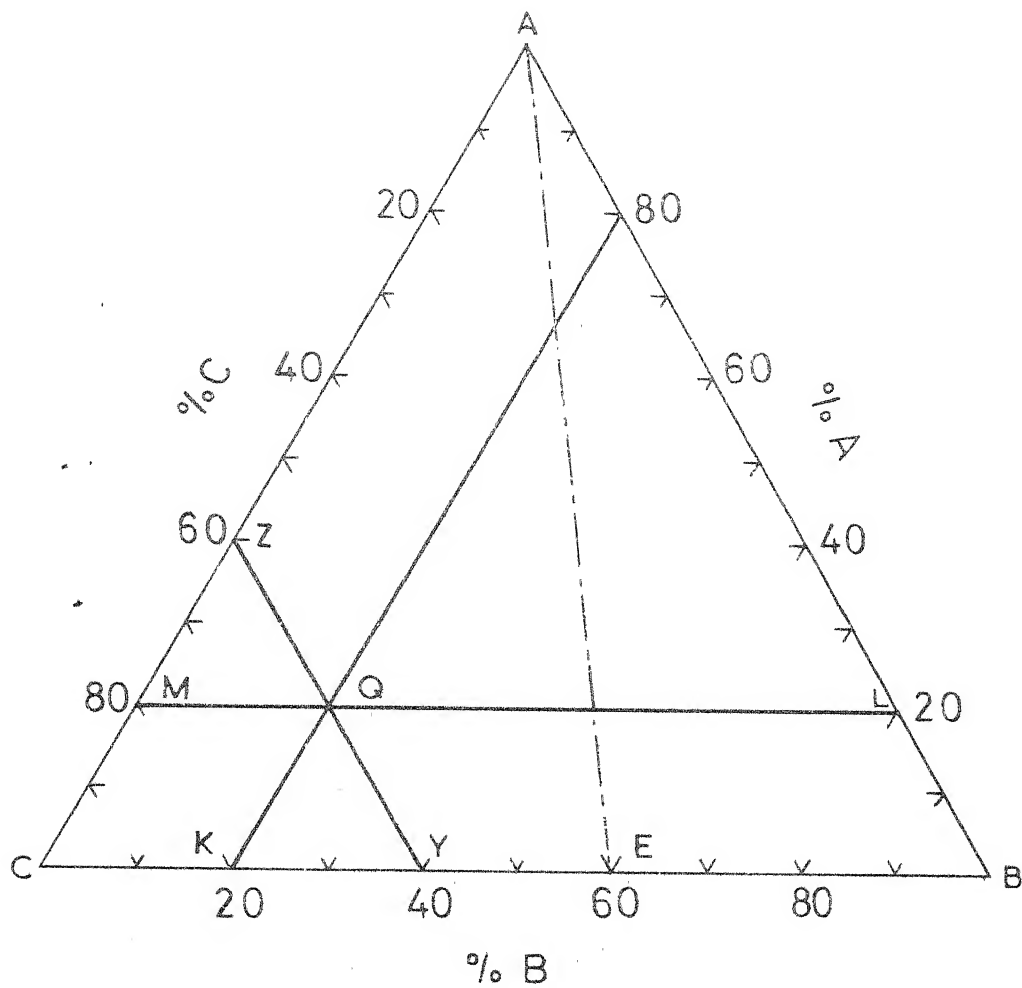
LITERATURE REVIEW ON LIQUIDUS TEMPERATURE IN BLAST FURNACE SLAG SYSTEM

3.1 Phase Diagrams of Three Component and Multicomponent Systems⁴⁵⁻⁴⁷:

3.1.1 Three Component Systems:

A three-component system may be described by specifying two of the three components. The total number of degrees of freedom in a ternary system is four (T , P , X_A and X_B) or three (T , X_A and X_B) when pressure is kept constant. Using phase rule it can be shown that the maximum number of phases which co-exist in equilibrium is four, which corresponds to an invariant point.⁴⁷

The composition field of a ternary system is usually represented by an equilateral triangle as shown in Figure 3-1. Each corner of triangle represents 100% of a pure component, each side, the composition of binary system involved, and any point within the triangle, a composition in the ternary system. For example in Figure 3-1 point A represents 100% A, point E, 60% B - 40% C, and point Q, 20% A - 20% B - 60% C. To obtain composition of point Q, three lines parallel to sides of the triangle are drawn



1 REPRESENTATION OF COMPOSITION IN A TERNARY SYSTEM

through it, then the lengths of BL (20%), CK (20%) and AZ (60%) represent the concentration of A, B, and C, respectively. Two important features of this scheme of composition representation are as follows.⁵³

1. Points on a line parallel to one side of the triangle represent compositions with a constant concentration of the component in the opposite corner. For example, in Figure 3-1 pct. of B is 60 on ZY.
2. Points on a straight line passing through one corner represent compositions with a fixed ratio between the concentrations of the components in the other two corners. For example, in Figure 3-1, the ratio of %B to %C is $2/3$ on AE.

A three dimensional diagram is necessary to represent the temperature vs. composition phase diagram of a ternary system. The temperature scale is drawn perpendicular to the composition triangle as shown in Figure 3-2 representing a ternary system with a simple eutectic without compound formation. The entire liquidus surface consists of intersecting curved surfaces representing the primary phase fields of compounds in the system. In the case of a congruently melting ternary, primary phase field is a domed surface, the highest elevation of which represents the

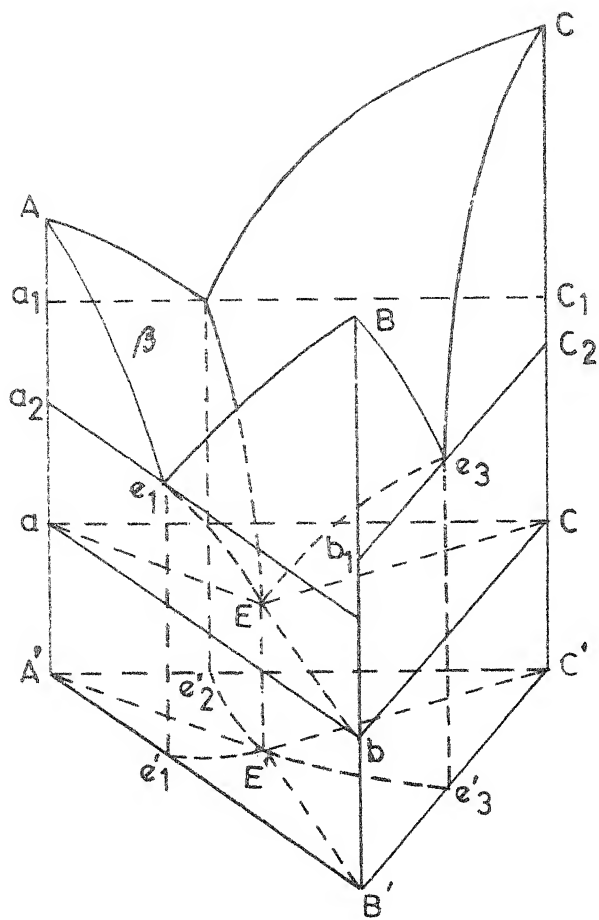


FIG.3 2 PERSPECTIVE DRAWING OF A SPACE MODEL
OF A TERNARY SYSTEM

melting point of the compound. Its field meets that of an adjacent congruently melting compound in a sloping valley or boundary line. In the case of an incongruently melting compound the intersection of the primary phase field of the first with that of second solid is a sloping terrace and not a valley.

It is not a simple task to present a ternary system completely. For complete representation one requires a space diagram and several isothermal and vertical sections. However, most of the ternary diagrams in the literature are simplified by projecting the valleys of liquidus on the composition triangles with arrows indicating direction of decreasing temperature. In addition to the liquidus projections, contours of isotherms and phase regions are marked. Usually this type of representation suffices for most practical purposes. A three-component system consisting of Al_2O_3 - CaO - SiO_2 is shown in Figure 3-3. It depicts

- a. Boundary curves as solid lines,
- b. Composition lines (Alkamade lines) as dashed lines.

The final product of crystallization (on slow cooling) of ternary solutions of this system always consists of three solid phases whose fields of stability are adjacent. The same three solid phases will be the final products of

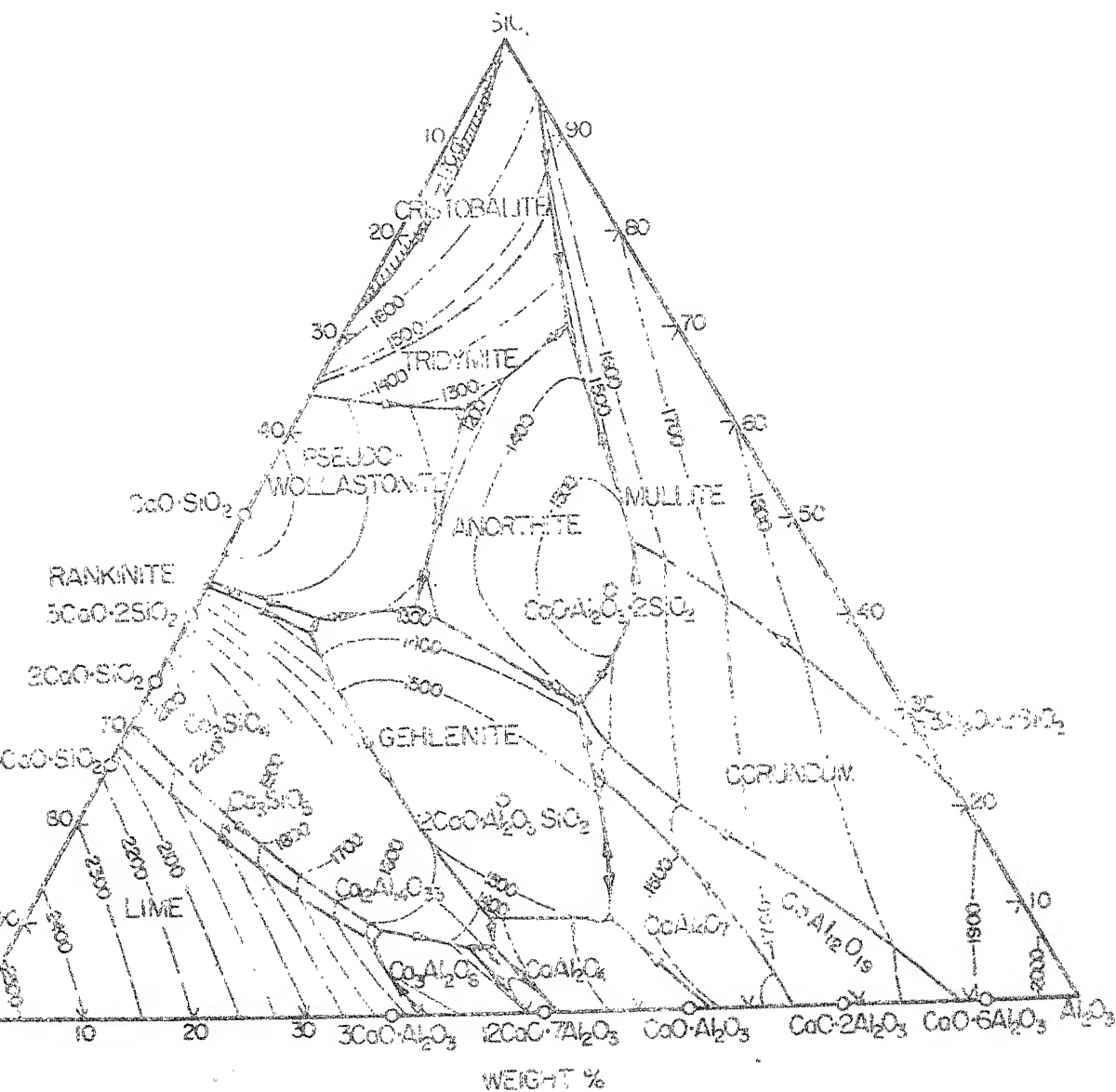


FIG. 3.3 Phase diagram for system CaO-Al₂O₃-SiO₂ (Ref. 48).

crystallization from any solution whose composition lies within the triangle formed by lines joining the compositions of these three phases.

3.1.2 Multicomponent Systems:

The arguments involved in representing and interpreting phase relations in binary and ternary systems applies also to quaternary and multicomponent systems. Beyond quaternary systems it is quite difficult to visualize and represent the systems. So in the present discussion, salient features of a quaternary system would be dealt with. If detailed data for a quaternary system are available, it is usually advantageous to build a tetrahedral model of the system in order to show satisfactorily phase relations at a particular temperature in the system in sufficient detail for practical use.

The complete graphical representation of a condensed quaternary phase, or one showing the relationships between temperature and all possible mixtures of four components, requires four dimensional space. All possible mixtures of four components, however, may be depicted by a regular tetrahedron, each apex representing 100% of one component. Various stable crystalline phases present in the system can be shown on the four faces. Considering the complex nature

of crystalline phases present, their modifications and their solubility at liquidus temperature, a systematic subdivision of the tetrahedron into smaller units is a must in order to obtain meaningful data and to convey them in a clear orderly manner.

Two different methods of representation are available as shown in Figure 3-4. One consists of choosing the planes representing compositions of mixtures having a constant content of one of the components at a given temperature. Such planes are parallel to one of the faces of the tetrahedron used to represent the quaternary system. Plane 'a' in Figure 3-4 is an example of such a plane, in which Al_2O_3 content is constant. The other choice consists in working along planes formed by joining triplets of points representing compositions of end members of crystalline phases present in the system. Plane 'b' in Figure 3-4 is an example of such a plane. Experimentally determined phase relations at liquidus temperature on each chosen plane are then usually drawn separately in the form of a triangular diagrams with liquidus temperatures indicated by liquidus isotherms, and boundary curves separating the various primary phase areas.

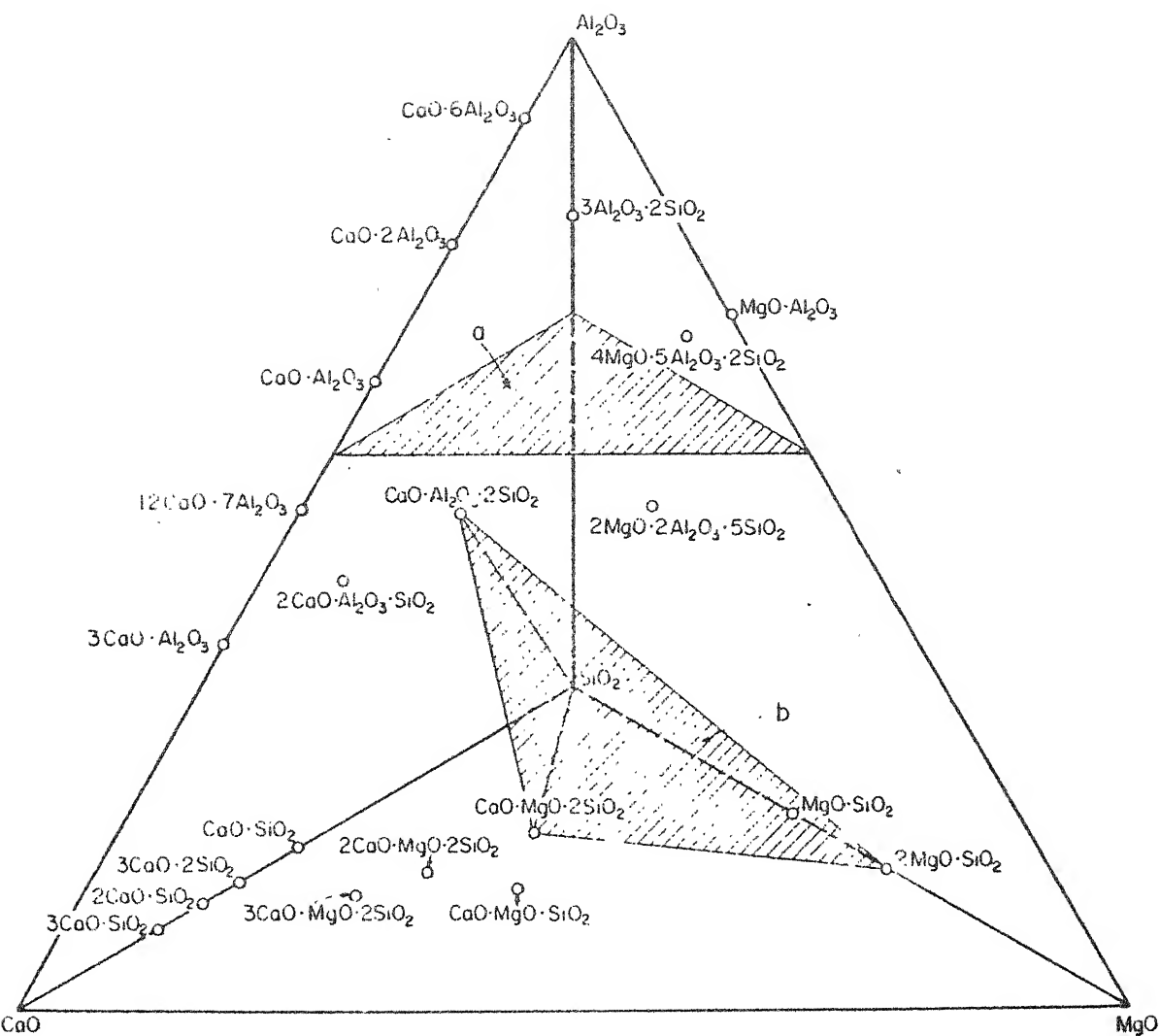


FIG. 3.4 Tetrahedron representing the quaternary system $\text{CaO-MgO-Al}_2\text{O}_3\text{-SiO}_2$. Planes (a) and (b) indicate alternative ways of representation (Ref. 48).

3.2 Synthetic Blast Furnace Slag Compositions:

A blast furnace slag can be considered approximately as a quaternary system comprising of $\text{CaO-Al}_2\text{O}_3\text{-SiO}_2\text{-MgO}$ without involving much error. An extensive work has been carried out by Osborn et al²² in order to understand the properties and to evaluate optimum slag compositions in terms of $\text{CaO-Al}_2\text{O}_3\text{-SiO}_2\text{-MgO}$ quaternary.

The primary phases present in the above quaternary system are listed in Table 3.1. Liquidus temperatures within each of these primary phase volumes vary with compositions in a manner which may be visualized by inspection of the liquidus isotherms in each plane of constant Al_2O_3 content.

The optimum slag composition with respect to desulphurizing power were deduced approximately from thermodynamic data for pure oxide and sulphide components.⁴⁸ From the free energy data it may be noted that K_2O and Na_2O are the best desulphurizers. However, because of their high vapour pressures and severe rate of attack on refractories, these oxides are not practical components of slags except as additions after tapping. The sulphur removal capacity of the practical slag ingredients increases in the order $\text{SiO}_2 < \text{Al}_2\text{O}_3 < \text{MgO} < \text{CaO}$. Clearly, low SiO_2 (and Al_2O_3) and high CaO (and MgO) content would be desirable in order to achieve the best possible sulphur retention by the slag.

Table 3.1
Various Compounds Present in B.F. Slags²⁵

| Chemical Formula | Name | Nomenclature |
|--|-----------------------|---------------------------|
| a) Single Component | | |
| Al_2O_3 | Corundum | A |
| CaO | Lime | C |
| MgO | Periclase | M |
| SiO_2 | Silica | S |
| b) Two Component | | |
| $\text{CaO} \cdot \text{SiO}_2$ | Calcium silicate | CS |
| $3\text{CaO} \cdot 2\text{SiO}_2$ | Tricalcium disilicate | C_3S_2 |
| $2\text{CaO} \cdot \text{SiO}_2$ | Dicalcium silicate | C_2S |
| $3\text{CaO} \cdot \text{SiO}_2$ | Tricalcium silicate | C_3S |
| $3\text{CaO} \cdot \text{Al}_2\text{O}_3$ | Tricalcium aluminate | C_3A |
| $12\text{CaO} \cdot 7\text{Al}_2\text{O}_3$ | | C_{12}A_7 |
| $\text{CaO} \cdot \text{Al}_2\text{O}_3$ | Calcium aluminate | CA |
| $\text{CaO} \cdot 2\text{Al}_2\text{O}_3$ | Calcium dialuminate | CA_2 |
| $\text{CaO} \cdot 6\text{Al}_2\text{O}_3$ | Calcium hexaaluminate | CA_6 |
| $3\text{Al}_2\text{O}_3 \cdot 2\text{SiO}_2$ | Mullite | C_3S_2 |
| $\text{MgO} \cdot \text{SiO}_2$ | Pyroxene | MS |
| $2\text{MgO} \cdot \text{SiO}_2$ | Forsterite | FO |
| $\text{MgO} \cdot \text{Al}_2\text{O}_3$ | Spinel | Sp |

Table 3.1 continued

| Chemical Formula | Name | Nomenclature |
|--|----------------------|--------------|
| c) Three Component | | |
| $\text{CaO} \cdot \text{Al}_2\text{O}_3 \cdot 2\text{SiO}_2$ | Anorthite | An |
| $2\text{CaO} \cdot \text{Al}_2\text{O}_3 \cdot \text{SiO}_2$ | Gehlenite | Ge |
| $2\text{CaO} \cdot \text{MgO} \cdot 2\text{SiO}_2$ | Akermanite | Ak |
| $\text{CaO} \cdot \text{MgO} \cdot 2\text{SiO}_2$ | Diopside | Di |
| $3\text{CaO} \cdot \text{MgO} \cdot 2\text{SiO}_2$ | Merwinite | Mer |
| $\text{CaO} \cdot \text{MgO} \cdot \text{SiO}_2$ | Monticellite | Mo |
| $2\text{Al}_2\text{O}_3 \cdot 2\text{MgO} \cdot 5\text{SiO}_2$ | Cordierite | Cor |
| $5\text{Al}_2\text{O}_3 \cdot 4\text{MgO} \cdot 2\text{SiO}_2$ | Sappharine | Sap |
| d) Solid Solution | | |
| $2\text{CaO} \cdot \text{Al}_2\text{O}_3 \cdot \text{SiO}_2 -$ $2\text{CaO} \cdot \text{MgO} \cdot 2\text{SiO}_2$ | Gehlemite-akermanite | Mel |
| $\text{CaO} \cdot \text{MgO} \cdot 2\text{SiO}_2 -$ $\text{MgO} \cdot \text{SiO}_2$ | Diopside-pyroxene | Pyr |

Osborn et al²² concluded that for all alumina concentrations, a better combination of desulphurizing power and liquidus temperature could be obtained by the addition of magnesia. These conclusions have been based on ternary sections at 5, 10, 15, 20, 25, 30 and 35 wt. % alumina. The variables in the slag/metal reaction are so complex that the effect of magnesia can be described by giving some typical numerical values. Given below is comparison of slags of the same desulphurizing power with and without addition of magnesia.

Table 3.2

A COMPARISON OF SLAGS OF THE SAME DESULPHURIZING POWER WITH AND WITHOUT MAGNESIA⁵²

| S.No. | Slag Composition (wt.%) | | | | Liquidus Temperature °C | Silica Activity X10 ² |
|-------|-------------------------|--------------------------------|------------------|------|----------------------------|-------------------------------------|
| | CaO | Al ₂ O ₃ | SiO ₂ | MgO | | |
| 1 | 51.0 | 10 | 39.0 | - | 1500 | 6.0 |
| 2 | 40.0 | 10 | 36.0 | 14.0 | 1450 | 8.0 |
| 3 | 48.5 | 15 | 36.5 | - | 1455 | 5.5 |
| 4 | 38.0 | 15 | 34.5 | 12.5 | 1430 | 8.0 |
| 5 | 46.5 | 20 | 33.5 | - | 1510 | 4.5 |
| 6 | 37.0 | 20 | 32.0 | 11.0 | 1450 | 6.0 |
| 7 | 44.0 | 25 | 31.0 | - | 1545 | 3.5 |
| 8 | 37.5 | 25 | 29.5 | 8.0 | 1470 | 5.0 |

The slags are estimated to have the same desulphurizing power, and the effect of magnesia on the silica activity and liquidus temperature is shown. In all cases, for the optimum magnesia content, the liquidus temperature is lowered and the silica activity raised. However since the equilibrium silicon value in the iron increases or decreases by a factor of 3 for $\pm 50^{\circ}\text{C}$ it would be seen that despite the slightly higher silica activities, the tendency for silica reduction decreases for the magnesia - containing slags.

So far only slags containing large concentrations of silica have been considered. Looking into $\text{CaO-Al}_2\text{O}_3\text{-SiO}_2$ ternary (Figure 3-3) it is seen that there is a low-melting region adjoining the $\text{CaO-Al}_2\text{O}_3$ binary. Slags from this range of compositions offer attractive possibilities. For this composition the desulphurizing power is high and the silica activities are so low that the possibility of extensive silica reduction is negligible.⁵² The problem faced is due to the critical nature of silica content because the liquidus temperature rises very steeply for concentrations of 10%. Practically there are a number of iron ores in which gangue is largely alumina that might be smelted with this type of slag. But unfortunately, the normal fuel, i.e. coke, always contains silica as a constituent of the ash and unless the silica present in the gangue of the ore is very

low, the slag liquidus temperature becomes uneconomically high.

Some of the more recent studies on the $\text{CaO-Al}_2\text{O}_3\text{-SiO}_2\text{-MgO}$ quaternary system have been reported by Koch et al^{24,25,44}, Glasser and Marr²⁶, Biggar and O'hara²⁷. Glasser and Marr²⁶ found that the system contains two 'quaternary' compounds which are Q = 42.2 CaO, 45.5 Al_2O_3 , 4.1 MgO, and 8.2 SiO_2 and R = 40.5 CaO, 48.0 Al_2O_3 , 9.4 MgO, 2.1 SiO_2 and these are thermodynamically stable compounds. However it may be noted that these compounds are of very low silica content and do not lie in the blast furnace slag composition regime. Thus the above work is not of much importance in the present context. Koch et al⁴⁴ studied the total equilibria between carbon-saturated molten iron and sulphur containing blast furnace slags of lime-silica-alumina and magnesia. The "total equilibrium" was attained by bringing saturated slag system in contact with carbon-saturated iron phase at 1600° and 1500°C temperature and ensuring that the reactions in the system have come to rest. This helped in determining the appropriate sulphur distribution values. They found that although equilibrium ranges were very small in comparison to data of Osborn et al²², the respective sulphur distribution can be clearly related to slag components. The effect of silica was found to be

negligible whereas magnesia exhibited an appreciably adverse effect on sulphur distribution. Also, the range of homogeneous slags in system $\text{Al}_2\text{O}_3\text{-CaO-SiO}_2$ was quantitatively indicated.

Koch et al²⁴ described saturated surfaces in $\text{Al}_2\text{O}_3\text{-CaO-MgO-SiO}_2$ by isothermal sections in the concentration range of blast furnace slags for 1600°, 1500° and 1400°C temperatures. Homogeneous slag zone interfaces were checked and reestablished by saturated melt method mentioned above. Also the homogeneous slag zone interfaces were represented by three dimensional tetrahedra and isothermal plane projections. It was found that homogeneous slag ranges were even smaller than presumed earlier. The quantitative projections to determine the liquidus for blast furnace slag regime obtained by Koch et al²⁴ are shown in Figure 3-5. Figure clearly shows the diminishing trend of homogeneous slag range with decrease in temperature. Koch et al²⁵ also renewed the quaternary system of $\text{Al}_2\text{O}_3\text{-CaO-MgO-SiO}_2$ by supplementing the recent data available. The tetrahedral model representing the quaternary system and all three dimensional regions corresponding to various crystallization regions were also worked out.

Si Solubility line

Δ Heterogenous

* Homogenous

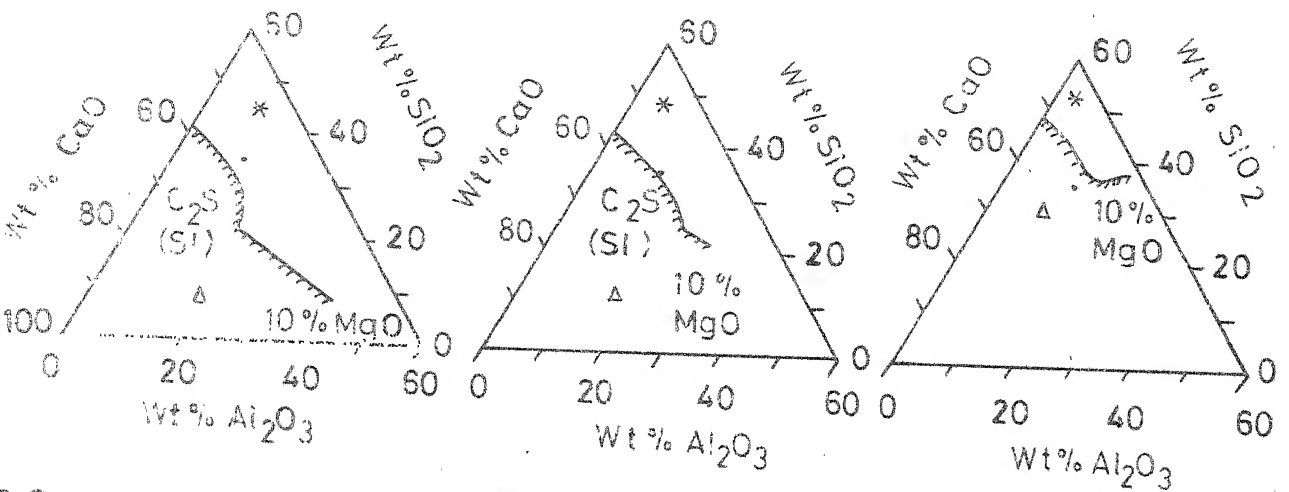


FIG. 3.5 SELECTED SATURATION LINES AS ORIENTATION AID TO ASSESS BLAST FURNACE SLAGS OF THE SYSTEM Al_2O_3 - CaO - MgO - SiO_2 AT (a) 1600 °C (b) 1500 °C (c) 1400 °C (Ref. 24)

3.3 Actual Blast Furnace Slags:

The actual slag compositions on recalculated basis (in terms of Al_2O_3 , SiO_2 , CaO and MgO totalling to 100 weight pct.) were plotted on ternary equilibrium diagram by Osborn et al²². They found that the predicted liquidus temperature were about 100°C more than the actual liquidus temperature of the slag. On the basis of measurements of liquidus temperature of actual slags, this liquidus temperature lowering was estimated to be of the order of 100°C on the steep liquidus slopes of the periclase and dicalcium silicates fields, and somewhat less in the plateau region. They also concluded that minor constituents were mainly responsible for lowering of liquidus surface without affecting the overall configuration, or relationship.

However Baldwin²⁰ performed liquidus temperature measurements on actual blast furnace slag samples and concluded that the actual liquidus temperatures of the blast furnace slags were close to that predicted by considering it as a quaternary system and also emphasized the reliability of diagrams published by Osborn et al²² for selection of optimum blast furnace compositions. Burgess and Baldwin²⁸ compared the measured liquidus temperatures of the slag samples with those calculated from quaternary diagrams of

Osborn et al²² and found the measured values lay, on an average, 15°C below the calculated values.

3.4 Crystallization of Blast Furnace Slag:

With rapid cooling, blast furnace slags remain glassy. In order to study these slag sample by DTA and to find out liquidus and solidus temperatures, it is necessary to have a crystalline sample to start with. Thus to convert a glassy sample to crystalline one, an annealing treatment is required. Clue was taken from the manufacture of slag-ceram, where a crystalline body is obtained from glassy matrix by an annealing process.^{33,35} The transformation into a new phase, ~~whether glassy or crystalline~~ always occurs by the process of nucleation and growth. Thus the salient features of nucleation and growth rate would be discussed briefly.

Modern theories of formation of crystal nuclei are based on thermodynamic principles first put forward by Gibbs and later developed by Volmer³⁰. These general considerations would be applicable to any substance. Looking at it from thermodynamic stand point, glass, like any other supercooled liquid is in a metastable state until a nucleus of the stable phase appears in it. It

then passes spontaneously into a stable phase - a process accompanied by decrease of the free energy of the system. However, a certain amount of work is required for formation of the nucleus, and this accounts for the stability of a metastable system. For homogeneous nucleation, the change in free energy during formation of a spherical nucleus is given by

$$G = \frac{4}{3}\pi r^3 \Delta g_v + 4\pi r^2 \Delta g_s \quad (3.1)$$

where Δg_s is the change in free energy per unit surface area of nucleus created and Δg_v is the change in bulk free energy per unit volume of the nucleus formed and r is the radius of nucleus.

The nucleation rate (J) is proportional to the probability of formation of stable nuclei, i.e.

$$J = A \exp\left(-\frac{\Delta G^*}{KT}\right) \quad (3.2)$$

where ΔG^* corresponds to the maximum value of ΔG at $r = r^*$, where

$$r^* = \frac{2 \Delta g_s}{\Delta g_v} \quad (3.3)$$

and

$$\Delta G^* = \frac{16}{3} \pi \frac{(\Delta g_s)^3}{(\Delta g_v)^2} \quad (3.4)$$

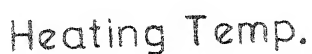
For a general case ΔG^* can be written as

$$\Delta G^* = K \frac{(\Delta g_s)^3}{(\Delta g_v)^2} \quad (3.5)$$

where K is a constant called shape factor and depends on the shape of the nuclei (for spherical shape, $K = \frac{16\pi}{3}$). On the basis of the Theory of Absolute Reaction Rates, the nucleation rate may be expressed as:

$$J = \frac{N^* K T}{h} \exp\left(-\frac{\Delta G^* + Q}{T}\right) \quad (3.6)$$

where N^* is the number of atoms in unit volume, h is the Plank's constant, K is Boltzmann's constant, T is the absolute temperature and Q is the activation energy for diffusion. From the equation (3.6) it is seen that if ΔG^* and Q remain constant with temperature then with the increase in temperature nucleation rate should increase. However this does not occur as ΔG^* decreases with decrease in temperature. The two terms, viz. ΔG^* and $\frac{1}{T}$ produce opposing effects with increase or decrease in temperature giving rise to a maximum nucleation rate at a certain temperature. Thus equation (3.6) leads to an optimum temperature of maximum nucleation. A plot of J vs. T is shown in Figure 3-6.



u Rate of crystal growth

FIG.3.6 SCHEMATIC DIAGRAM FOR THE CRYSTALLIZATION OF A VISCOUS LIQUID

U. S. AIR FORCE
CENTRAL LIBRARY
Acc. No. A 50869

The kinetics of heterogeneous nucleation of a crystalline phase is governed by similar principles as those of homogeneous nucleation excepting that the interfacial free energy (i.e. interfacial tension) term in equation (3.6) is different. The interfacial energy is decided by the type of interaction between the embryo and substrate crystal. According to Turnbull²⁹, the important parameter is the contact angle.

The expressions discussed above have been derived for single component system. For multicomponent systems, the derivations become more complex. When a system is in a supercooled condition with respect to several phases, the first to crystallize is the one with the lowest energy of activation for nucleation. Then as the composition alters as a result of crystallization, consecutive deposition of several crystalline phases becomes possible. Because of low diffusion coefficients, deposition of equilibrium phases may not occur during the finite crystallization time. Thus factors which favour decrease of activation energy for nucleation accelerate and facilitate crystallization.

Tamman³² studied crystal growth rate and found that, provided nuclei were present, below the liquidus, the crystal growth decreased as shown in Figure 3-6. Many workers have derived both empirical and theoretical

equations to describe crystal growth rate. These have been reviewed by Morley³³. Underlying all the approaches, is the idea that rate is controlled by diffusion processes and Frenkel³⁴ expressed the rate as follows

$$u = A \exp - \frac{CT_1}{\Delta H(T_1 - T)KT} - \frac{Q}{KT} \quad (3.7)$$

where A and C are constants, T_1 is the liquidus temperature, T is the interface temperature between glass and crystal, ΔH is the heat of two dimensional condensation and Q the activation energy for diffusion. Empirically it has found that activation energy for viscosity can be used and thus Frenkel expression becomes

$$u = \frac{A}{\eta_l} \exp - \frac{ZT_1}{T_1(T_1 - T)} \quad (3.8)$$

where η_l is the viscosity and Z is a constant. This implies that species whose movement controls crystal growth also determines viscosity. This looks reasonable because large, slow moving species are involved in both cases.

Thus to obtain a crystalline body, an annealing treatment has to be decided upon depending upon the morphology of crystals (coarse or fine) required, with the help of Figure 3-6 (which is also referred to as

Tanman curve). For illustration, if we require large crystal size, a moderate rate of nucleation combined with a high growth rate is necessary, while for a small crystal size the maximum nucleation rate combined with moderate, not maximum crystal growth rate ought to be chosen.

CHAPTER 4

PREPARATION AND CHARACTERIZATION OF SLAG SAMPLES

4.1 Preparation of B.F. Slag Sample:

4.1.1 Crushing and Grinding:

Rourkela Blast Furnace slag was crushed in a jaw crusher to a size of about 1 cm. After primary crushing the material was mixed properly and about 5 Kgs representative slag sample was taken for grinding following standard sampling procedure. The grinding was performed in a ball mill. Final particle size of the slag was primarily -325 mesh.

4.1.2 Magnetic Separation:

A representative part of finely ground slag was subjected to magnetic separation in a drum type laboratory magnetic separator. Since the particle size was very fine, the separation of iron particles was not up to the mark, because slag particles adhered to free iron particles. Thus in the final stage the magnetic separation was carried out manually with a strong permanent bar magnet.

The finally prepared slag sample after drying was stored in desiccator to avoid absorption of moisture.

4.2 Additives-Specifications and Preparations:

a. Alumina (Al_2O_3); ALCOA, U.S.A.

Maximum Impurities; SiO_2 - 0.03%

Fe_2O_3 - 0.05%

Ta_2O_5 - 0.06%

Loss on Ignition - 1%

b. Calcium Oxide (CaO);

Sufficiently pure CaO was not available. Therefore it was prepared by calcining CaCO_3 at 1100°C for a long time in order to drive out CO_2 completely. The completion was checked by weight loss measurements.

Calcium Carbonate (CaCO_3); BDH-LR grade

Mixed Oxides - 0.23%

Loss on Ignition - 1.5%

c. Titanium Dioxide (TiO_2), BDH-LR grade

Fe Content - 0.05%

Loss on Ignition - 0.5%

4.3 Preparation of Various Compositions With and Without Additives:

The slag samples and additions were weighed to an accuracy of 1 mg and then thoroughly mixed in mortar and pestle. The samples were then melted in graphite crucible

in a 6 KW Type "CH" AJAX-NORTHROP Induction furnace. Since the slag itself is a poor conductor of electricity it needs to be indirectly heated through the use of graphite crucible. Due to above reason melting took a long time. Mostly the sample at the bottom of the crucible melted while top portion remained in solid or semisolid state. This was taken care of by stirring with a graphite rod. It took about 15 minutes to homogenize the melt. The liquid slag was finally poured over a copper plate and quenched. This quenching was performed to exclude any possibility of segregation of the melt. The quenched samples were then again crushed and ground. A hand magnet was used to separate metallic iron particles if any. The samples were remelted and quenched again for ensuring proper homogeneization. The quenched samples were again crushed, ground and then stored in desiccator. Figure 4-1 shows a sketch of the crucible used in melting.

4.4 Chemical Analysis of Blast Furnace Slags:

In order to find out the percentage of constituents in the plain blast furnace slag without additives, it was chemically analysed a number of times. The results are shown in Table 4.1. It was, however, found that the

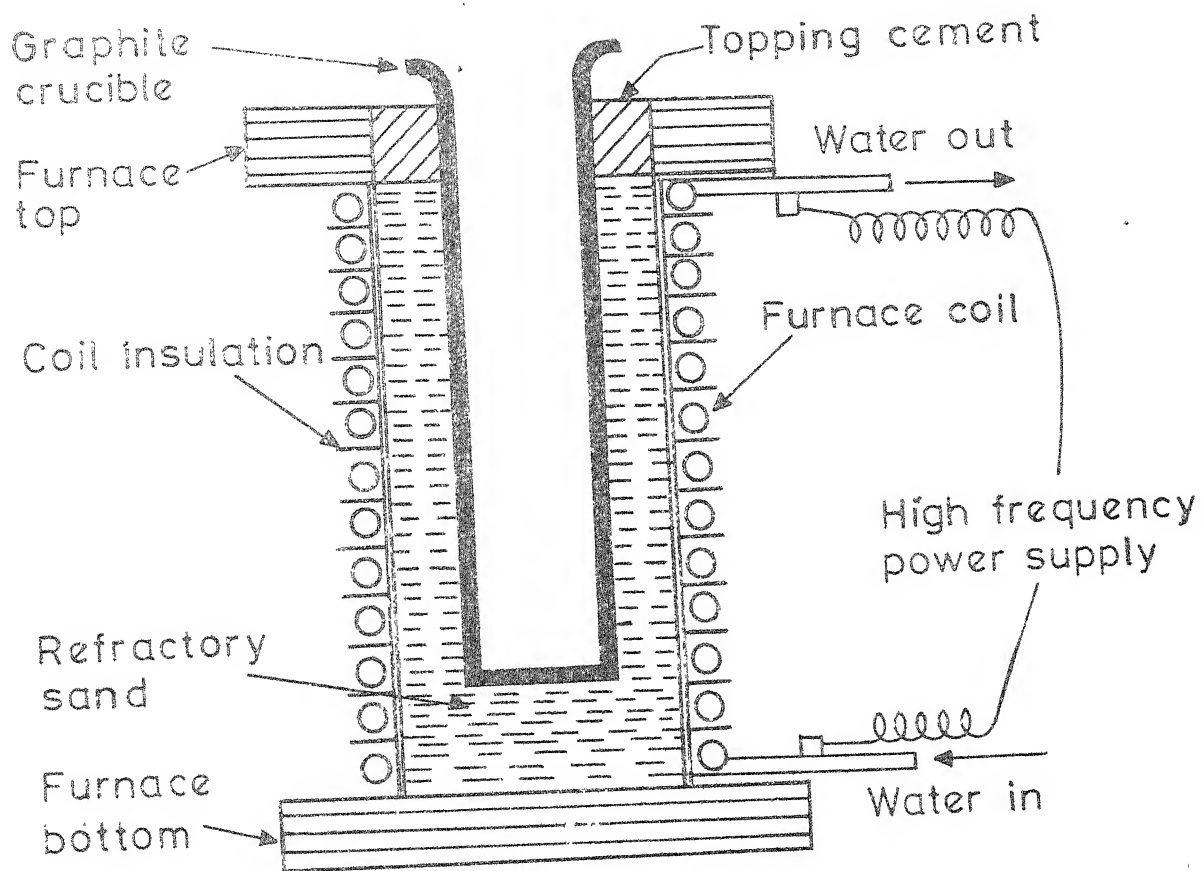


FIG.4.1 INDUCTION MELTING CRUCIBLE

Table 4.1

Slag Analysis from Various Sources

| Source of Analysis | Slag-Analysis | | | | | | Total |
|--------------------|------------------|-------|------|--------------------------------|--------------------------------|------------------|--------|
| | SiO ₂ | CaO | MgO | Al ₂ O ₃ | Fe ₂ O ₃ | TiO ₂ | MnO |
| I.I.T. Kanpur | 36.1 | 31.24 | 6.83 | 21.224 | 2.25 | 0.208 | 1.016 |
| " | 34.27 | 30.44 | 7.01 | 21.112 | 2.37 | 0.209 | 1.216 |
| " | 36.8 | 29.10 | 3.0 | 27.8 | 2.2 | 0.21 | - |
| " | 35.8 | 29.70 | 3.60 | 27.5 | 2.1 | 0.26 | - |
| " | 34.2 | 28.2 | 6.3 | 25.1 | 2.3 | 2.1 | 2.6 |
| " | 34.2 | 29.5 | 6.4 | 26.0 | 1.0 | 1.9 | 1.9 |
| " | 37.0 | 24.0 | 3.0 | 28.2 | 0.32 | - | 6.8 |
| N.M.L. Jamshedpur | 35.34 | 26.53 | 9.85 | 21.00 | 3.50 | 1.00 | 1.3 |
| | | | | | | | 98.978 |
| | | | | | | | 96.627 |
| | | | | | | | 99.1 |
| | | | | | | | 98.96 |
| | | | | | | | 101.0 |
| | | | | | | | 100.9 |
| | | | | | | | 99.32 |
| | | | | | | | 98.52 |

analysis results were not reproducible. It is evident that no two sets of analysis match and the reliability of any one set cannot be substantiated. As such acceptance of a set of values needed a judgement. A discussion was carried out with HSL (R & D) regarding expected ranges of various constituents. Some analyses results were altogether discarded, while in other analyses, averages were taken for the major constituents viz. Al_2O_3 , CaO , SiO_2 and MgO . For minor constituents also, average values were taken wherever possible. The amount of iron oxide and sulphur were fixed as 1.0 and 0.5 pct. respectively. Thus the blast furnace slag composition finally accepted is as follows.

| Constituents | Weight Percent |
|-------------------------|----------------|
| Al_2O_3 | 25.5 |
| CaO | 29.0 |
| MgO | 4.5 |
| SiO_2 | 35.5 |
| MnO | 3.8 |
| TiO_2 | 0.2 |
| FeO | 1.0 |
| Sulphur | 0.5 |
| <hr/> | |
| Total | 100.0 |

4.5 Chemical Characterization of Various Compositions:

On the basis of the final chemical composition of the slag, calculations were performed to obtain the chemical composition of each sample in weight percent. These are shown in Table 4.2A and 4.2B.

4.6 Annealing Procedure of Blast Furnace Slags:

It consists of heating the slag samples at a given temperature such that nucleation of the crystalline phases occurs. This was achieved by holding the sample at certain temperature T_1 for certain time t_1 . In order to accelerate the growth of crystallites formed, the sample temperature was raised to T_2 and held there for time t_2 . This was expected to lead to a well-crystallized sample. The annealing temperatures and times T_1 , T_2 and t_1 , t_2 respectively, depend on the individual composition and can be roughly predicted by theoretical considerations.³⁵ But the actual values have to be ascertained experimentally.

Since the theoretical considerations about annealing time and temperature are quite involved, a common heat treatment scheme was selected, which is usually applied in slag-ceram manufacture.³⁶

The procedure consisted of heating the samples in zirconia crucibles to 750°C and holding at this temperature for 24 hours. Subsequently the temperature was raised to 850°C and held there for 24 hours more.

Table 4.2A

Computed Chemical Analysis of Samples of Region A

S = slag, Y = Al_2O_3 , Z = CaO

| S.No. | Sample No. | Designation of Sample | Weight Percent | | | | | | | |
|-------|------------|-----------------------|-------------------------|------|----------------|-----|-----|-----|----------------|-----|
| | | | Al_2O_3 | CaO | SiO_2 | MgO | MnO | FeO | TiO_2 | S |
| 1 | A1 | 100 S | 25.5 | 29.0 | 35.5 | 4.5 | 3.8 | 1.0 | 0.2 | 0.5 |
| 2 | A2 | 100 S + 10 Z | 23.2 | 35.5 | 32.3 | 4.1 | 3.5 | 0.9 | 0.2 | 0.5 |
| 3 | A3 | 100 S + 20 Z | 21.3 | 40.8 | 29.6 | 3.8 | 3.2 | 0.8 | 0.2 | 0.4 |
| 4 | A4 | 100 S + 30 Z | 19.6 | 45.4 | 27.3 | 3.5 | 2.9 | 0.8 | 0.2 | 0.4 |
| 5 | A5 | 100 S + 30Z + 10 Y | 25.4 | 42.1 | 25.4 | 3.2 | 2.7 | 0.7 | 0.1 | 0.4 |
| 6 | A6 | 100 S + 30 Z + 20 Y | 30.3 | 39.3 | 23.7 | 3.0 | 2.5 | 0.7 | 0.1 | 0.3 |
| 7 | A7 | 100 S + 40 Z + 10 Y | 23.7 | 46.0 | 23.7 | 3.0 | 2.5 | 0.7 | 0.1 | 0.3 |
| 8 | A8 | 100 S + 40 Z + 20 Y | 28.4 | 43.1 | 22.2 | 2.8 | 2.4 | 0.6 | 0.1 | 0.3 |
| 9 | A9 | 100 S + 50 Z + 10 Y | 22.2 | 49.4 | 22.2 | 2.8 | 2.4 | 0.6 | 0.1 | 0.3 |
| 10 | A10 | 100 S + 50 Z + 20 Y | 26.8 | 46.5 | 20.9 | 2.6 | 2.2 | 0.6 | 0.1 | 0.3 |

CHAPTER 5

DESIGN, FABRICATION AND PERFORMANCE OF HOT FILAMENT MICROSCOPE (HFM)

As discussed earlier HFM technique consists of heating a tiny slag sample kept at a thermocouple tip in the form of a filament which is heated by passing current through it. The thermocouple tip also acts as a temperature sensing device in the absence of the heating current. The dual purpose of heating and temperature sensing is served by the help of a switch, solid state or mechanical in nature, which connects the heating element alternatively either to heating voltage or to potentiometer as shown in Figure 5.1. The hot filament is observed under a long focus microscope for detection of melting and crystallization of the sample. The schematic diagram of the microscope and hot filament assembly is shown in Figure 5.2.

The essential components involved in HFM are:

1. Filament with supporting leads of thermocouple grade wires
2. Switching device, solid state or mechanical
3. Intense light source
4. Long focus microscope
5. Low voltage, high current power supply
6. Potentiometer to measure temperature

These above components are described in the following sections.

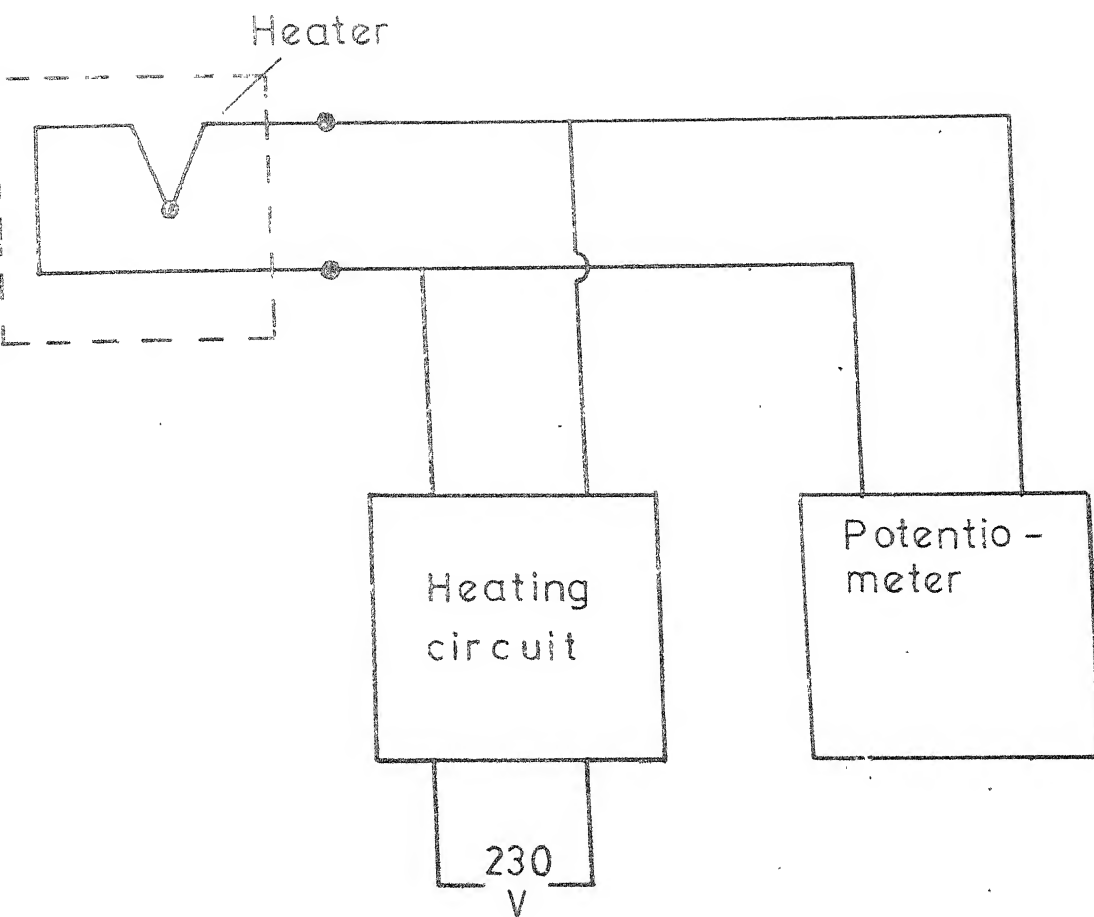


FIG. 5.1 HEATING & MEASUREMENT CIRCUIT

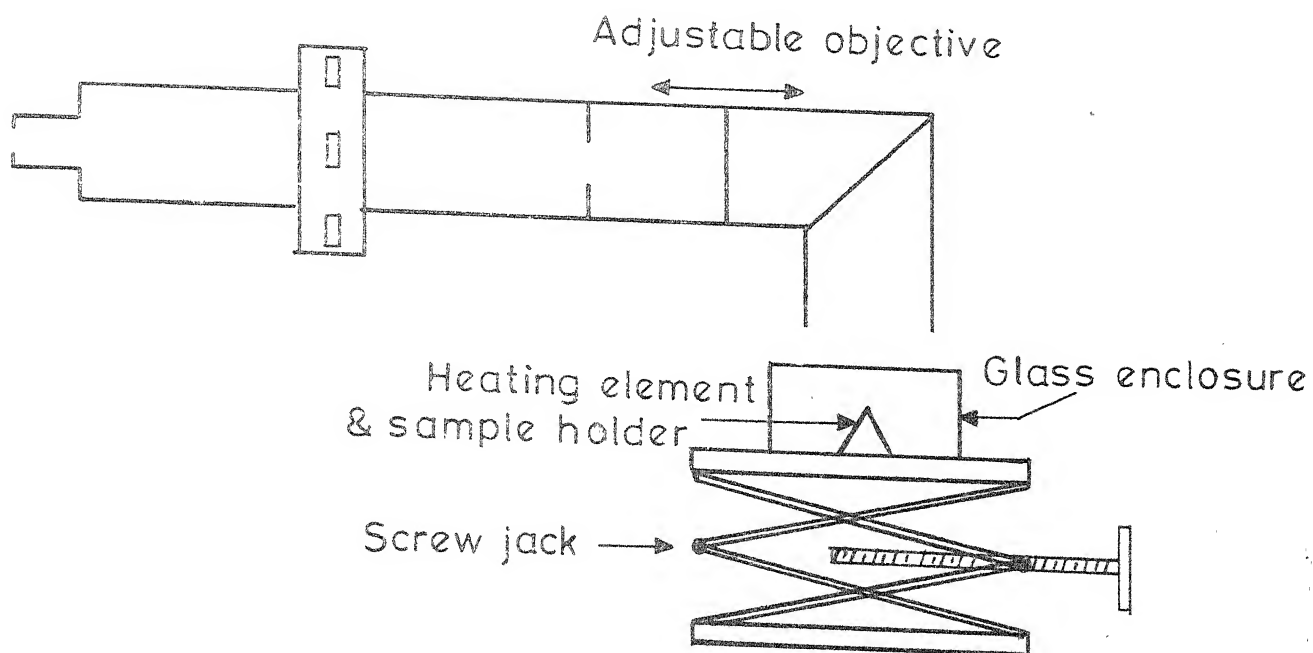


FIG.5.2 HOT STAGE MICROSCOPE

5.1 Apparatus:

5.1.1 Filament Assembly:

It consisted of the filament and the support lead wires which were supported with the help of screws to binding post. These brass binding posts were fixed over a thick perspex plate. About 2 cm of length of each thermocouple wire were taken and spot welded at their tips. A schematic diagram of the fabricated filament is shown in Figure 2.6(a). Free ends of filament wires were joined to wires of similar composition and of 0.5 mm diameter. These thick wires were used to save the binding posts from excessive heating. The filament was bent in a U-shape such that the gap between wires was around 0.02 to 0.025 mm only. The gap is a critical factor in order to maintain a uniform temperature zone. The filament was tightened to brass binding posts fixed over a non-conducting base made of perspex plate. The whole assembly was placed over a movable platform under the microscope. The filament was enclosed in a glass enclosure to cut down convective heat loss. The glass enclosure was fitted with a optically flat glass top.

5.1.2 Power Supply:

The characteristic feature of power supply for the HFM is the requirement of low voltage and high current. The

high current is needed because of extremely low resistance of filament (approximately 0.2 ohm). Thus the mains voltage of 230 V was stepped down to 10 V by means of a step down transformer which in turn was connected to an autotransformer variac. The autotransformer variac is to regulate the filament voltage for temperature control. The output of the variac was fed to the filament through a switching device. The mains voltage of 230 V was taken through a voltage stabilizer to get rid of line voltage fluctuations.

5.1.3 Switching Devices:

A switching device for HFM technique is basically meant to allow the voltage to filament intermittently such that in the absence of heating voltage, the filament is connected across a potentiometer to measure the thermocouple e.m.f. The frequency of intermittent voltage supply has to be maintained such that a steady-state heating of filament is obtained. Keeping in view the problem faced by Welch^{2,55}, and others^{54,56}, different types of switches were tried which are described below.

a. Solid State Device: At first an attempt was made to develop a solid-state switching device, due to inherent limitations of the mechanical switches used by Welch^{2,55}. The high current led to severe contact erosion, and required

constant maintenance and adjustments of the contacts.

In the solid state device circuit shown in Figure 5.3, the filament was heated by a D.C. voltage which was controlled by an A.C. signal. The filament was to be heated in the positive part of the voltage cycle while for the negative part of the cycle, the power to the filament was to be cut off and thermocouple e.m.f. developed was to be sensed by a potentiometer through an amplifier circuit. This amplifier circuit acts as an open switch during the positive heating cycle. This would shield the millivolt potentiometer against high voltages. The main components used in solid state circuit were power transistor ECN055, diode CD21, operational amplifier A 741, carbon resistances and variable resistors. This circuit did not give the required performance due to the small overlap of heating voltage with that of thermocouple e.m.f. This was due to the inherent limitation of a solid state junction which always gives some leakage voltage in the non-conducting cycle.

Thus it was decided to try a switch giving rise to a physical make or break contact with heating voltage and potentiometer.

b. Electromagnetic Switch: This type of switch shown in Figure 5.4 mechanically transfers the contact from one circuit to the other and thus any kind of overlap of the two voltages

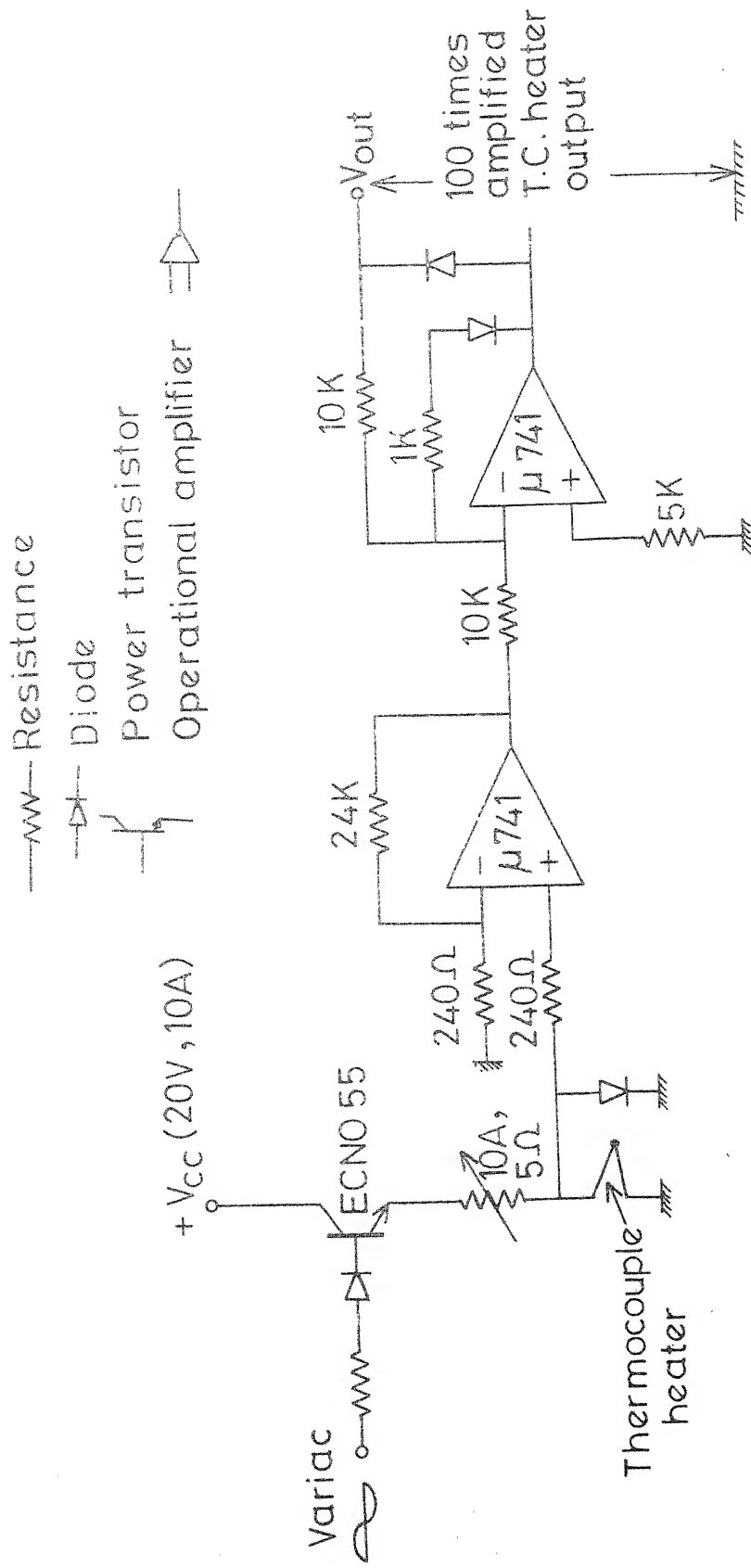


FIG.5.3. Solid state switching circuit

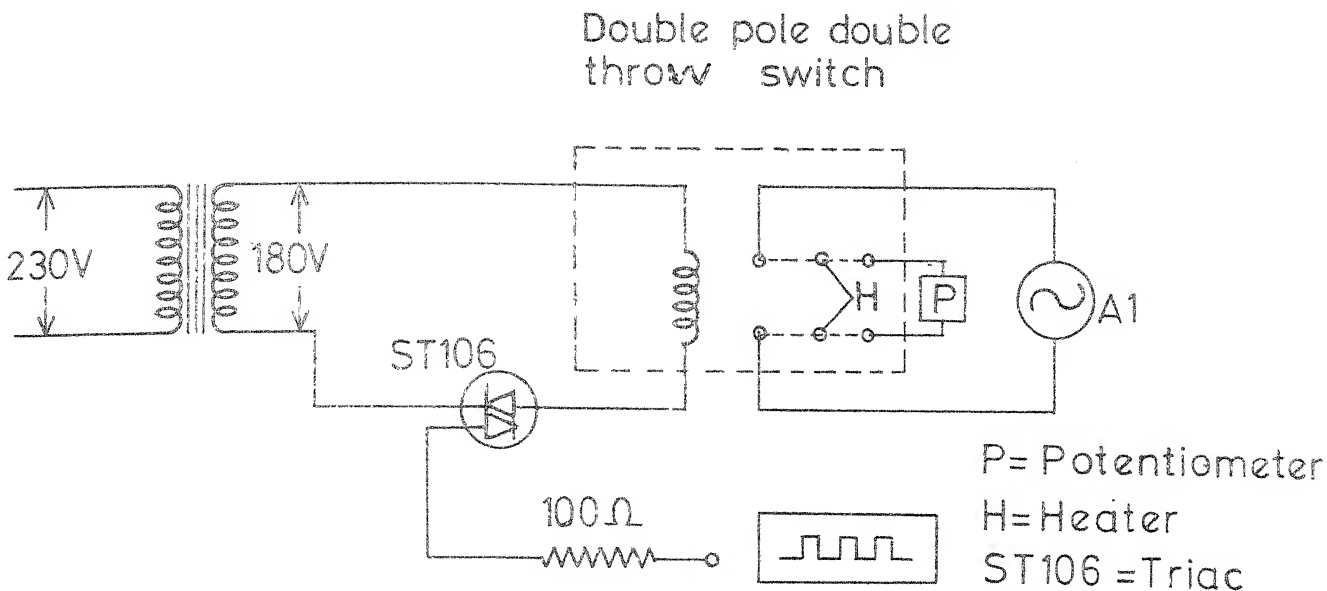


FIG 5.4(a) Circuit using DPDT relay switch

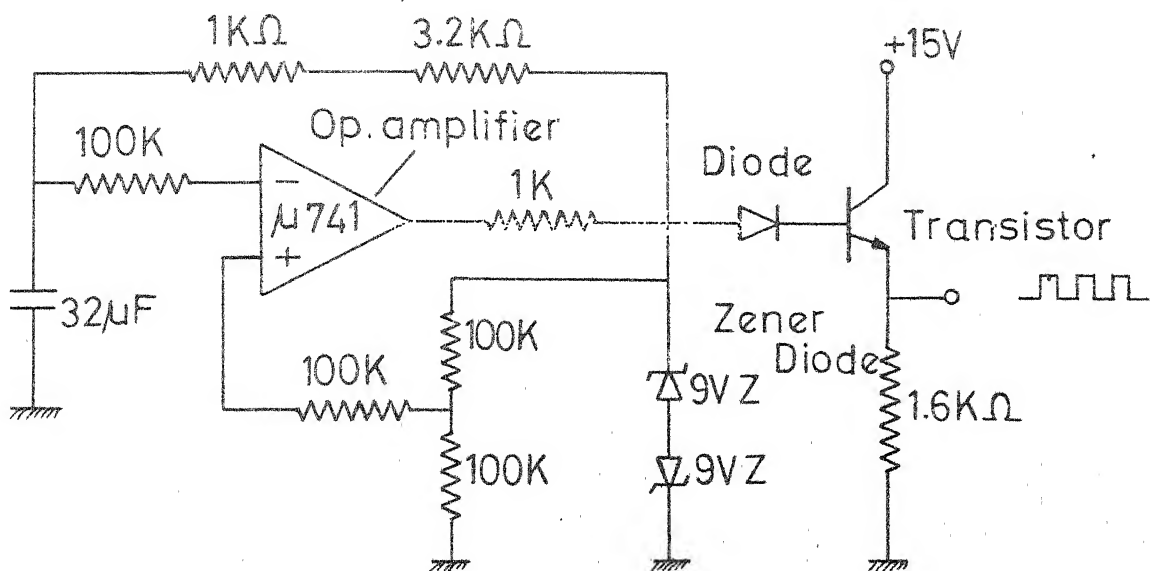
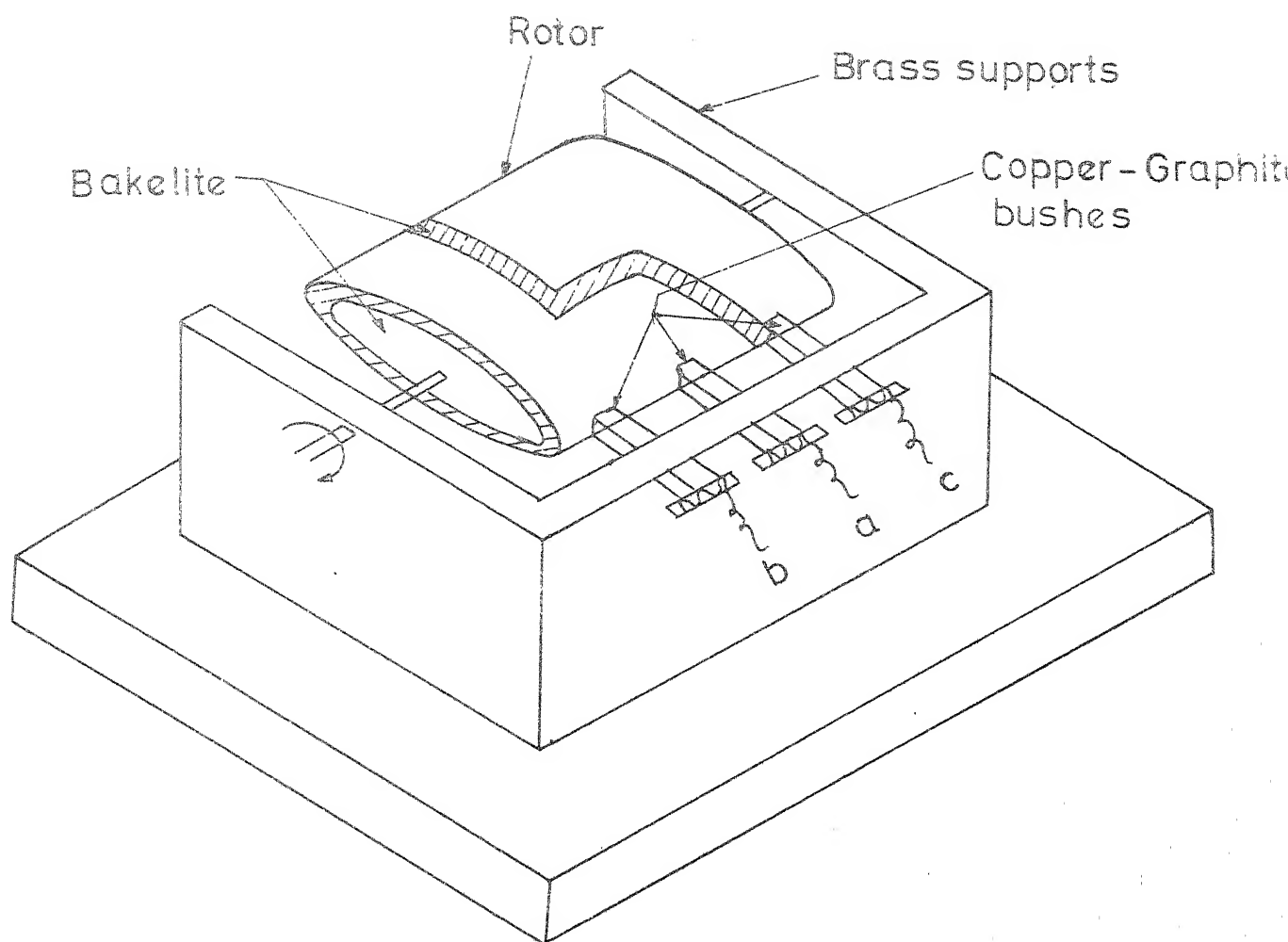


FIG 5.4(b) Low frequency squarewave circuit

was not possible. This employed a double-pole, double-throw mechanical relay (AB 11 type). The relay was energized by a triac circuit using a square wave. The relay contact terminals were capable of taking 10 amperes current. Here the filament was connected to moving poles of the switch which either made contacts with heating voltage when the relay was energized to the potentiometer when the relay was off. The components used were DPDT relay, triac ST106, step down transformer, zener diode, diode, operational amplifier (.4741) capacitor and resistances.

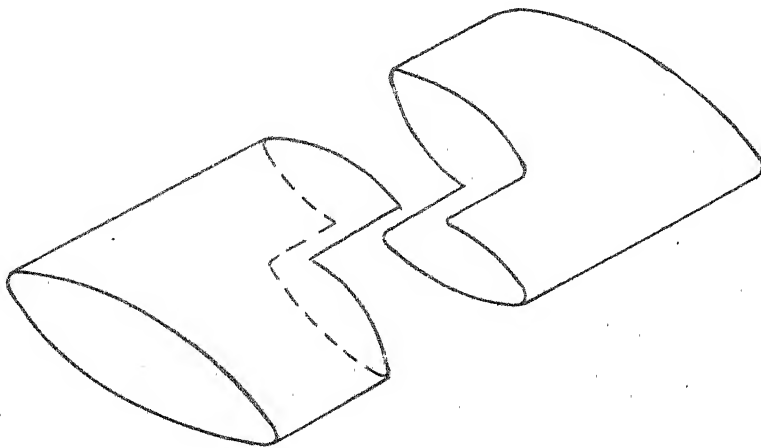
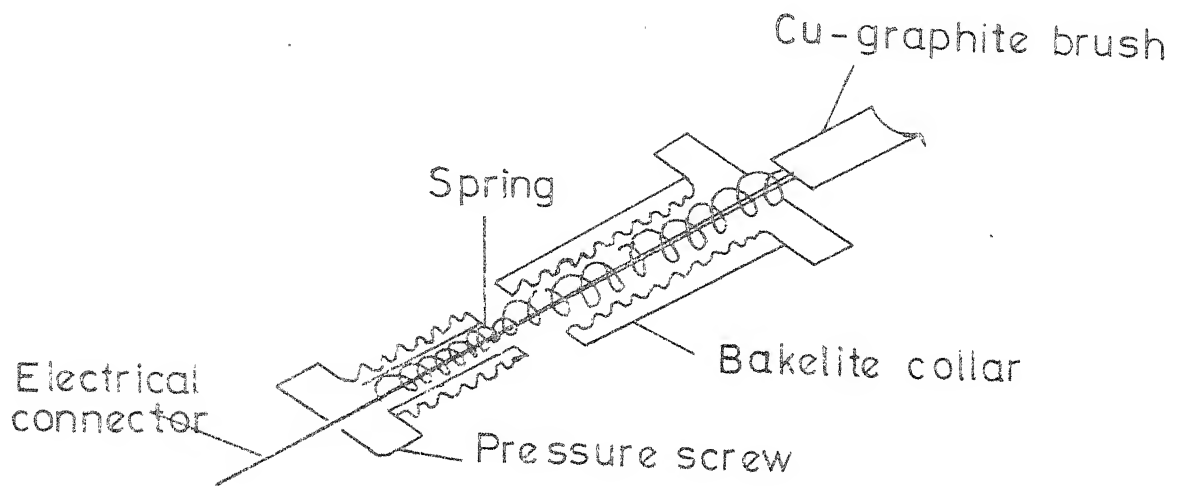
The performance of this switch was not up to the mark due to the large temperature fluctuations of the filament. These temperature fluctuations could be reduced only if the switching frequency was higher. However the relay could not operate beyond a frequency of 15 cycles/sec. Thus the switch could not be used effectively for liquidus measurements due to large temperature variations during heating and non-heating cycles.

c. Mechanical Switch: Keeping in view the limited switching frequency of the electromagnetic switch, a rotary switch was fabricated as shown in Figure 5.5. It was a simple single-pole double-throw (SPDT) switch. It consists of a rotor mounted with bakelite disks over which two copper rings are fitted. These rings shown in Figure 5.6(b) are insulated from



G.5.5 SINGLE POLE DOUBLE THROW ROTARY SWITCH.

(a) SPRING LOADED BRUSH



(b) TWO COPPER RINGS

G.5.6 COMPONENTS OF ROTARY SWITCH

each other, the gap between them being covered with bakelite so as to allow smooth contact with the brush. The rotor assembly is mounted over two ball bearing supports on either side in a brass frame. From one side three spring-loaded brushes are mounted over the rotor. These brushes were of copper-graphite composites to enable them to carry large current. The spring-loaded brush assembly is shown in Figure 5.6(a). The central brush 'a' acts as the single pole which alternately gets connected with 'b' or 'c'. The gap between the two copper rings was adjusted to give break-before-make contact. This arrangement is necessary to safe-guard the millivolt-potentiometer from damage by overlap of high voltage.

5.1.4 Optical System:

This comprised of a long focus microscope and an illumination source. The microscope had been manufactured by American Optical Company (U.S.A.). It has three different magnifications viz. 17.5, 35, and 70. The illumination source comprised of a high wattage projection lamp. The light of the source was focused by means of a condenser lens on to the plane of the filament. This type of illumination is necessary because the incandescent light of the filament itself was not sufficient to allow visualization of the process of crystallization. However, one could see the

physical rounding of the sample due to surface tension forces along the filament as the softening of the sample started. To observe the crystals, during solidification of the melt, an intense light beam has to be focused over the filament. It would also be very difficult to visualize the crystals if the amount of the sample is large.

5.2 Performance of the Apparatus:

During trial of the filament assembly, the filament was directly heated without the switching device and it showed good performance. The fine adjustments of temperature could be made by the autotransformer variac. The microscope could be focused easily to observe the sample. The illumination system was not upto the mark. This could be attributed to a large sample which increased the opacity. However, a few more trials are required to ascertain the performance of the optical system.

The major problem was associated with the switching device. In the case of solid-state switching device, the circuit developed to isolate the heating voltage from thermocouple e.m.f. did not give the desired performance. The failure was due to limitation of the device to filter out the undesirable voltage completely. In the case of electromagnetic switching device, the separation of heating voltage

from thermocouple e.m.f. was upto the mark because of the mechanical isolation of contacts. The problem arose due to limited switching frequency of relay. The maximum frequency attainable for the switching cycle was about 15 cps. Though the slag melted down at this switching frequency, the temperature fluctuations seemed to be quite large which did not allow accurate measurements and control of temperature. The mechanical switching scheme gave the switching at high frequencies depending on the speed with which it was rotated. But excessive sparking at the contacts led to power fluctuations resulting into fluctuations in the filament temperature. Contact quenching with lubricants like petroleum jelly and others were tried but the problem remained.

Shortage of time did not allow pursuing these any further and set the apparatus right.

CHAPTER 6

DIFFERENTIAL THERMAL ANALYSIS (DTA): APPARATUS AND EXPERIMENTAL PROCEDURE

DTA consists of heating or cooling a pair of thermocouples, one immersed in or in contact with a standard material and the other with the sample when the difference between the two thermocouples is recorded as a function of time or temperature, a DTA curve is obtained. The DTA curve gives rise to a peak when the sample thermocouple absorbs or releases heat due to some kind of change occurring in it.

The main features of DTA apparatus are as follows:

- a. Furnace and power supply
- b. DTA cell comprising of crucibles and thermocouples
- c. Measuring and recording instruments for temperature and difference of temperature.

The DTA set-up used in the present work is shown in Figure 6.1.

6.1 Apparatus:

6.1.1 Furnace and Power Supply:

The salient feature of a DTA furnace is the requirement of fast temperature response. For a fast temperature

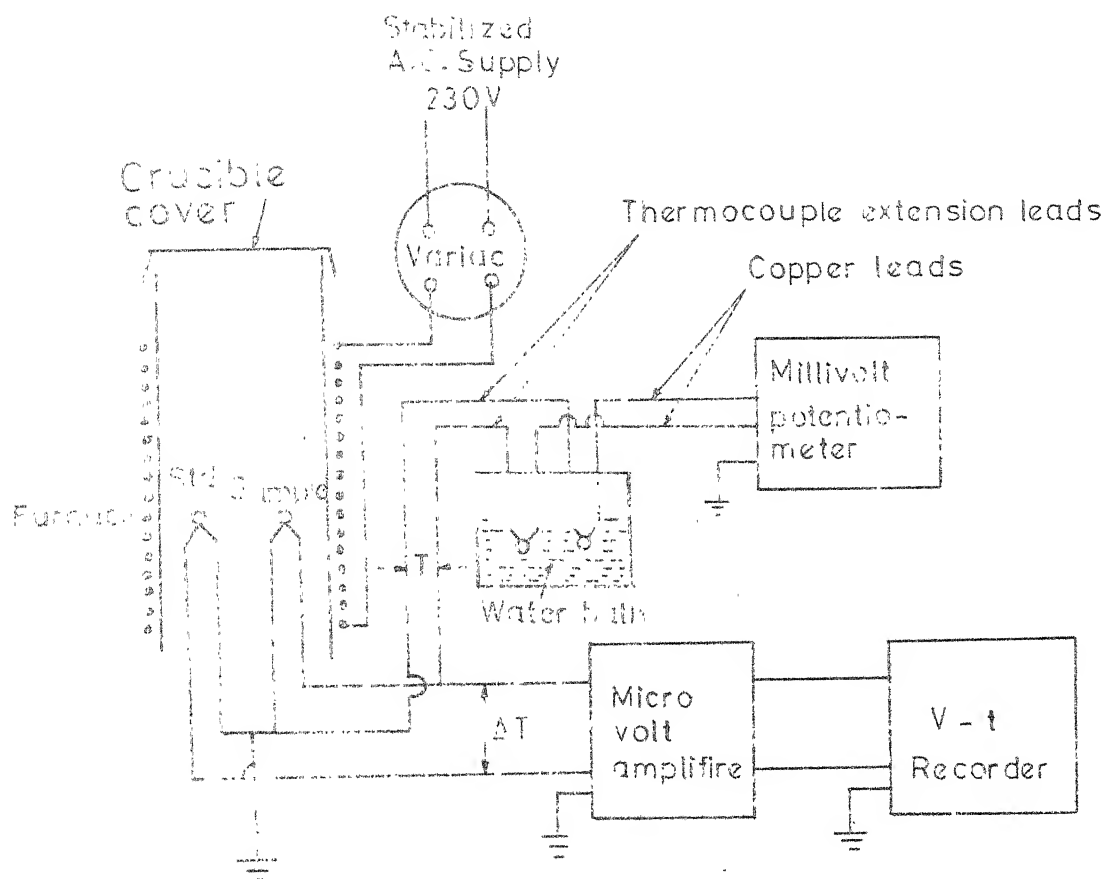


FIG.6.1 SET-UP FOR DIFFERENTIAL THERMAL ANALYSIS.

response, a furnace with as small an insulation as possible is a must. Keeping the above fact in mind, a furnace was designed for an operating temperature of 1600°C . The heat flux calculations were performed using graphical method developed by Heilman⁵⁷. A heavily insulated furnace is less subject to minor fluctuations in temperature due to fluctuation in line voltage. It also requires less power. However, one drawback of a heavily insulated furnace is that it will take a longer time to cool down and heat up thus slowing the response of the furnace to temperature changes.

The high working temperature requirement prompted the use of 20% Rhodium-Platinum alloy wire of 0.5 mm diameter as the heating element. The furnace set-up is shown in Figure 6.2. The wire was helically wound on recrystallized alumina tube of 1.5 cm I.D., 2.25 cm O.D. and 42.0 cm long. The pattern of winding is shown in Figure 6.3. The ends contained winding of 4 turns/cm while the centre 2 turns/cm. This gives a constant temperature zone of about 4-5 cm. The winding was cemented into place with high temperature Norton Alundum refractory cement. Chemically pure alumina powder of -200 mesh size was employed as insulating material. The optimum shell diameter was decided by taking into the surface temperature, insulation effect and the requirement of rapid response of the furnace to temperature changes. A 15 cm

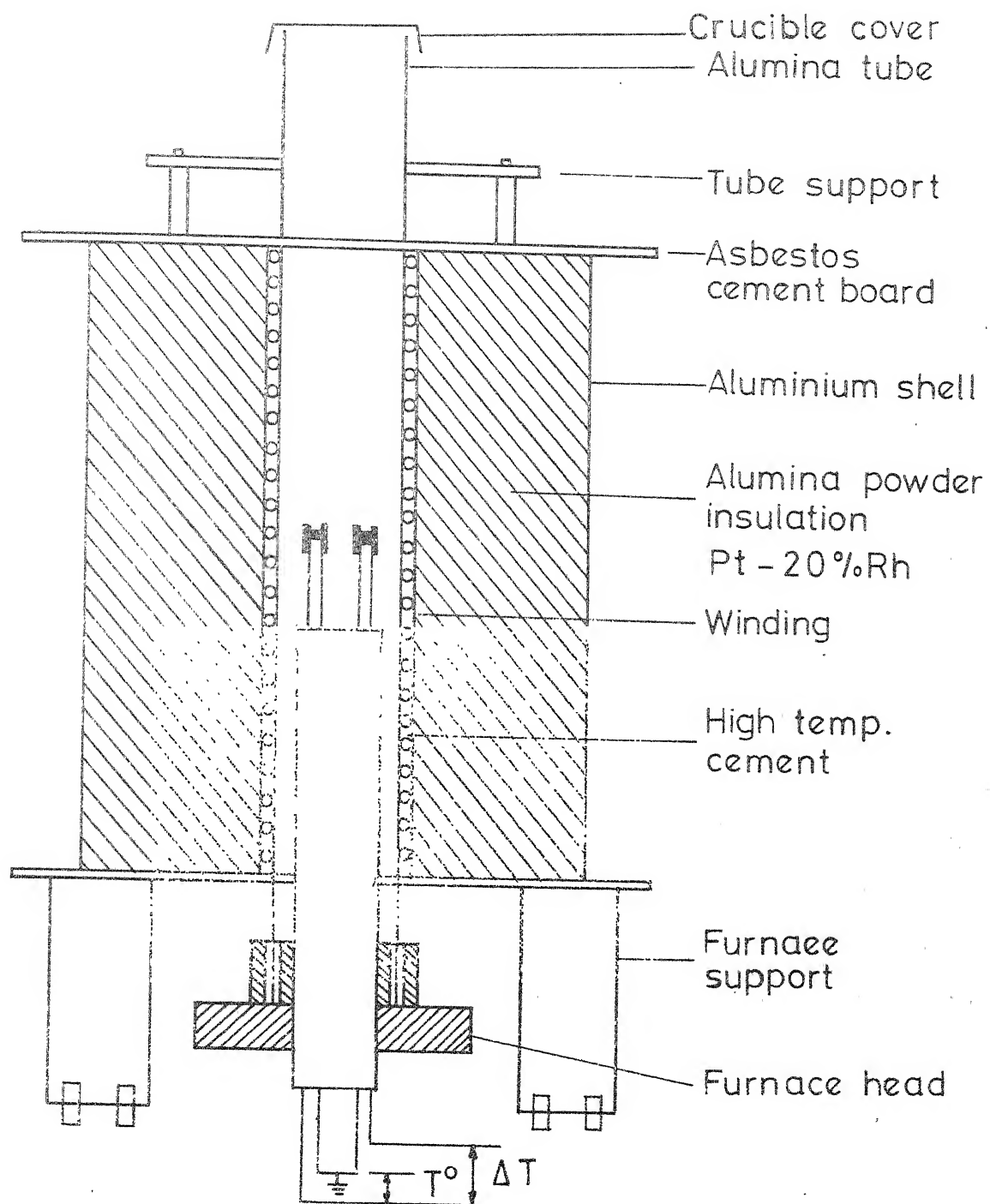


FIG 6-2 Furnace assembly

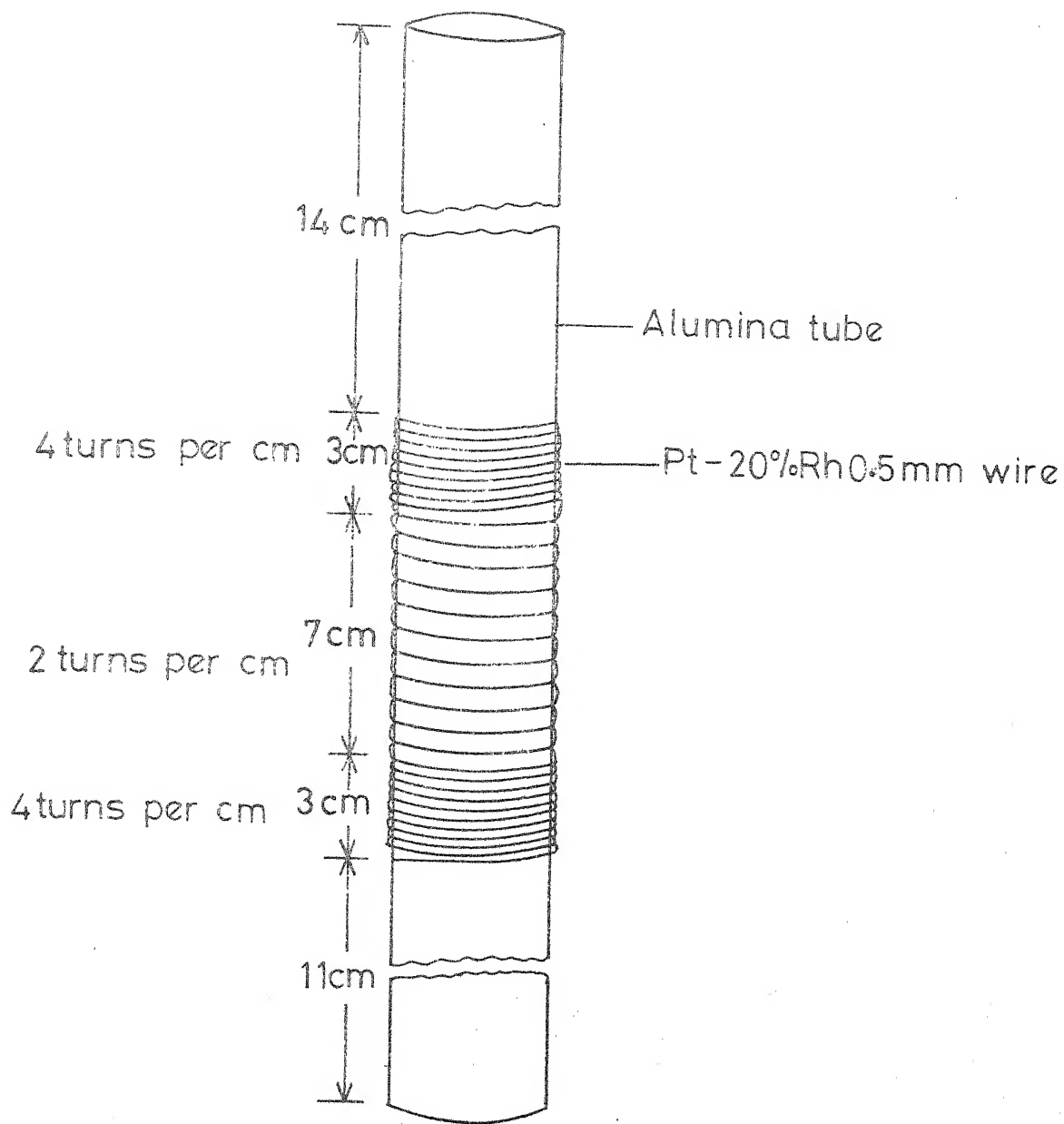


FIG 6.3 Helical winding on insulating tube

diameter outer shell was taken. The shell was made of aluminium sheet. The two ends of the furnace were closed with 1 cm thick asbestos cement sheets.

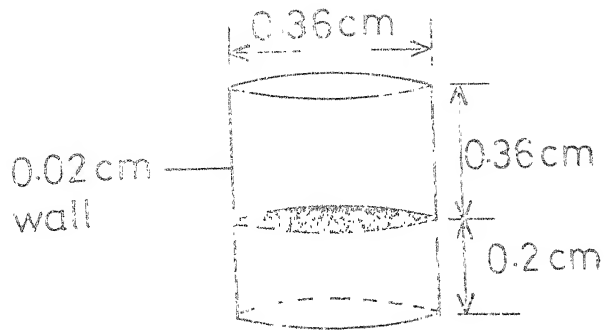
Power to furnace was taken from 230 A.C. stabilized voltage source through a autotransformer variac. The heating and cooling of the furnace was also controlled by the Variac by changing the voltage manually.

6.1.2 The DTA Cell Assembly:

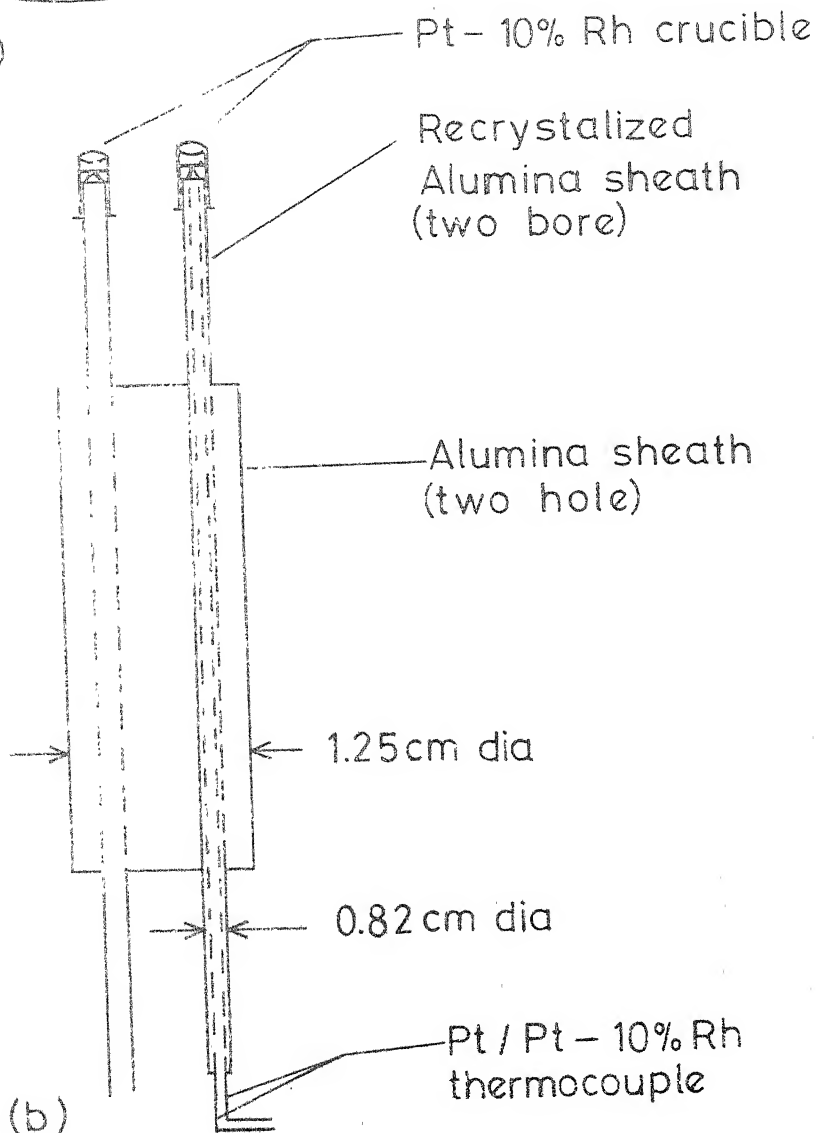
The schematic diagram of the DTA cell assembly is shown in Figure 6.4. It consisted of two specially shaped platinum -10% rhodium crucibles supported over two double-hole alumina sheaths of 0.32 cm diameter. These in turn were supported by a double-bore mullite sheath of 1 cm diameter. The two matched pair of 10% rhodium-platinum and platinum thermocouple of diameter 0.02 cm passed through thin alumina sheaths. The large diameter sheath was fixed to the furnace head at the bottom with the help of three screws.

The specially shaped crucibles were chosen so as to avoid the need for sample block for containing crucibles. Moreover crucibles rested over the thermocouple junction to give a good thermal contact. Since the thermocouple junctions were not in direct contact with the sample they were safe from corrosive nature of slags. The furnace top was closed with the help of an alumina crucible to avoid heat loss.

Pt - 10 % Rh crucible



(a)



(b)

FIG.6.4 D.T. A Cell

6.1.3 Measuring Instruments:

These were required to record the ΔT signal and the temperature. For recording differential temperature (ΔT) signal, a strip chart recorder in conjunction with a DC micro-volt amplifier was employed. The recorder was manufactured by Digital Electronics Ltd. It has various chart speeds ranging from 0.2 cm/min to 10 cm/min. Microvolt indicating amplifier was manufactured by Leeds & Northrup Co., U.S.A. It can magnify the input signal by factors of 5, 10, 20, 50, 100 and 200 when switched to recorder position. A millivolt potentiometer of Leeds & Northrup Co. was employed to measure the temperature of the sample intermittently. It has an accuracy of ± 5 microvolts. With the above set-up a continuous record of temperature was not possible during the DTA runs.

In order to check the possibility of stray e.m.f. pick ups by the measuring instrument, several precautions were taken. All electrical connections were made with coaxial cables. The recorder, potentiometer and millivolt amplifier were also grounded separately with the help of copper wire. Moreover, the outer shell of furnace was also grounded. To avoid the disturbances arising due to line voltage fluctuations, all the instruments were operated by stabilized voltage.

A photograph of the DTA set-up used is presented in Figure 6.5.

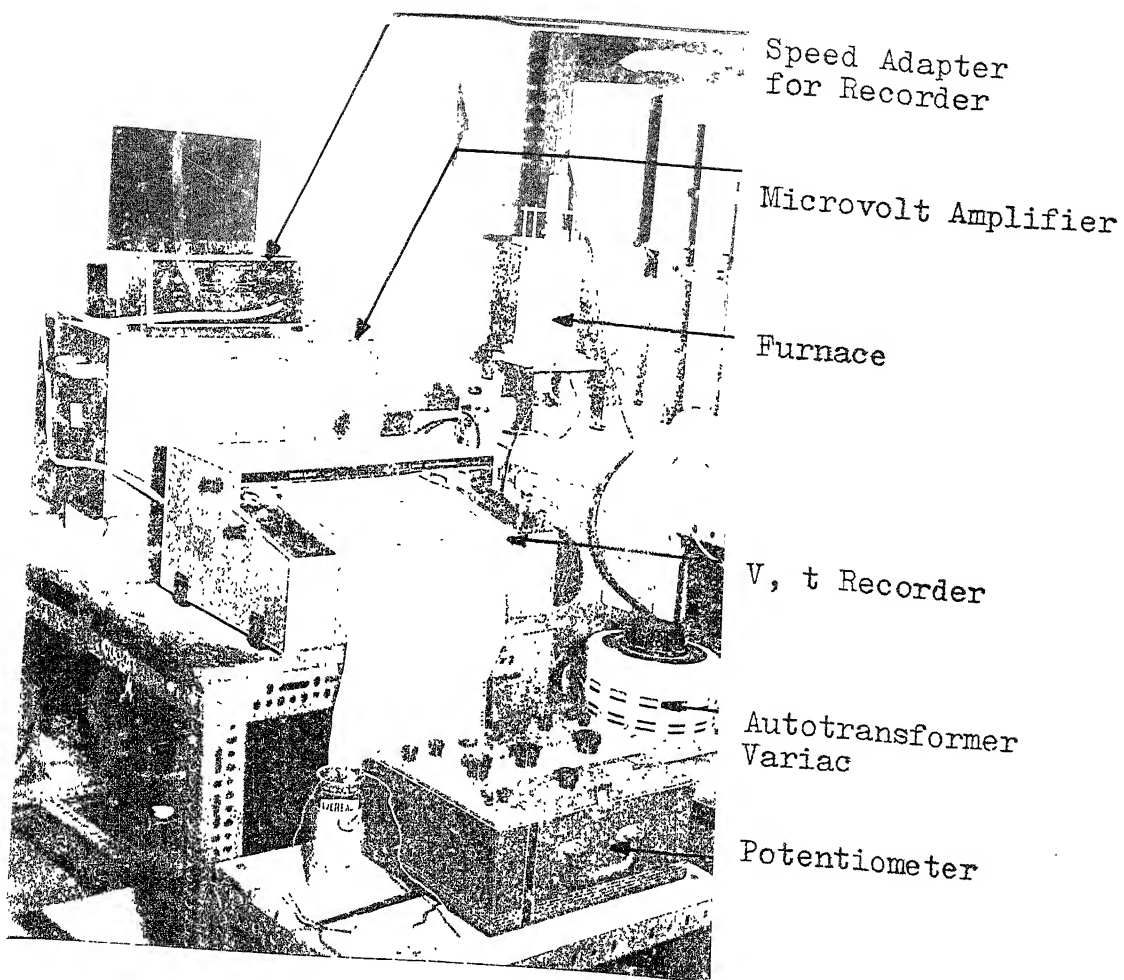


FIG. 6.5: Photograph of DTA set-up.

6.2 Experimental Procedure:

The sample weighing about 36 mg was taken in the crucible. The crucible was mildly tapped over a flat surface to ensure a uniform packing. To ensure complete filling of crucible, slightly more slag was taken, the excess fell out during tapping. This procedure was adopted in order to obtain uniform and reproducible packing of sample for all the DTA runs. A similar procedure was followed for filling standard substance in the crucible. However the standard sample was not removed and renewed for every sample. Usually the standard substance was replaced only after three runs or in some cases earlier, if it fell out during adjustments of the DTA cell inside the furnace. Under normal packing a crucible contained about 13 mgs of alumina. After proper filling, the crucibles were mounted over the alumina sheaths ensuring a good contact between them and the thermocouple tips. The physical contact was checked by a multimeter. Afterwards the DTA cell was introduced in the furnace in a vertical position. Finer adjustments of the DTA cell were made in order to ensure that the two crucibles were in a symmetrical position around the vertical axis of the furnace tube. This minimizes the temperature difference between the two crucibles.

Under steady-state conditions the DTA furnace temperatures with respect to voltage were as follows.

| Temperature (°C) | Voltage V |
|---------------------|--------------|
| 1000 | 50 |
| 1100 | 56 |
| 1200 | 60 |
| 1400 | 75 |
| 1500 | 80 |

After the proper placement of the DTA cell inside the furnace and closing the furnace tube top by an alumina crucible, the furnace was slowly heated to 1000°C or so. During this period no DTA record was made. Afterwards the DTA was performed at controlled heating rates; ΔT signal being recorded as function of time. Meanwhile the temperature of the sample crucible was measured every minute to ensure the linearity of the heating rate. Finer adjustments of the voltage were made in between as per the requirement to obtain more or less an uniform heating rate. By trial runs, for different heating rates, the required voltage steps per unit time were ascertained. For heating rates of 6°C/min and 3°C/min, the required voltage steps were 1 volt change in 3 minutes and 6 minutes respectively. Usually the manual adjustment of the autotransformer gave heating and cooling rates within an accuracy of $\pm 1^\circ\text{C}/\text{min}$.

Most of the samples were heated upto 1500°C or so for the present DTA work. DTA traces were taken only during the heating cycle because during cooling peaks did not appear.

Between the experiments, the thermocouple calibrations were performed with the help of a reference thermocouple (supplied by Engelhardt Inc., U.S.A.) to keep track of any deterioration of the thermocouples in use.

After a DTA run was finished, the crucible containing slag sample was washed by boiling in concentrated HCl. This required around 24 hours, so a set of crucibles were kept for the work.

6.3 Performance of the Apparatus at Moderate Temperature:

Moderate temperature trials were performed with quartz samples for $\alpha \rightarrow \beta$ transformation at around 575°C. The apparatus gave well defined endothermic and exothermic peaks during heating and cooling. The transition temperatures were matching with the values reported in literature after suitable compensation for the heating rate employed was made.

6.4 Performance of the Apparatus at High Temperature:

During high temperature trial runs, a major problem was appearance of broad peak above 1200°C. It appeared like

a DTA peak but this possibility was rejected because of its non-reversible nature during heating and cooling cycles (i.e. the peak was in the same direction both during heating and during cooling). First of all it was thought that this might be due to some kind of physical change occurring in the thermocouple or DTA cell components. Thus one by one all the components were individually checked by changing or replacement and taking blank runs. However the components seemed to be alright and no such change could be traced. Next it was thought that spurious peaks may be caused due to interference of furnace power supply. This was ruled out by ascertaining the behaviour when power to furnace was switched off.

At last the spurious signal was removed by grounding the common terminal of the thermocouples. It was eventually attributed to the D.C. components of asymmetric stray A.C. pick-up from some external source.

Trial runs with actual slag samples also did not yield any DTA peaks. Afterwards the slag samples were given annealing treatment in the furnace itself (Sec. 3.4). This yielded DTA peaks during the heating cycle. During the cooling cycle no DTA peak was obtained for annealed samples also.

CHAPTER 7

RESULTS AND DISCUSSIONS

7.1 DTA Traces:

Thirtynine DTA curves (24 samples) obtained under various conditions in the present work are given in the Appendix I. All the traces obtained are with packed powders during heating cycle only. The molten slag samples did not give DTA peaks during cooling presumably because of difficulty of crystallisation. Also the traces do not show temperatures below 1000°C. The curves shown are approximately to half scale from the original traces. The salient features of each trace are indicated on the diagrams. Table 7.1 summarizes the main observations deduced from these curves while most of the traces are for the same heating rate (6-7°C/min), some traces were obtained with other heating rates (Figures I-18, I-34).

The salient features of the DTA traces include initial base lines, single or multiple peaks, abrupt base line shifts, continuous and discontinuous changes in base line slopes. The base lines obtained during heating are initially wavy and subsequently relatively smooth. The traces then show well-defined single peaks or multiple peaks.

Table 7.1

Summary of Main Observations from DTA Traces

Heating Rate - All 6-7°C/min. Unless Otherwise Mentioned

Sample Condition - Annealed Powder Unless Otherwise Mentioned

S - Pure slag, Y - Al_2O_3 , Z - CaO , T - TiO_2

| Run No. | Sample No. | Designation of Sample | T _S , Solidus Temp., °C | T _L , Liquidus Temp., °C | Remarks* |
|---------|------------|-----------------------|--|---|-------------------------|
| 1 | A1 | 100S | 1135-1146 | -** | A,D,E |
| 2 | A1 | 100S | 1135-1145 | 1325(?)*** | Double annealed, B,F |
| 3 | A2 | 100S+10Z | 1195-1198 | - | A,D,F |
| 4 | A3 | 100S+20Z | 1225 | 1390-1400 | B |
| 5 | A4 | 100S+30Z | 1318-1335 | 1431(?) | F |
| 6 | A4 | 100S+30Z | 1315-1330 | 1426(?) | F |
| 7 | A4 | 100S+30Z | - | 1435(?) | Double annealed, F |
| 8 | A5 | 100S+30Z+10Y | 1360 | 1485-1490 | A,F |
| 9 | A6 | 100S+30Z+20Y | 1215 | - | A,E |
| 10 | A6 | 100S+30Z+20Y | 1240-1245 | 1512 | A,D |
| 11 | A7 | 100S+40Z+10Y | 1335 | 1464 | B,D |
| 12 | A7 | 100S+40Z+10Y | 1328-1333 | 1464 | B,D |
| 13 | A8 | 100S+40Z+20Y | 1324 | 1487-1491 | A,D |
| 14 | A8 | 100S+40Z+20Y | 1329 | 1488 | A,F |
| 15 | A9 | 100S+50Z+10Y | 1325 | 1520-1522 | A,D |
| 16 | A10 | 100S+50Z+20Y | 1329 | 1468 | E |

Table 7.1 (Continued)

| Run No. | Sample No. | Designation of Sample | T _S , Solidus Temp., °C | T _L , Liquidus Temp., °C | Remarks |
|---------|------------|-----------------------|--|---|--|
| 17 | A10 | 100S+50Z+20Y | 1320 | 1450 | B |
| 18 | A10 | 100S+50Z+20Y | 1335 | 1446 | Heating rate (2-3°C/min.), Broad peak |
| 19a | B2 | 100S+10Y | 1105-1115 | - | B |
| 19b | B2 | 100S+10Y | 1110-1115 | 1320-1322 | Repeat run on 19a peak less pronounced |
| 20 | B3 | 100S+20Y | 1200 | 1408 | Single broad peak |
| 21 | B3-1 | 100S+20Y+1.2T | 1220 | 1372 | Single broad peak |
| 22 | B3-2 | 100S+20Y+2.4T | 1288 | 1458(?), 1483(?) | B,E |
| 23 | B4 | 100S+30Y | 1242 | 1377 | Single narrow peak |
| 24 | B5 | 100S+30Y+20Z | 1250-1258 | 1426 | Single broad peak |
| 25 | B6 | 100S+50Y+20Z | 1295 | 1446 | Single broad peak |
| 26 | B7 | 100S+40Y+30Z | 1258 | - | C,F |
| 27 | B7 | 100S+40Y+30Z | - | 1455(?) | F, Appearance of small peak |
| 28 | B7 | 100S+40Y+30Z | 1228-1269 | 1454(?) | F, No clear peak, small thermal arrest at 1400°C |
| 29 | B7 | 100S+40Y+30Z | - | 1459(?) | F, No clear peak, small thermal arrest at 1400°C, Double annealed |

Table 7.1 (Continued)

| Run No. | Sample No. | Designation of Sample | T _S , Solidus Temp., °C | T _L , Liquidus Temp., °C | Remarks |
|---------|------------|------------------------------|------------------------------------|-------------------------------------|-------------------------------------|
| 30 | B8 | 100S+60Y+30Z | 1337 | 1452 | Single peak, F |
| 31 | B8-1 | 100S+60Y+30Z+1.9T | 1225 | 1354 | Single large peak |
| 32 | B8-1 | 100S+60Y+30Z+1.9T | 1227 | 1370 | Single large peak |
| 33 | B8-1 | 100S+60Y+30Z+1.9T | 1230 | 1355(?) | Heating rate 2-3°C/min, Simple peak |
| 34 | B8-2 | 100S+60Y+30Z+3.8T | 1209-1219 | 1345(?) | Single large peak |
| 35 | B9 | 100S+50Y+40Z | 1230(?) | - | C, F |
| 36 | B9 | 100S+50Y+40Z | - | - | C, F, Double annealed |
| 37 | B10 | 100S+70Y+40Z | - | - | C, F |
| 38 | B10 | 100S+70Y+40Z | - | - | C, F, Double annealed |
| 39 | S | .8 Anorthite + .2 Akermanite | 1240 | 1470 | Single peak, F |

- * A - Multiple peaks (refer to Figures I-10; I-15)
 B - Double peak (refer to Figures I-11, I-12)
 C - No peak (refer to Figures I-38, I-39)
 D - Spurious effects before melting (refer to Figures I-11; I-12)
 E - Spurious effect after melting (refer to Figures I-6, I-16)
 F - Shifting of base line slope (refer to Figures I-8, I-30)

** - No value could be obtained

***? - Uncertainty exists.

Anorthite - $\text{CaO} \cdot \text{Al}_2\text{O}_3 \cdot 2\text{SiO}_2$

Akermanite - $2\text{CaO} \cdot \text{MgO} \cdot 2\text{SiO}_2$

Ultimately the traces show a sudden upward swing i.e. a drastic change in base line slope. This is associated with completion of the melting process. In some cases the trace tends to droop again or even exhibits some secondary peaks. These have been found to be associated with formation of bubbles in the solidified slag samples, ejection of sample from the crucible etc. The lack of smoothness of base line may be attributed to initial adjustments problems in measuring apparatus and changes in packing density.

The solidus and liquidus temperatures have been obtained using a simple graphical procedure of extended base line-tangent intercept as shown on the diagrams. A small error is certainly present because of subjective judgement. The possible errors have been indicated in Table 7.1.

7.2 Results:

Table 7.1 summarizes the main results obtained by the DTA. It shows the beginning and end of melting, i.e. the solidus and liquidus temperatures. Salient features of individual DTA traces are also indicated. The liquidus temperatures reported are the temperatures corresponding to complete melting. In several instances such as those where a plateau exists after the peak, the actual temperatures may be somewhat lower.

7.2.1 Effect of Heating Rate:

Figures I-18 and I-34 in Appendix I show the effect of heating rate on the DTA trace for two samples. The traces demonstrate that the record of transformation temperature is reproducible within a few degrees centigrade with no detectable effect of heating rate. This is consistent with the observation made earlier in Chapter 2.

7.2.2 Reproducibility:

Additional DTA traces for some samples with the same heating rate (Figures I-5, I-6; I-11, I-12; I-13, I-14; I-32, I-33) showed that the results are fairly reproducible. For example, Figure I-11 obtained for slag A-7 gives solidus and liquidus temperatures as 1335 and 1464°C. A second trace for the same sample yields the temperatures as 1328-1333 and 1464°C respectively.

7.2.3 Sources of Errors and Troubles:

The problems associated with stray voltage pick-ups at elevated temperatures (1200°C onwards), noncrystallinity etc. and the measures for their elimination have been discussed in Chapter 4. There were, however, several other problems which had to be overcome.

The main problem involves foaming of the viscous slags. It was found that some slags were so viscous that they tended to form bubbles once melting started. Such bubbles would invariably change the thermal characteristics of the samples significantly thus causing irregularities in the DTA traces. In some cases severe foaming caused actual ejection of the sample from the crucible. It was found that foaming and ejection caused the DTA trace to abruptly swing in the opposite direction. It was therefore necessary to make visual observation of slag sample after every run.

It was found out that slags containing TiO_2 gave the most well-defined peaks. This may perhaps be attributed to the well-known behaviour of TiO_2 as a promoter of nucleation and crystallization in glasses. While the height and area of peak would definitely depend on the extent of crystallization, it would be difficult to analyse the present traces in those terms.

Multiple peaks as such ought to indicate more than one transformation in the melting temperature range. However it has been inferred already that gas bubble formation disturbs the peak. As the entrapped bubble tries to escape or coalesces with other bubble and disrupts the semiliquid slag some kind of pseudo peaks may very well appear in the DTA curve due to fluctuations in sample temperature. Therefore multiple peaks are most likely due to troubles like this and do not depict multiple transformations.

7.3 Comparison with Liquidus Data Available in Literature:

Considering the actual slag sample to consist of four components viz. Al_2O_3 , CaO , SiO_2 and MgO only, and rejecting other constituents, the compositions of all the samples were recalculated and are presented in Table 7.2. Next liquidus temperature data of a few composition of such four-component representation were compared with those by Osborn et al.²² for the synthetic four-component system: Al_2O_3 - CaO - SiO_2 - MgO comparisons are presented in Table 7.3. Due to the limited matching of slag compositions with those investigated by Osborn et al.²², comparisons could be made only for a few compositions. From Table 7.3 it may be noted that for two slag compositions (viz. A1 and A8), the liquidus temperatures are in the proximity of the temperatures given by Osborn et al.²². However for samples A4 and B2 no such matching of liquidus temperature exists. The reasonable matching of liquidus temperatures for sample A1 and A8 and not samples A4 and B2 may be attributed to sensitiveness of liquidus temperatures to composition variations. It can be seen that for compositions falling in range of sample A1 and A8; slight variations in compositions do not effect the liquidus temperatures on the other hand for the compositions falling in the range of samples A4 and B2, slight variations in composition drastically change the liquidus temperatures

Table 7.2A

Slag Analyses of Samples of Region A In Terms of Four
Components viz. Al_2O_3 , CaO , SiO_2 and MgO

S = Pure slag, Y = Al_2O_3 , Z = CaO

| S.N. | Sample No. | Designation of Sample | wt. pct. | | | |
|------|---------------|--------------------------|-------------------------|--------------|--------------|----------------|
| | | | Al_2O_3 | CaO | MgO | SiO_2 |
| 1 | A1 | 100S | 26.98 | 30.69 | 4.76 | 37.57 |
| 2 | A2 | 100S+10Z | 24.53 | 36.99 | 4.33 | 34.15 |
| 3 | A3 | 100S+20Z | 22.48 | 42.24 | 3.97 | 31.31 |
| 4 | A4 | 100S+30Z | 20.75 | 46.68 | 3.66 | 31.31 |
| 5 | A5 | 100S+30Z+10Y | 26.41 | 43.35 | 3.40 | 26.84 |
| 6 | A6 | 100S+30Z+20Y | 31.32 | 40.46 | 3.17 | 25.05 |
| 7 | A7 | 100S+40Z+10Y | 24.65 | 47.13 | 3.17 | 25.05 |
| 8 | A8 | 100S+40Z+20Y | 29.36 | 44.18 | 2.98 | 23.48 |
| 9 | A9 | 100S+50Z+10Y | 23.11 | 50.43 | 2.98 | 23.48 |
| 10 | A10 | 100S+50Z+20Y | 27.64 | 47.46 | 2.80 | 22.10 |

Table 7.2B

Slag Analyses of Samples of Region B In Terms of Four
Components viz. Al_2O_3 , CaO , SiO_2 and MgO

S = Pure slag, Y = Al_2O_3 , T = TiO_2 , Z = CaO

| S.N. | Sample No. | Designation of Sample | wt. pct. | | | |
|------|------------|-----------------------|-------------------------|--------------|--------------|----------------|
| | | | Al_2O_3 | CaO | MgO | SiO_2 |
| 1 | B1 | 100S | 26.98 | 30.69 | 4.76 | 37.57 |
| 2 | B2 | 100S+10Y | 33.62 | 27.90 | 4.33 | 34.15 |
| 3 | B3 | 100S+20Y | 39.15 | 25.58 | 3.97 | 31.31 |
| 4 | B3-1 | 100S+20Y+1.2T | 38.76 | 25.32 | 3.93 | 31.00 |
| 5 | B3-2 | 100S+20Y+2.4T | 38.38 | 25.07 | 3.89 | 30.69 |
| 6 | B4 | 100S+30Y | 43.83 | 23.61 | 3.66 | 28.90 |
| 7 | B5 | 100S+30Y+20Z | 37.99 | 33.79 | 3.17 | 25.05 |
| 8 | B6 | 100S+50Y+20Z | 45.28 | 29.82 | 2.80 | 22.10 |
| 9 | B7 | 100S+40Y+30Z | 39.40 | 35.70 | 2.80 | 22.10 |
| 10 | B8 | 100S+60Y+30Z | 45.78 | 31.94 | 2.51 | 19.77 |
| 11 | B8-1 | 100S+60Y+30Z+1.9T | 45.33 | 31.63 | 2.48 | 19.58 |
| 12 | B8-2 | 100S+60Y+30Z+3.8T | 44.88 | 31.32 | 2.46 | 19.39 |
| 13 | B9 | 100S+50Y+40Z | 40.52 | 37.21 | 2.51 | 19.77 |
| 14 | B10 | 100S+70Y+40Z | 46.18 | 33.66 | 2.27 | 17.89 |

Table 7.3

Comparison of Some Liquidus Temperatures of the Present Investigation with Those Obtained by Osborn et al.²² for Synthetic CaO-Al₂O₃-SiO₂-MgO System

| Sample No. | Present investigation | | | | | Osborn et al. ²² | | | | |
|------------|--------------------------------|-------|------------------|------|---------------------|--------------------------------|------|------------------|-----|---------------------|
| | Al ₂ O ₃ | CaO | SiO ₂ | MgO | T _L , °C | Al ₂ O ₃ | CaO | SiO ₂ | MgO | T _L , °C |
| A1 | 26.98 | 30.69 | 37.57 | 4.76 | 1325 | 25 | 30.0 | 40.0 | 5.0 | 1320±5 |
| | | | | | | 25 | 30.0 | 39.0 | 6.0 | 1316±3 |
| | | | | | | 25 | 30.0 | 38.0 | 7.0 | 1350±1 |
| | | | | | | 25 | 31.0 | 36.0 | 8.0 | 1417±3 |
| A4 | 20.75 | 46.68 | 28.90 | 3.66 | 1426 | 20 | 46.5 | 26.0 | 7.5 | 1536 |
| | | | | | 1431 | 20 | 45.0 | 30.0 | 5.0 | 1505 |
| | | | | | | 20 | 44.5 | 28.5 | 7.0 | 1465 |
| | | | | | | 20 | 48.0 | 28.0 | 4.0 | >1575 |
| A8 | 29.36 | 44.18 | 23.48 | 2.98 | 1488 | 30 | 37.0 | 25.0 | 8.0 | 1493±1 |
| | | | | | | 30 | 44.0 | 20.0 | 6.0 | 1455±4 |
| | | | | | | 30 | 43.0 | 19.0 | 8.0 | 1416±3 |
| | | | | | | 30 | 42.0 | 19.0 | 9.0 | 1422±2 |
| B2 | 33.62 | 27.90 | 34.15 | 4.30 | 1322 | 35 | 28.0 | 33.0 | 4.0 | 1447±4 |
| | | | | | | 35 | 24.0 | 33.0 | 8.0 | 1561±2 |
| | | | | | | 35 | 32.0 | 29.0 | 4.0 | 1480±3 |
| | | | | | | 35 | 28.0 | 29.0 | 8.0 | 1597±4 |

and therefore correlation of data of present investigation with literature data ought to be difficult.

Table 7.4 shows the comparison of present work with liquidus temperatures obtained by Baldwin²⁰ on some actual blast furnace slags. Here only the compositions of two samples could be matched with those of Baldwin²⁰ work. It is to be noted that for one sample (A4), the temperature is off by about 100°C while for the other sample (A6) there is only a difference of about 15°C. On closer look at the compositions, we find that MnO content is very high in the slag samples of present work. Thus it is difficult to correlate the present data with other similar work reported in the literature. Moreover due to limited data it is difficult to ascertain whether the compositions of samples A4 and A6 fall in composition sensitive range or not.

Table 7.4

Comparison of Some Liquidus Temperatures of the Present Study with Those of Baldwin²⁰ on Actual Blast Furnace Slag Samples

| Slag Constituents | Present Investigation A4 | Baldwin ²⁰ | Present Investigation A6 | Baldwin ²⁰ |
|-------------------------|--------------------------------|-----------------------|--------------------------------|-----------------------|
| Al_2O_3 | 19.6 | 19.5 | 30.3 | 29.0 |
| CaO | 45.4 | 43.8 | 39.3 | 39.0 |
| SiO_2 | 27.3 | 30.8 | 23.7 | 26.2 |
| MgO | 3.5 | 4.6 | 3.0 | 3.7 |
| MnO | 2.9 | 0.5 | 2.5 | 0.2 |
| FeO | 0.8 | 0.1 | 0.7 | 0.3 |
| TiO_2 | 0.2 | - | 0.1 | - |
| S | 0.4 | 1.6 | 0.3 | 1.8 |
| <hr/> | | | | |
| Liquidus Temp. °C | 1430 | 1510* 1530** | 1512 | 1525* 1530** |

* Calculated liquidus

** Measured liquidus

CHAPTER 8

SUMMARY AND CONCLUSIONS

8.1 Summary:

- a) Differential thermal analysis (DTA) and hot filament microscopy (HFM) units were designed and fabricated.
- b) Determination of liquidus and solidus temperatures of Rourkela blast furnace slag with and without additions of Al_2O_3 , CaO and TiO_2 were made using the DTA apparatus.
- c) HFM assembly and filament design were perfected.

Various switching devices were tried. However, all the problems could not be resolved.

8.2 Conclusions:

The findings of the present investigation are:

- a) Without annealing and crystallization, no DTA peak could be obtained.
- b) DTA peak could be obtained for heating cycle only.
- c) Variation in heating rate did not influence the solidus and liquidus temperatures.
- d) Data were reproducible within 10°C .
- e) Formation and evolution of gas bubbles led to irregularities in the DTA traces at some compositions.

Multiple peaks obtained in several DTA traces may be attributed to these factors as well as possible multiple transformations in the slag during heating.

- f) Comparison with data from other sources for few compositions did not yield any systematic matching. It seems sensitivity of the liquidus temperature to composition variations is at least partly responsible for this behaviour pattern.
- g) It is contended that a fair amount of confidence can be placed on the results. However some cross checking by the HFM, quench method and/or viscosity-temperature behaviour would perhaps be desirable.

REFERENCES

1. Industrial R&D Plans for Iron & Steel; Published by Hindustan Steel Ltd. (1975)
- 1A. F. Ordway: J. Res. Nat. Bur. Standards, 48, 152 (1952)
2. J.H. Welch: J. Sci. Instrum., 31, 458 (1954)
3. J.H. Welch: J. Iron & Steel Inst., 83, 275 (1956)
4. R.C. Mackenzie: Basic Principles and Historical Developments in 'Differential Thermal Analysis', Vol. I, R.C. Mackenzie (Ed.), Academic Press, N.Y. (1970)
5. R.C. Mackenzie (Ed.): 'Differential Thermal Analysis', Vol. I, II, Academic Press, N.Y. (1970)
6. W.J. Smothers, Yao Chiang: 'Hand Book of Differential Thermal Analysis', Chemical Publ. Comp., Inc., N.Y. (1966)
7. RNDr, Ph Mr. Anton Blazek: 'Thermal Analysis', von Nostrand Reinhold Comp. Ltd., (1973)
8. R.C. Mackenzie: 'The Differential Thermal Investigation of Clays', Mineralogical Soc., London (1957)
9. P.D. Garn: 'Thermoanalytical Methods of Investigation', Academic Press, N.Y. (1965)
10. R.F. Schwenker Jr., P.D. Garn (Ed.): 'Thermal Analysis', Vol. 1, 2, Academic Press, N.Y. (1969)
11. T. Daniels: 'Thermal Analysis', Kogan Page Ltd., London, (1973)
12. P.L. Arens: 'A Study of the Differential Thermal Analysis of Clays and Clay Minerals', Excelsiors Foto Offset (1951)
13. R.W. Nurse: Proc. Intern. Symposium Chem. Cement, 3rd Symp. London, 56 (1952)
14. K. Grupner: in, 'Research in Chemical and Extraction Metallurgy', J.T. Wood Cock, A.E. Jenkins, G.M. Willis (Ed.), (1965)

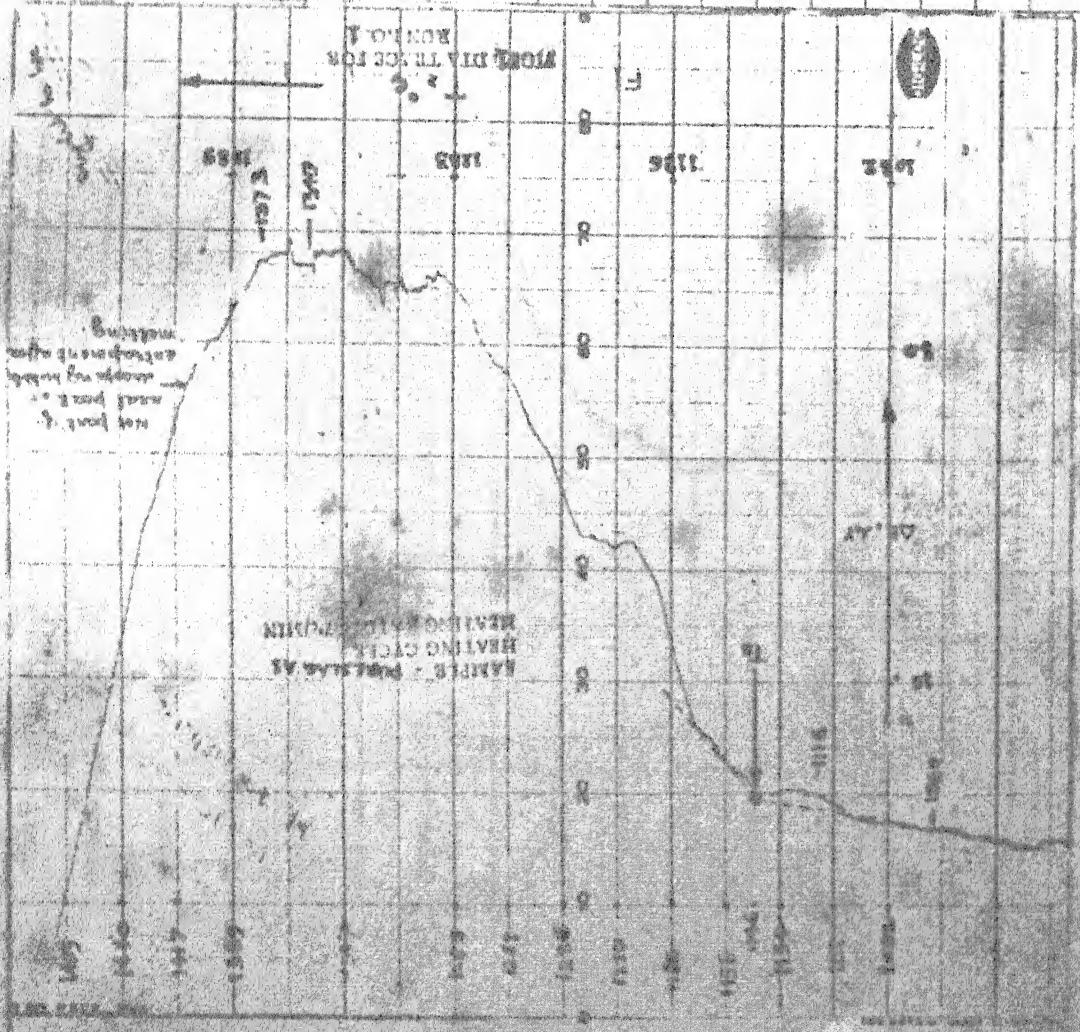
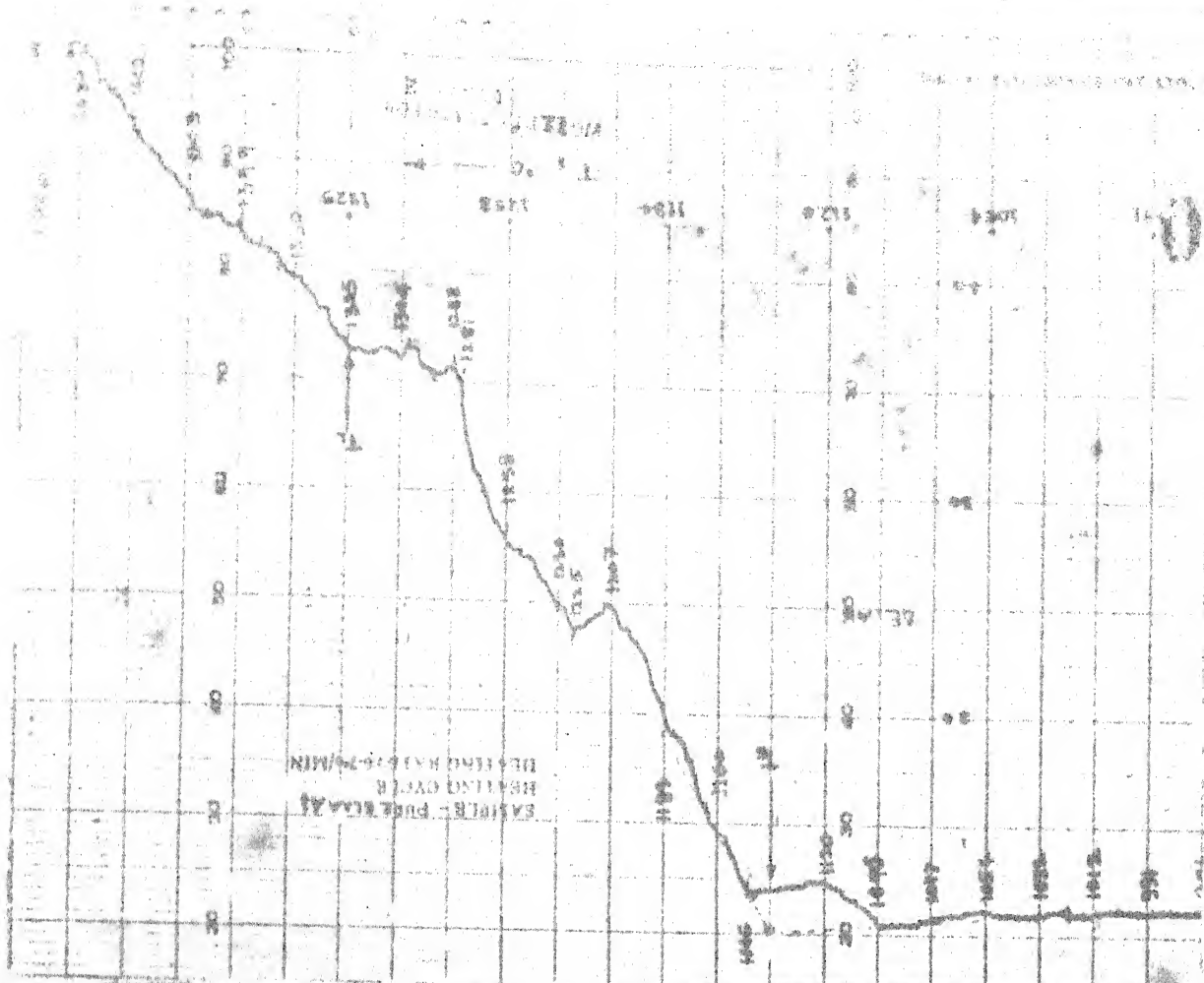
15. W. Richard Ott, Malcolm G. McLaren: in, 'Thermal Analysis', R.F. Schevenker Jr., P.D. Garn (Ed.), Vol. 2, 1329 (1969)
16. Ralph H. Nafziger: 'High Temp. Sci.', 7, 179 (1975)
17. J.J. Byerely: Univ. Toronto, M.A.Sc. Thesis (1959)
18. A. Ohno: Univ. Toronto, Ph.D. Thesis (1962)
19. Gerhard Derge: Trans. Met. Soc. AIME, 239, 1480 (1967)
20. B.G. Baldwin: J. Iron & Steel Inst., 186, 388 (1957)
21. A. Ohno, H.U. Ross: Can. Met. Quat., 2, 243 (1963)
22. E.F. Osborn, R.C. DeVries, K.H. Gee, H.M. Kraner: J. Metals Trans., 200, 33 (1954)
23. J. Taylor: J. Iron & Steel Inst. Lon., 200, 701 (1962)
24. Klaus Koch, Gerhard Tromel: Arch. Eisenhüttenwes, 46, 165 (1975)
25. von Klauskoch, Gerhard Tromel, Gerd Heinz: Sonderdruck aus Tonind. - Ztg, 99, 3 (1975)
26. F.P. Glasser, J. Marr: Trans. & J. Brit. Ceram. Soc., 4, 133 (1975)
27. G.M. Biggar, J. O'hara: Miner. Magz., 38, 918 (1972)
28. A.J. Burgess, B.G. Baldwin: J. Iron & Steel Inst., 186, 227 (1957)
29. D. Turnbull: J. Chem. Phys., 18, 198 (1950)
30. M. Volmer: Z. Electrochem., 35, 555 (1929)
31. N.H. Fletcher: J. Chem. Phys., 29, 572 (1958)
32. G. Tamman: J. Soc. Glass. Tech., 90, 166 (1925)
33. J.G. Morley: Glass Technol., 6, 77 (1965)
34. J. Frenkel: 'Kinetic Theory of Liquids', Oxford, Clarendon Press (1946)

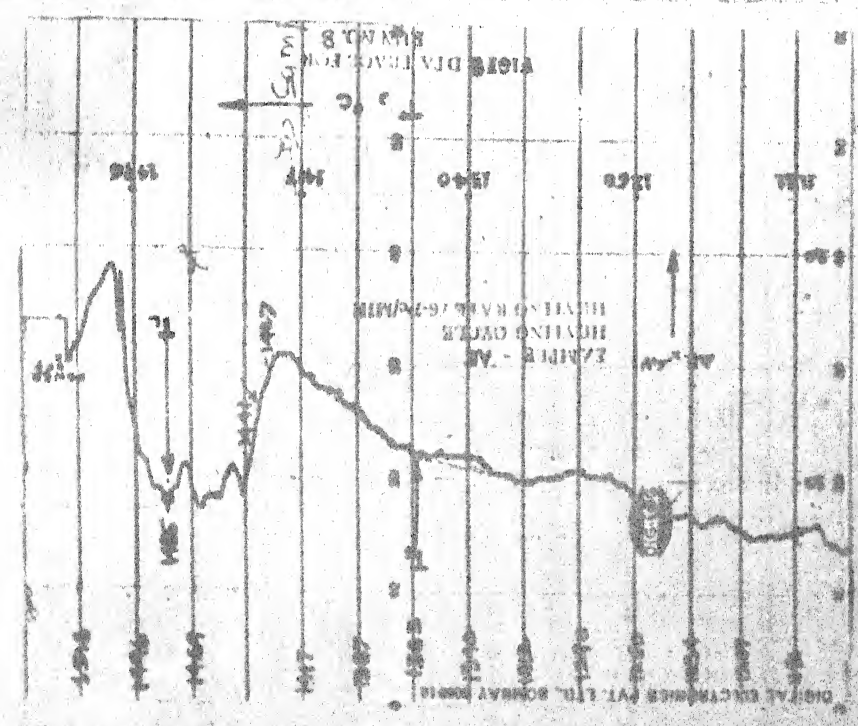
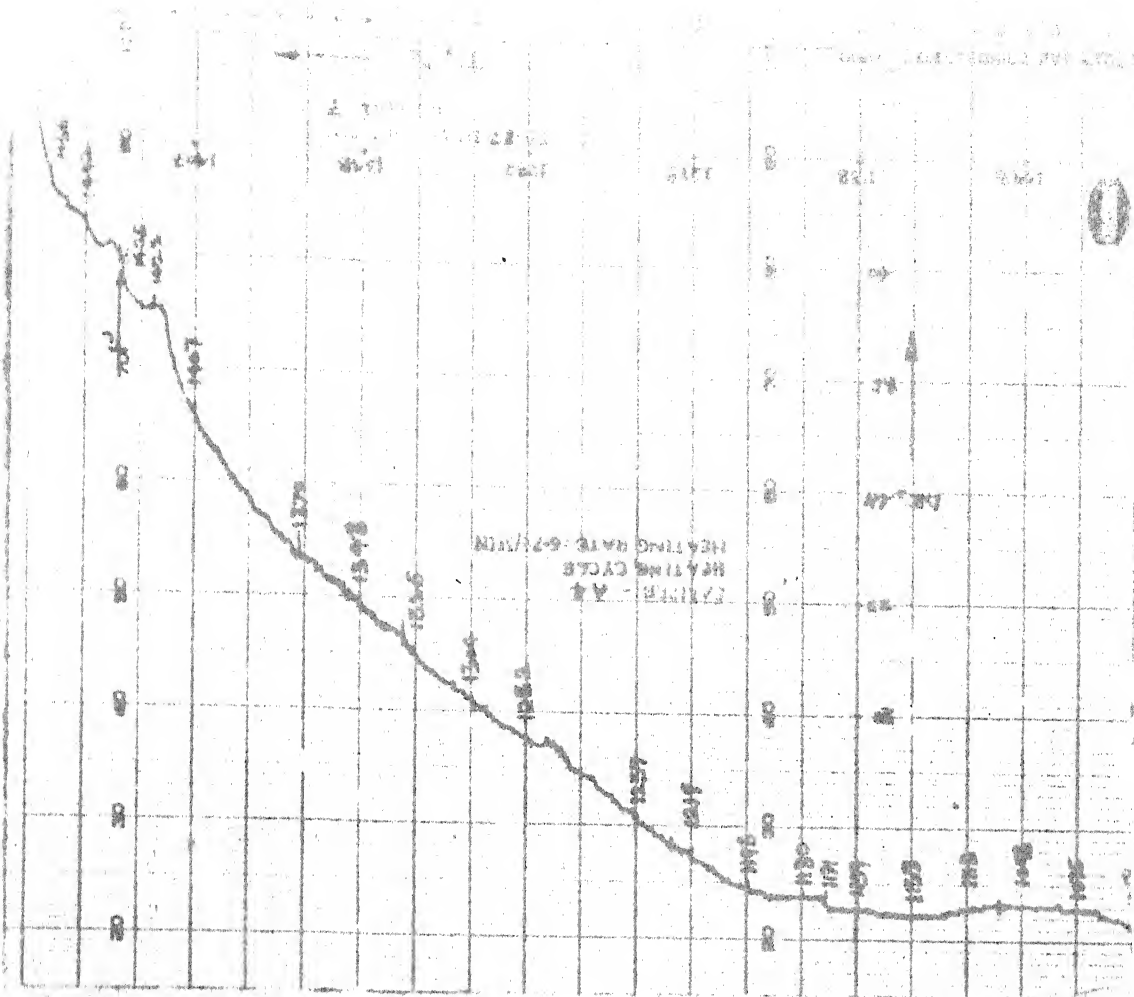
35. V.V. Vargin (Ed.): 'Catalyzed Controlled Crystallization of Glasses, Part 1, Chap. 2', Consultants Bureau, N.Y. (1965)
36. Kirk Othmor: 'Encyclopedia of Chemical Technology', second completely revised edition, supplement volume, 876 (1971)
37. P.D. Garn: 'Thermoanalytical Methods of Investigation', Chap. III, Academic Press, N.Y. (1965)
38. R.C. Mackenzie (Ed.): 'Differential Thermal Analysis', Chap. 4, Vol. 1, Academic Press, N.Y. (1970)
39. S.L. Boersma: J. Am. Ceram. Soc., 38, 281 (1955)
40. N.A. Nedumov: Zh. fiz. Khim., 84, 181 (1960)
41. P.L. Arens: Soil Science, 72, 406 (1951)
42. H.E. Kissinger: J. Res. Natl. Bur. Std., 57, 217 (1956)
43. H.T. Smyth: J. Am. Ceram. Soc., 34, 221 (1951)
44. Klauskoch, et al.: Arch. Eisenhüttenwes, 46, 83 (1975)
45. A.M. Alpher (Ed.): 'Phase Diagrams', Vol. I, II, Academic Press (1970)
46. A. Muan, E.F. Osborn: 'Phase Equilibria Among Oxide in Steelmaking', Addison-Wesley Pub. Comp. Inc., Mass. (1965)
47. E.M. Levin et al.: 'Phase Diagrams for Ceramists', Am. Ceram. Soc., Columbus, Ohio (1964)
48. M.R. Kalyanram, et al.: J. Iron Steel Inst. London, 195, 58 (1960)
49. G.G. Hatch, J. Chipman: Trans. AIME, 185, 274 (1949)
50. A.B. Samaddar, D. Lahiri: Trans. Ind. Ceram. Soc., 21, 75 (1962)
51. J.E. Kruger: Cement and Lime Manuf., London, 25, 104 (1962)
52. J. Taylor: in 'Phase Diagrams', A.M. Alper (Ed.), Vol. II, Chap. 6, Academic Press, N.Y. (1970)

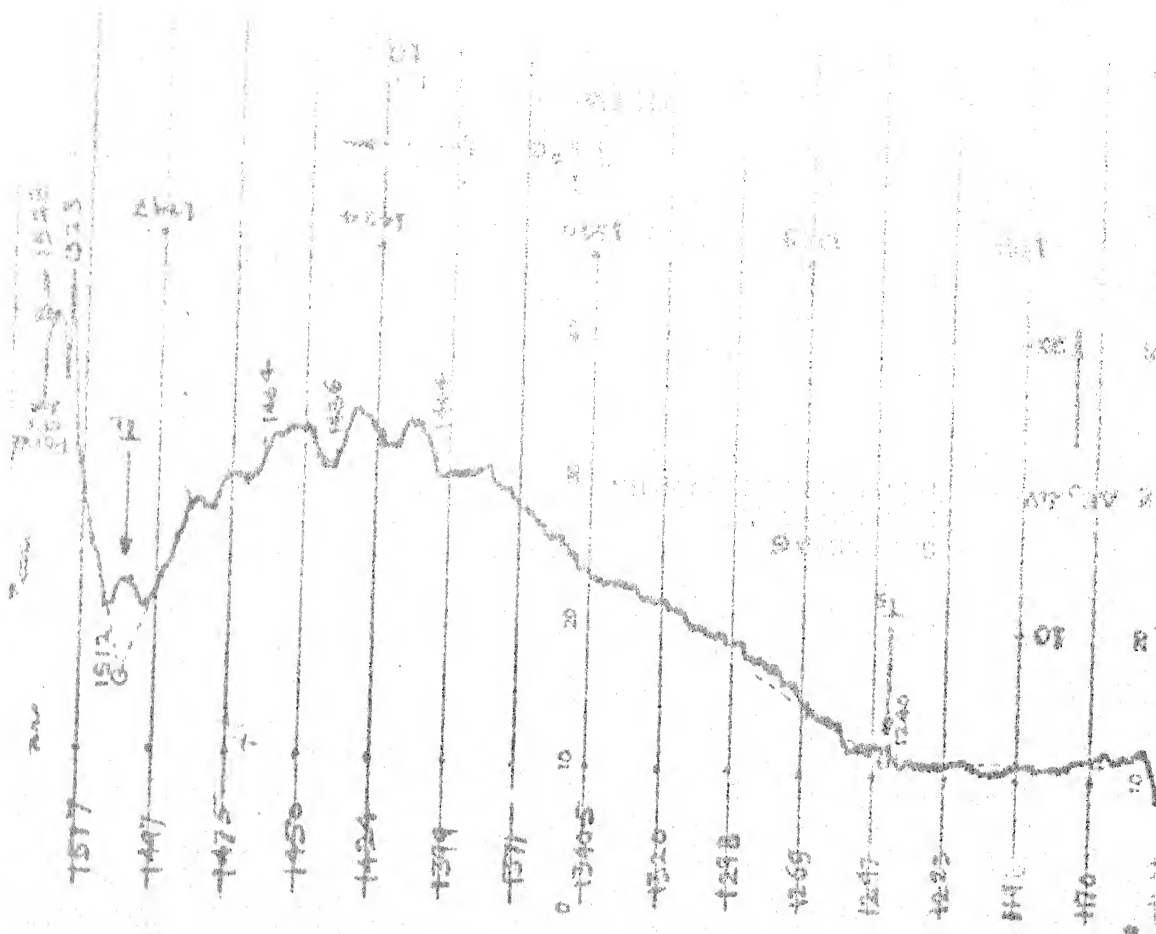
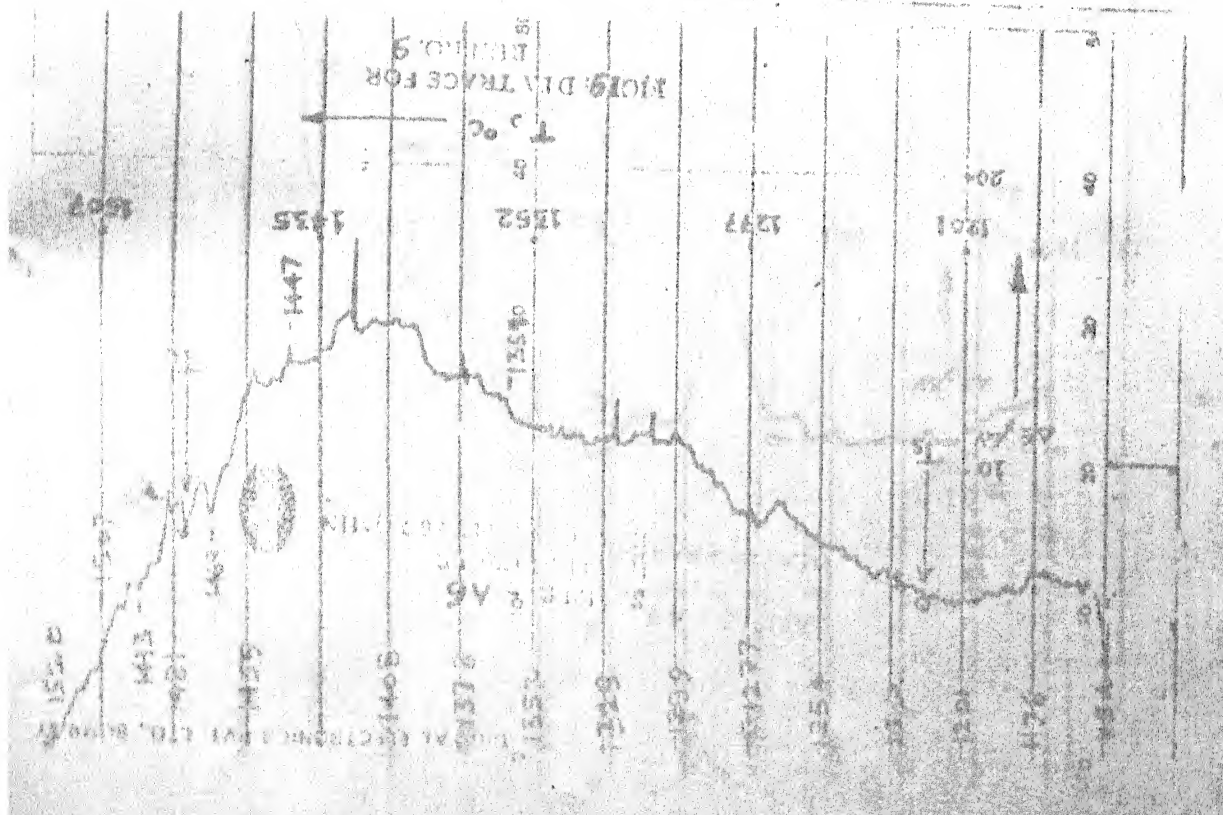
53. H.C. Yeh: *ibid*, Vol. I, Chap. 6 (1970)
54. E. Aruja, J.H. Welch, W. Gutt: *J. Sci. Instrum.*, 36, 162 (1959)
55. J.H. Welch: *ibid*, 38, 402 (1961)
56. R.L. Causer: *ibid*, 43, 650 (1966)
57. J.O.M. Bockris, et al.: 'Physicochemical Measurements at High Temperatures', pp. 65, Butterworths Scientific Publ., London.

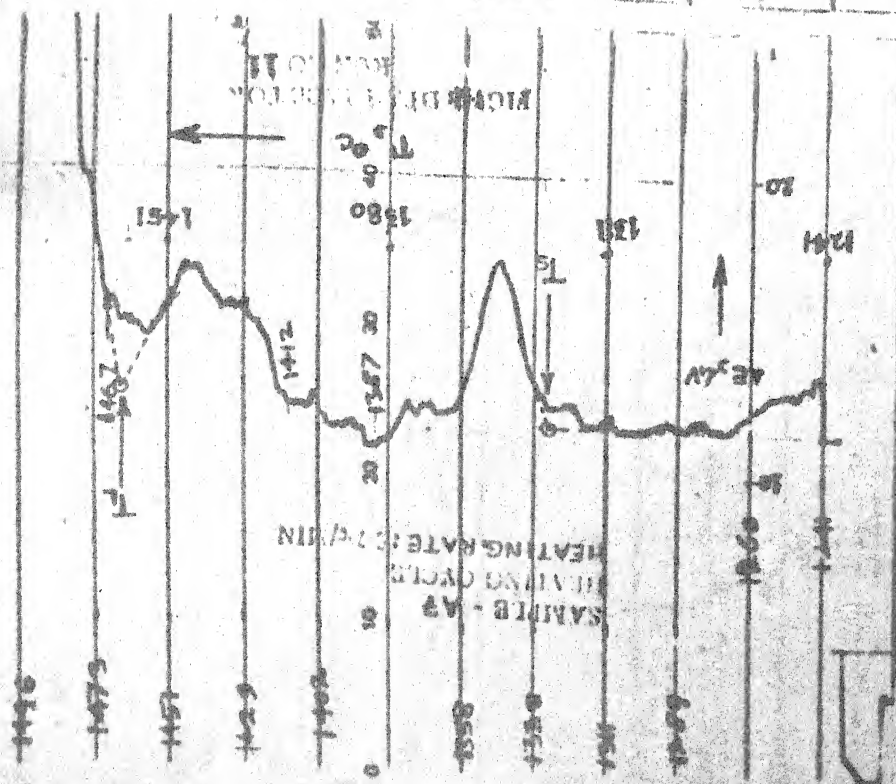
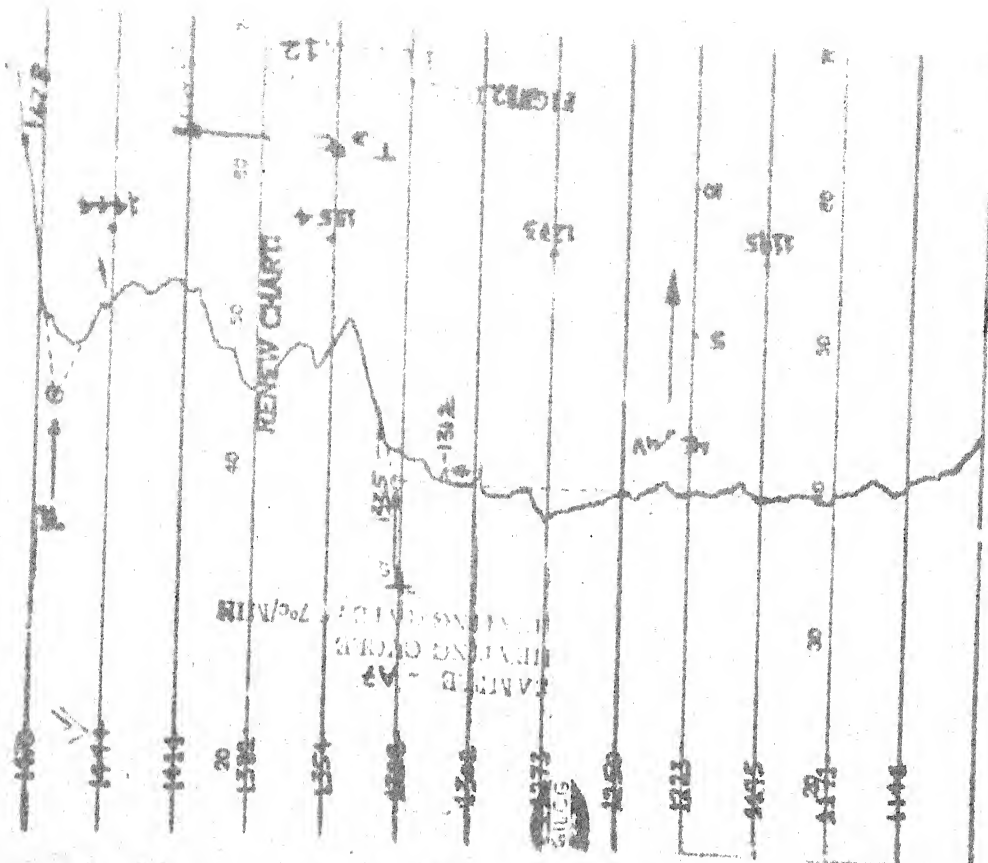
APPENDIX - I

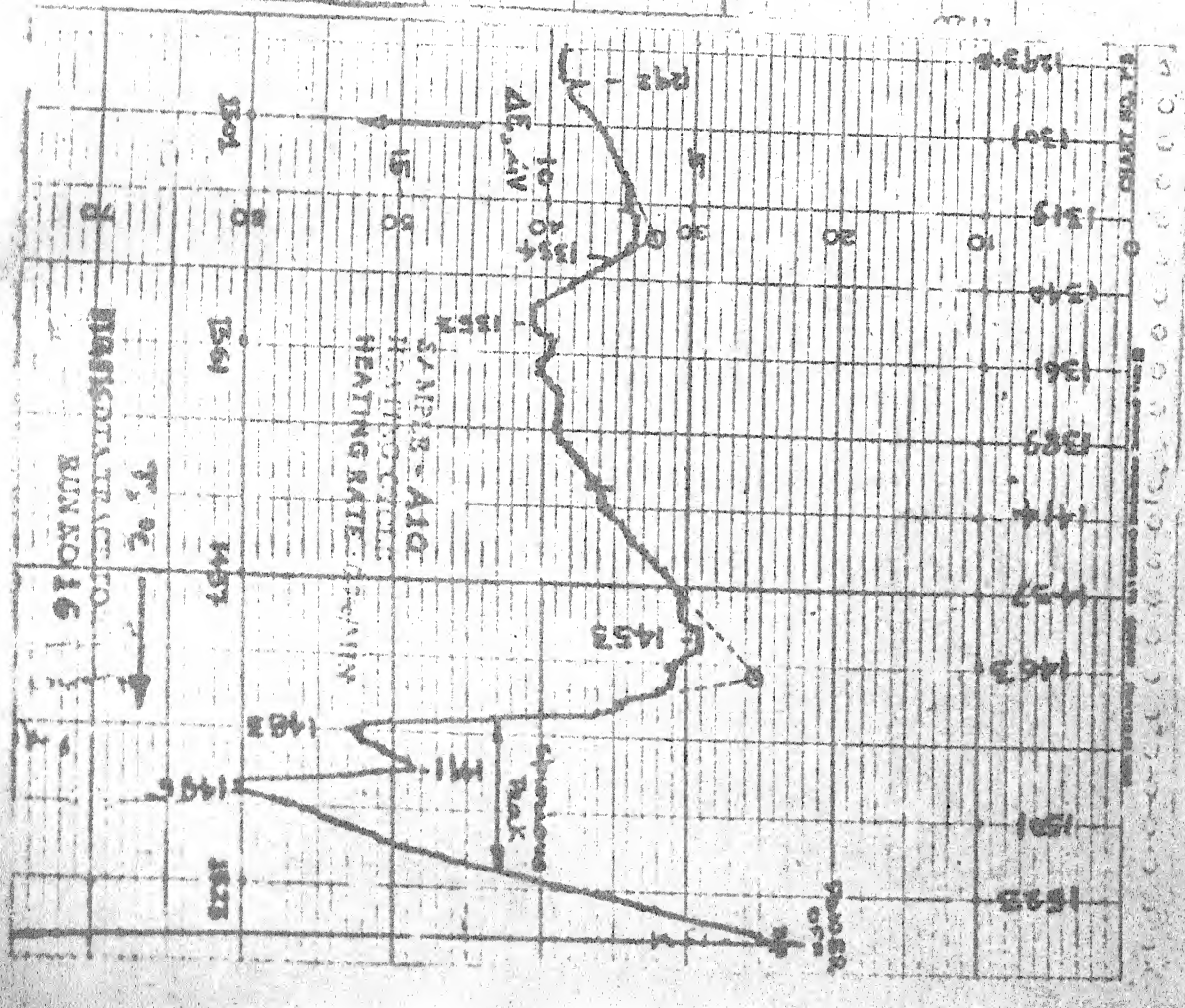
DTA TRACES

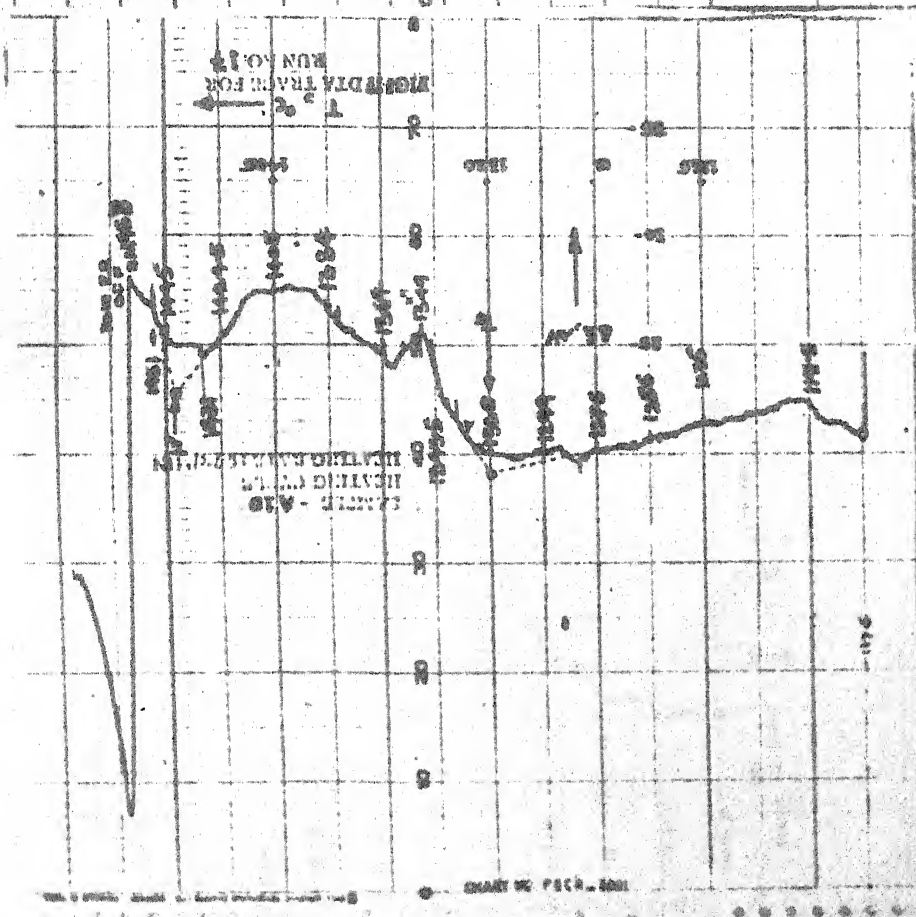
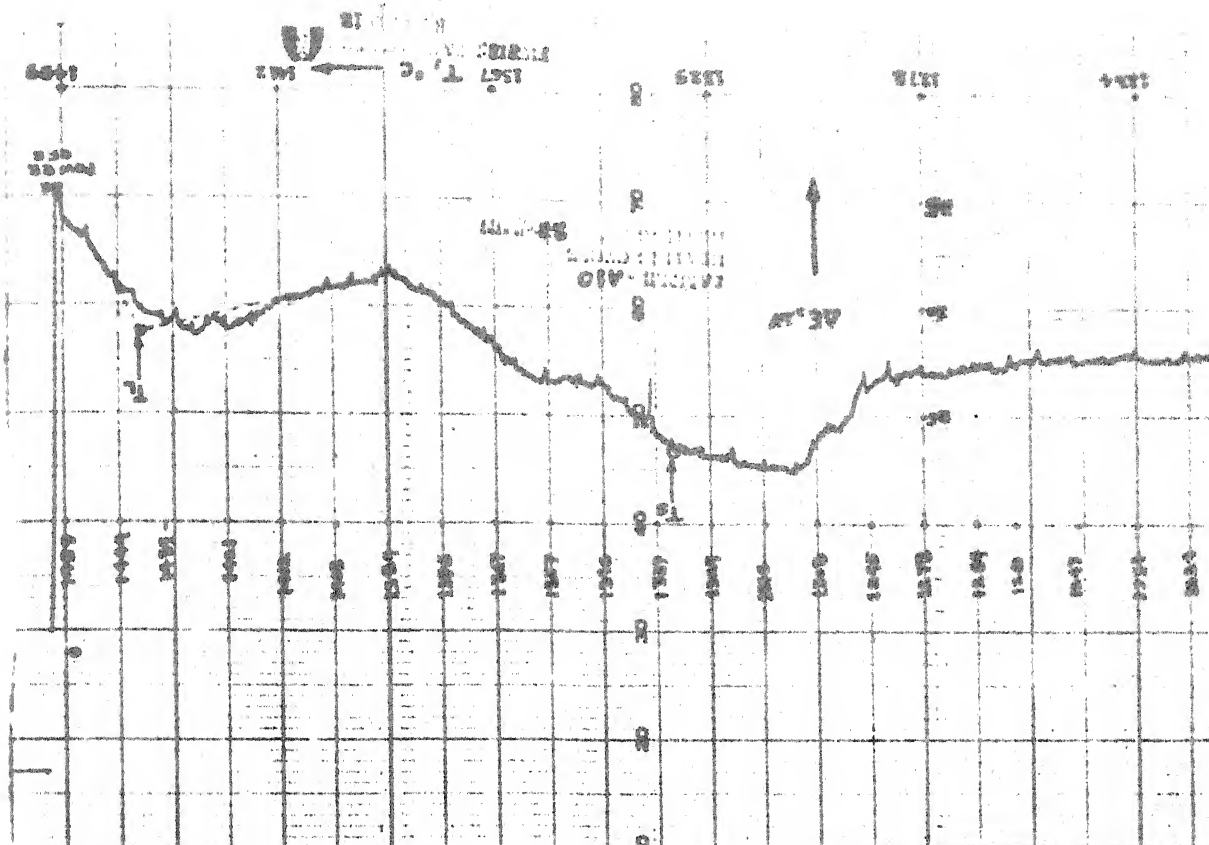


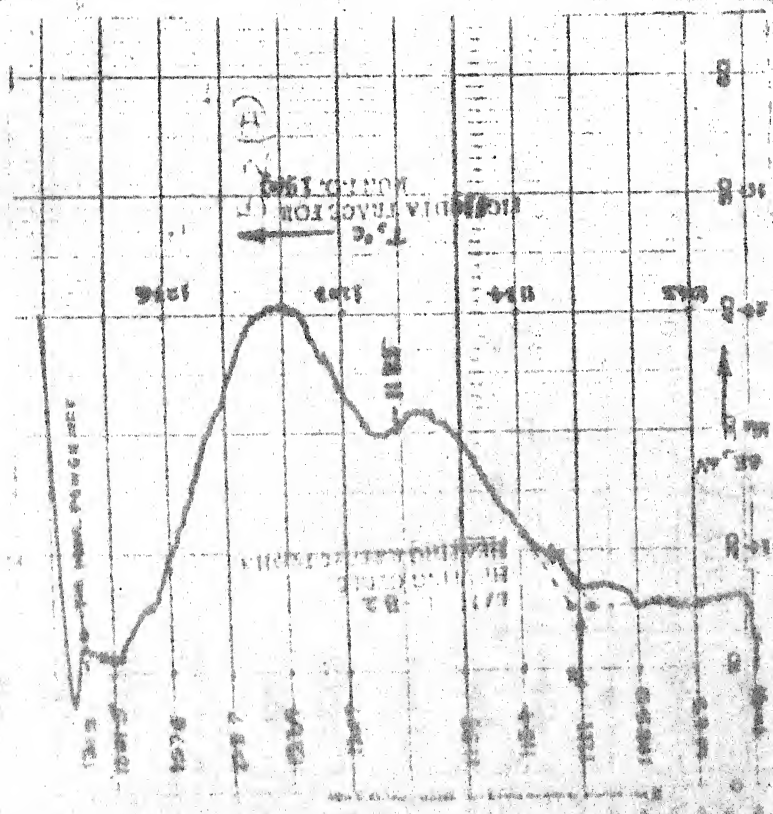
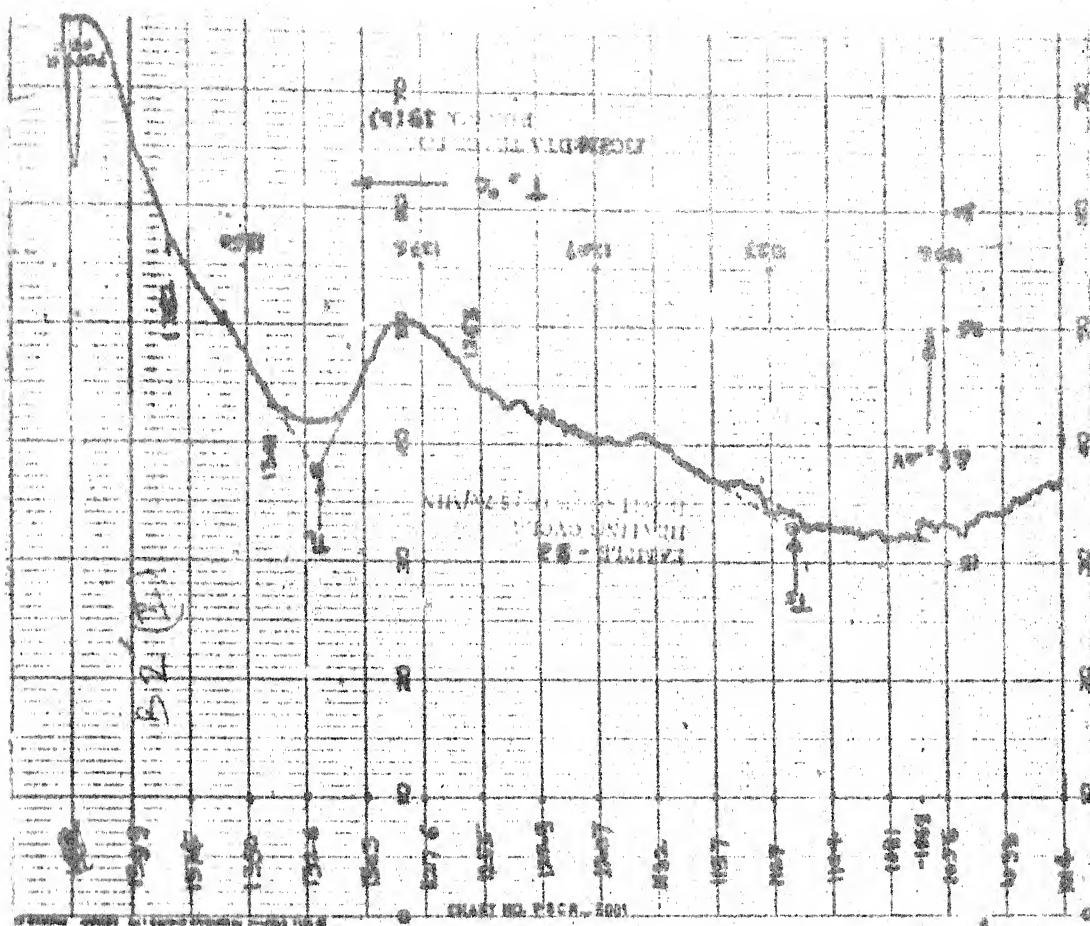


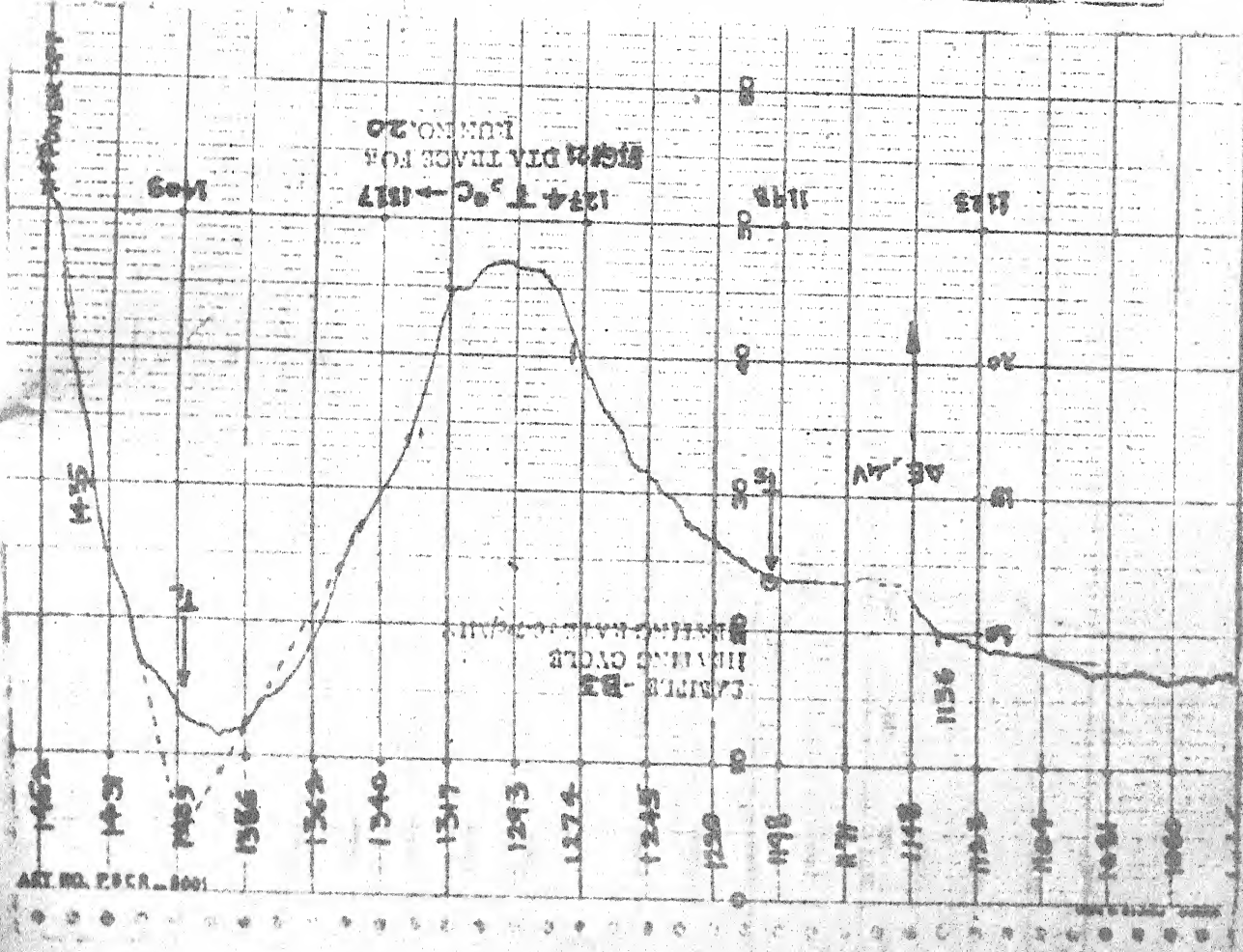
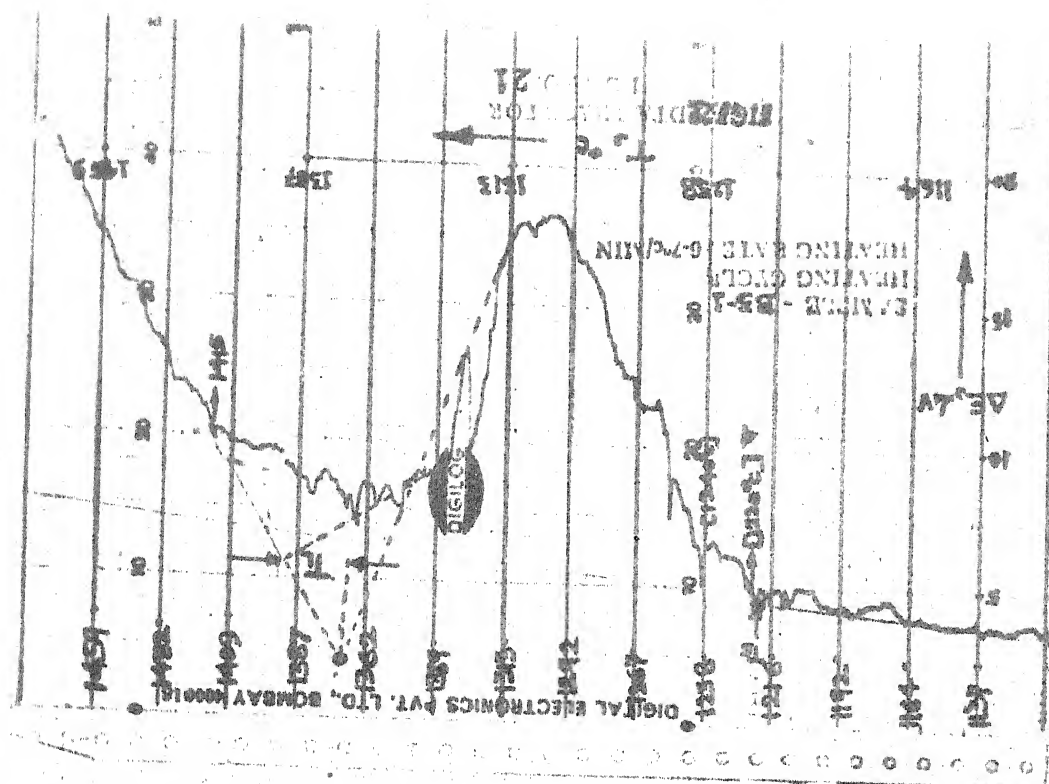


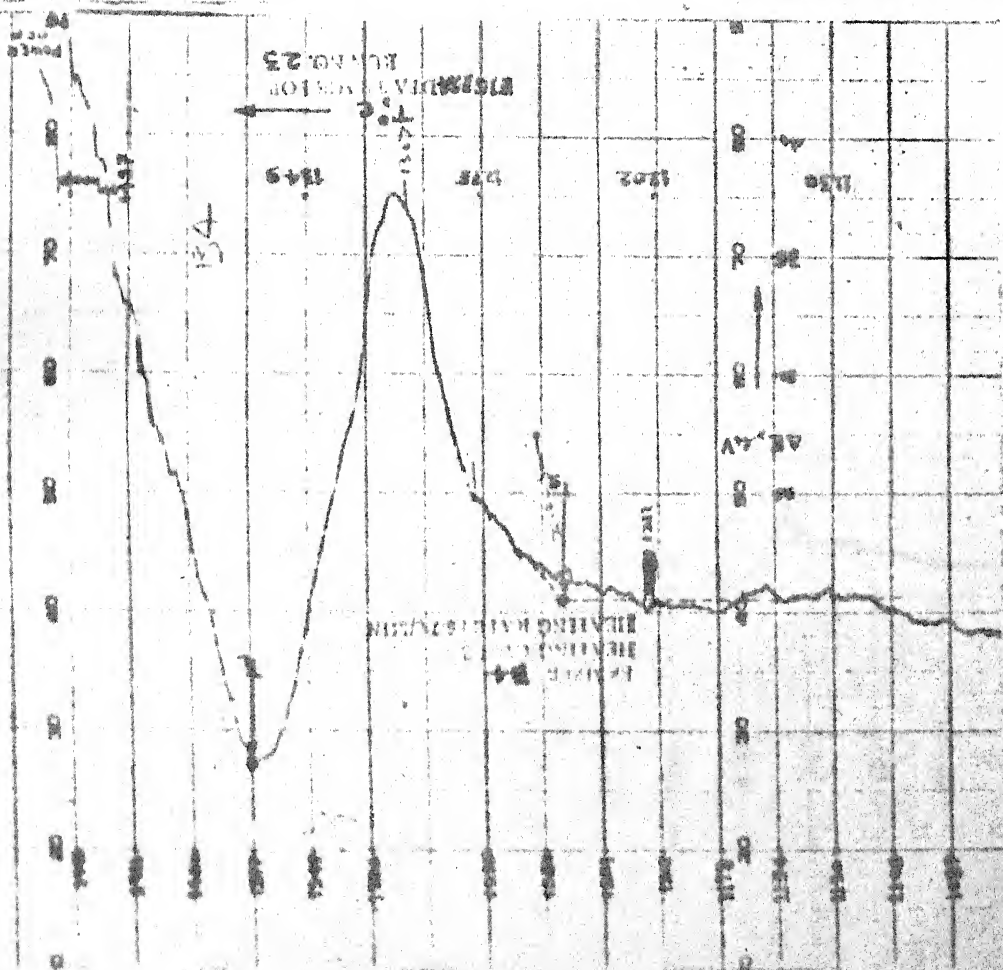
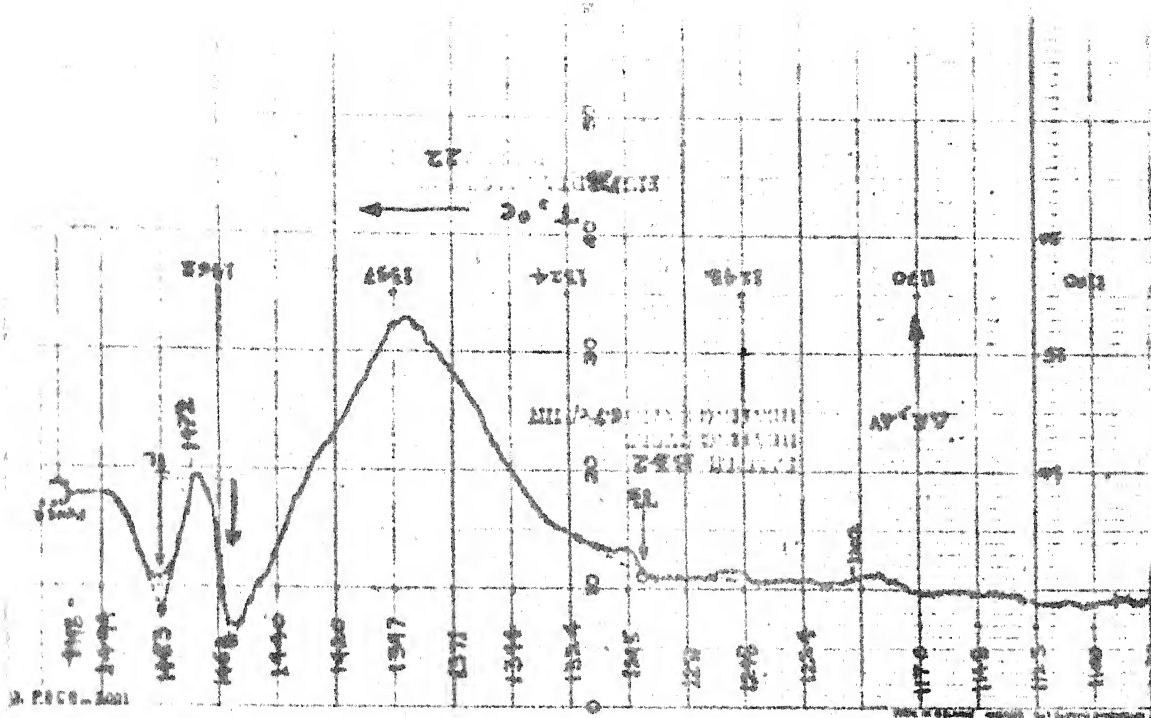


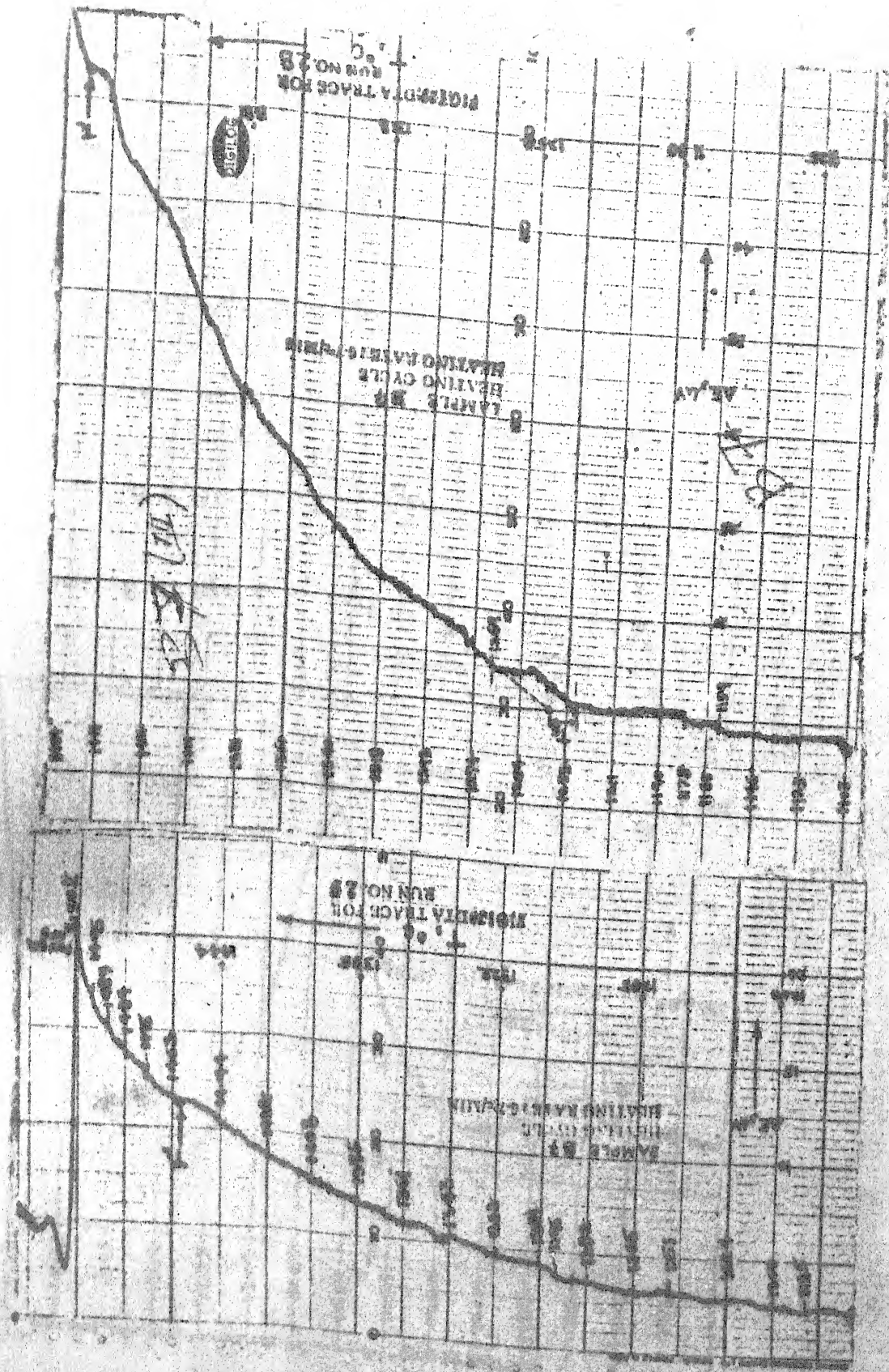


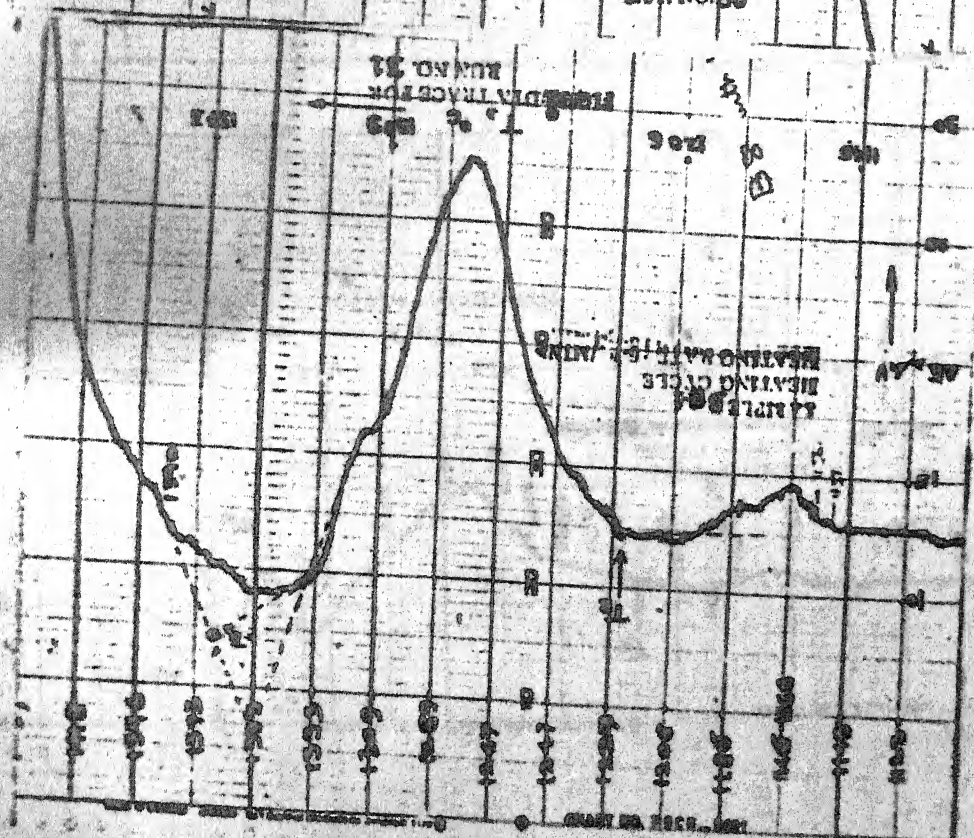
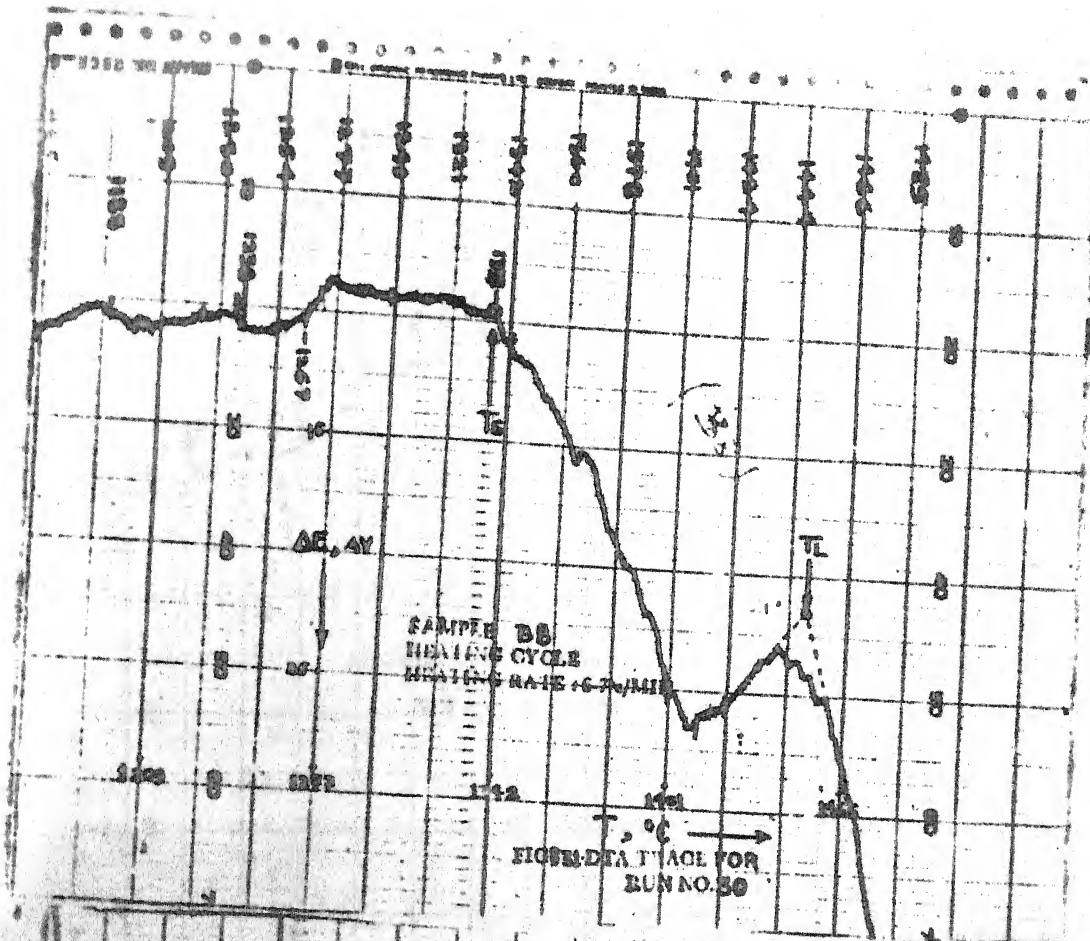


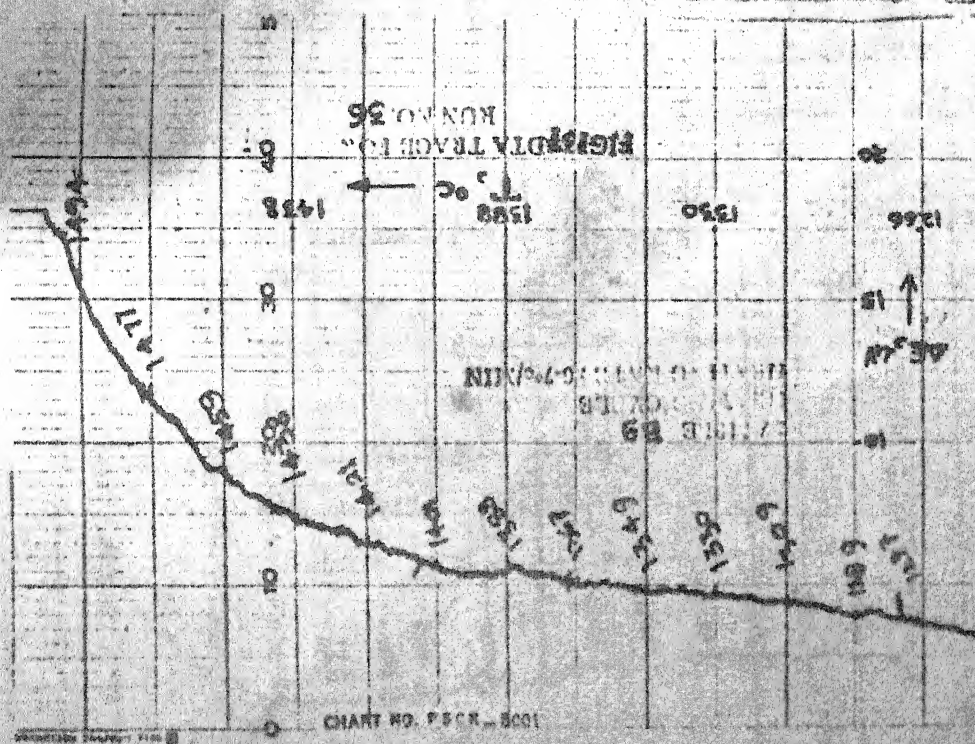
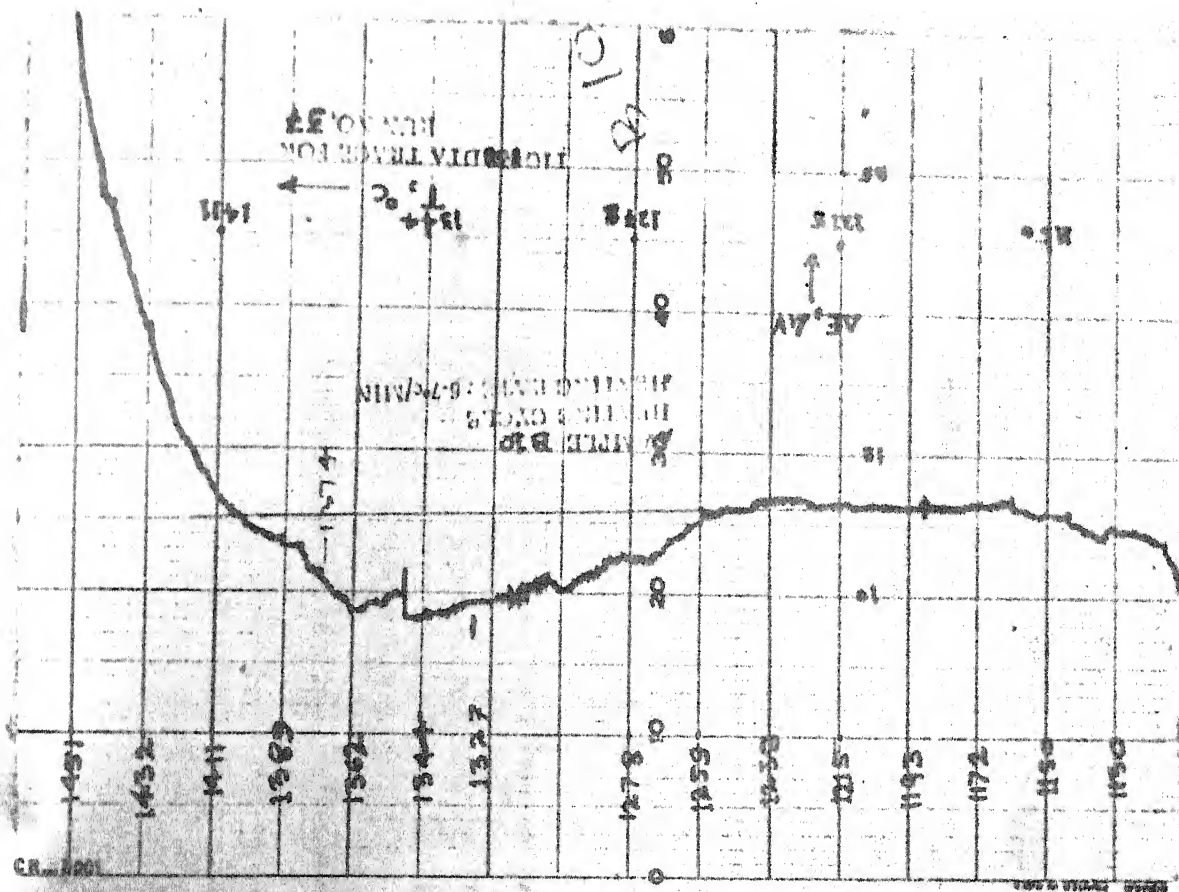


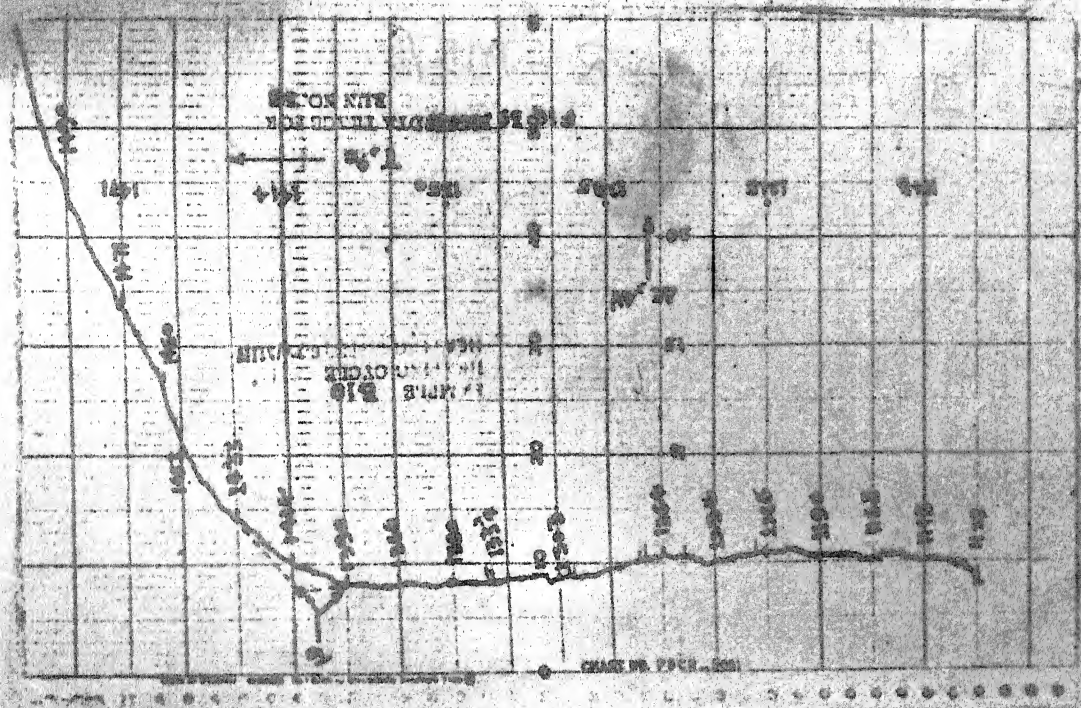
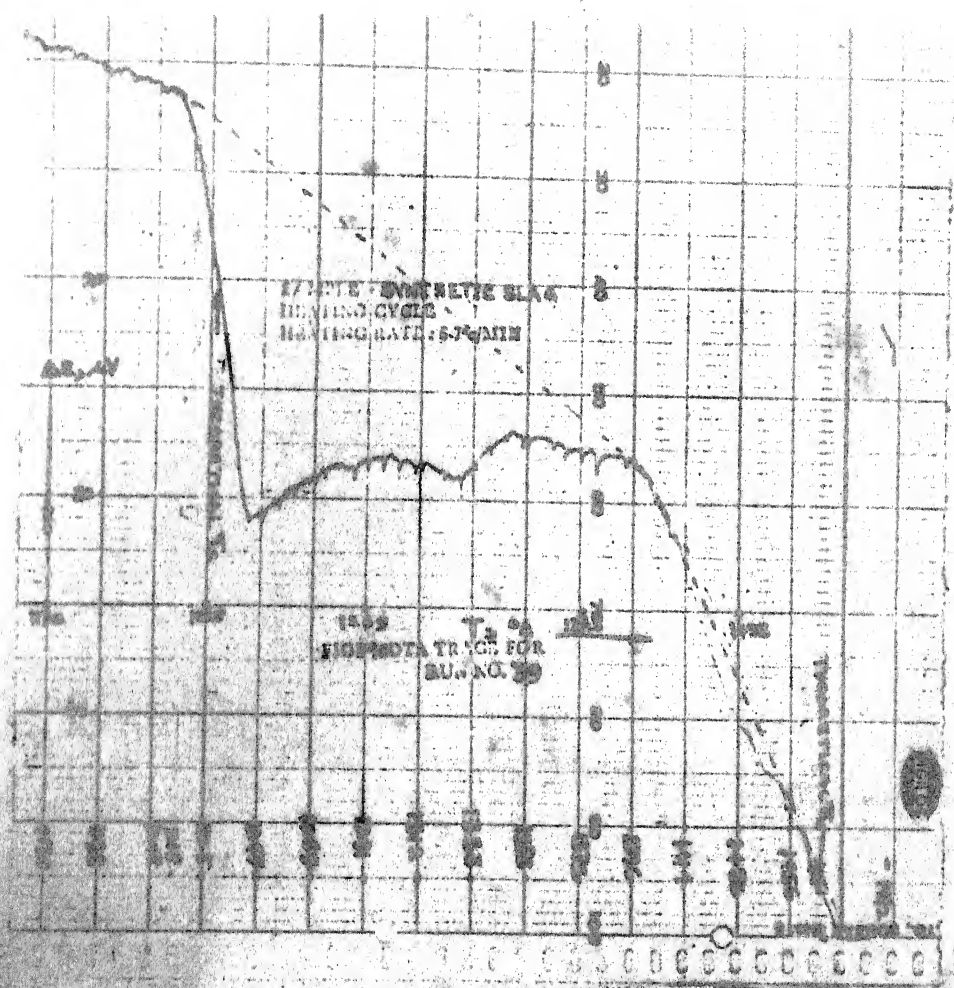












Date Slip

A 50869

This image shows a blank sheet of white paper with horizontal ruling lines. A single vertical line runs down the center of the page, creating two equal-width columns. The horizontal lines are evenly spaced and extend across the entire width of the paper, including both columns. There is no handwriting or other markings on the page.

CD 6 72.9

ME-1977-M-VER-MEA